This is Chapter 3 "Some properties of rocks and rock masses" including the related Appendix B "Some mechanical properties of rocks" from my PhD thesis

Kluckner, A. 2023. Tunnelling at greater depths: Study on the ground and system behaviour when passing a stiff rock block in a weak zone. PhD thesis. Graz University of Technology, Graz, Austria.

The full thesis can be downloaded from the TU Graz repository: LINK

If you have any questions or remarks, you can contact me on

ResearchGate: LINK

or on

LinkedIn: LINK.

Enjoy reading.

Best regards, Alexander Kluckner



Dipl.-Ing. Alexander Kluckner, BSc

Tunnelling at greater depths: Study on the ground and system behaviour when passing a stiff rock block in a weak zone

DOCTORAL THESIS

to achieve the university degree of Doktor der technischen Wissenschaften

submitted to

Graz University of Technology

Reviewers

Em.Univ.-Prof. Dipl.-Ing. Dr.mont. Wulf Schubert Faculty of Civil Engineering Sciences Graz University of Technology, Graz, Austria

Univ.-Prof. Dr. Nobuharu Isago Faculty of Urban Environmental Sciences Tokyo Metropolitan University, Tokyo, Japan

Contents

Li	st of	Figures	xxi
Li	st of	Tables	xxix
Li	st of	Acronyms, Symbols, and Notations	xxxv
1	Intr	roduction	1
	1.1	Research motivation	. 1
	1.2	Research questions	. 4
	1.3	Methodology	. 5
	1.4	Thesis structure and objectives	. 6
	1.5	Research limitations	. 7
2	Abo	out fault zones and block-in-matrix rocks	9
	2.1	Brittle fault zones	. 12
	2.2	Block-in-matrix rocks	. 14
3	Son	ne properties of rocks and rock masses	19
	3.1	Geometric properties of bimrock blocks	. 19
		3.1.1 Block shape	. 19
		3.1.2 Block location and orientation	. 21
		3.1.3 Block size	. 21
	3.2	Mechanical properties of rocks and rock masses	. 22
		3.2.1 Shear strength of the matrix material	. 22
		3.2.2 Uniaxial compressive strength of the matrix material	. 28
		3.2.3 Shear strength of the block material	. 28
		3.2.4 Uniaxial compressive strength of the block material $\ \ldots \ \ldots \ \ldots$. 28
		3.2.5 Tensile strength	. 30
		3.2.6 Dilation angle	. 32
		3.2.7 Poisson's ratio	. 33
		3.2.8 Density	. 36
		3.2.9 Young's modulus	. 36
		3.2.10 Block-matrix contacts	. 40
4	Son	ne characteristics of shotcrete	45
	4.1	Hardening of concrete	. 47
	4.2	Origin of strength and stiffness growth	. 47
	4.3	A note on the behaviour under pressure	. 48
	4.4	About strain in shotcreted tunnel linings	. 49
	15	Postroints	50

CONTENTS

	4.6	Strain	n components	51
		4.6.1	Elastic (instantaneous) strain	52
		4.6.2	Thermal elastic (instantaneous) strain	52
		4.6.3	Shrinkage (delayed) strain	54
		4.6.4	Creep (delayed) strain	57
		4.6.5	Plastic (instantaneous) strain	60
		4.6.6	Irrecoverable strain due to ageing	62
	4.7	Peak	strain	62
	4.8	Shotc	rete strength	63
	4.9	Shotc	rete deformability	66
		4.9.1	Poisson's ratio	67
		4.9.2	Empirical approximation	67
5	The	rmo-cl	nemo-mechanical shotcrete model	69
	5.1	Displa	acement and strain field	70
	5.2	Shotc	rete model	71
		5.2.1	Chemo-thermal coupling	73
		5.2.2	Thermo-mechanical coupling	74
		5.2.3	Chemo-mechanical coupling	74
6	Stiff	f block	next to excavation (2D): Parametric study	81
	6.1		erical model setup	82
		6.1.1	Modelling of system features	82
		6.1.2	Modelling of material behaviour	84
		6.1.3	Mesh	86
		6.1.4	Model size	87
		6.1.5	Boundary conditions and initial state	87
		6.1.6	Solve criterion and damping	87
		6.1.7	Excavation method	88
	6.2	Nume	erical input parameters	89
		6.2.1	Tunnel shape and size	90
		6.2.2	Primary stress state	90
		6.2.3	Block shape	90
		6.2.4	Block location and orientation	90
		6.2.5	Distance of the block from the tunnel and block size	94
		6.2.6	Internal angle of friction of the matrix material	94
		6.2.7	Internal angle of friction of the block material	94
		6.2.8	Cohesion of the matrix material	95
		6.2.9	Uniaxial compressive strength of the matrix material	96
		6.2.10	Uniaxial compressive strength of the block material	97
		6.2.11	Cohesion of the block material	98
		6.2.12	Tensile strength	98
		6.2.13	Dilation angle	100
		6.2.14	Poisson's ratio	100
		6.2.15	Density	100
		6.2.16	Young's modulus	100
		6 2 17	Interface properties	101

CONTENTS xv

	6.3	Evalu	ation approach	103
		6.3.1	Angular deviation of in-plane tunnel displacement vectors	105
		6.3.2	Total in-plane tunnel displacements	107
		6.3.3	Shear strain increment along tunnel periphery	108
		6.3.4	Maximum in-plane block-matrix interface slip, and other interface related	
			variables	109
		6.3.5	Block bending	109
		6.3.6	Horizontal evaluation plane	
		6.3.7	Path of highest secondary in-plane major principal stresses	
		6.3.8	Parameter development with ongoing relaxation	
		6.3.9	Zone-by-zone comparison of different cases	
			Orientation of stresses along block periphery	
			Spalling limit and damage threshold	
			Work	
	6.4		ts: Summary	
	0.1	6.4.1	In-plane block-matrix interface slip	
		6.4.2	Shear strain increment	
		6.4.3	Block deformation	
		6.4.4	Block displacement	
		6.4.5	Path of the highest secondary in-plane major principal stresses	
		6.4.6	Shear strain increment along tunnel periphery	
		6.4.7	Displacement of the tunnel periphery	
		6.4.8	Yielded zones	
		6.4.9	Block failure	
			In-plane stresses	
			Orientation of in-plane stresses	
			Elastic work	
	6.5		pretation and discussion	
	0.0	6.5.1	The block-matrix interface rules	
		0.0.1		
		6.5.2	•	
		6.5.3	Small block distance: hazardous	
		6.5.4	Identification on site? It depends	
		6.5.5	Underestimation of the situation	
		6.5.6	About installing support	157
		6.5.7	On dynamic effects	
		6.5.8	Most probable scenario	158
7	Stiff	f block	next to excavation (3D): Supplementary study	159
	7.1		erical model setup	159
		7.1.1	Modelling of system features	159
		7.1.2	Mesh	160
		7.1.3	Model size	160
		7.1.4	Boundary conditions and initial state	
		7.1.5	Construction sequence and excavation method	
	7.2		erical input parameters	161
		7.2.1	Block shape	161
		7.2.2	Block location	
		_		

CONTENTS xvi

		7.2.3 Block distance from the tunnel	61
	7.3	Evaluation approach	61
	7.4	Results	62
	7.5	Interpretation and discussion	67
8	Fibi	re optic monitoring section: Data evaluation 1	69
	8.1	Distributed fibre optic sensing	
	8.2	Geological and hydrogeological conditions	
	8.3	Rock mass types	
	8.4	Primary stress state	
	0.1	8.4.1 General	
		8.4.2 Primary stress at the analysed section	
	8.5	Tunnelling method	
	0.0	8.5.1 Excavation sequence	
		8.5.2 Support	
		8.5.3 Work steps	
	0.6	•	
	8.6	Position of monitoring devices	
	8.7	Observed system behaviour: Geodetic measurements	
		8.7.1 Time-dependent displacements	
		8.7.2 Out-of-plane displacements	
		8.7.3 In-plane displacements	
	8.8	Observed system behaviour: DFOS	
		8.8.1 Strain in the circumferential and longitudinal direction	
		8.8.2 Evolution of strain with time	
		8.8.3 Strain rate	
	8.9	Observed system behaviour: Temperature	96
9	Fib	re optic monitoring section: Calibration case (3D)	01
	9.1	Limitations	02
		9.1.1 Time-dependent rock deformation	02
		9.1.2 Swelling	02
		9.1.3 Porewater pressure	02
	9.2	DFOS section: Strain components utilising a micromechanical model 2	03
		9.2.1 Neglecting thermal strain	04
		9.2.2 Neglecting shrinkage strain	05
	9.3	Burgers model	05
		9.3.1 Basic rheological models	207
		9.3.2 Combined rheological models	207
	9.4	•	10
		9.4.1 Modelling of system features	12
		9.4.2 Modelling of material behaviour	
		~	14
			15
			15
			15
		r o	16
		9.4.8 Creep time step	

CONTENTS xvii

	9.5	Numerical input parameters	20
		9.5.1 Tunnel shape and size	20
		9.5.2 Primary stress state	20
		9.5.3 Rock mass	20
		9.5.4 Backfill	25
		9.5.5 Shotcrete lining	25
		9.5.6 Rock bolts	33
	9.6	Evaluation approach	36
	9.7	Results	36
	9.8	Interpretation and discussion	40
10		,	43
	10.1	Limitations	
	10.2	Geological and hydrogeological conditions	
	10.3	Rock mass types	
	10.4	Primary stress state	
		10.4.1 General	
		10.4.2 Primary stress at the analysed section	
	10.5	Tunnelling method	
	10.6	Position of monitoring devices	
	10.7	Observed system behaviour: Geodetic measurements	
	10.8	Numerical model setup	
		10.8.1 Modelling of system features	
		10.8.2 Modelling of material behaviour	
		10.8.3 Mesh	
		10.8.4 Model size	
		10.8.5 Boundary conditions and initial state	
		10.8.6 Construction sequence	
	10.9	Numerical input parameters	
		10.9.1 Tunnel shape and size	
		v	60
			61
		9	67
			68
		**	68
			69
	10.12	Interpretation and discussion	71
11	Disc	ussion 2'	77
	11.1		77
	11.2	·	78
	11.3		79
	11.4		79
	11.5		81
	11.6		81
			81
		11.6.2 Tunnel support	
		* *	

CONTENTS xviii

	11.6.3 Tunnelling sequence	284
12 Con	clusion	285
Bibliog	raphy	287
Appen	dix A: Equations	317
A.1	Stress invariants	317
A.2	Strain invariants	317
A.3	Mohr-Coulomb failure criterion	318
A.4	Size of the yield zone in a homogeneous, isotropic rock mass	318
A.5	Elastic secondary tangential in-plane stresses around a circular opening in a	
	homogenous, isotropic medium	319
A.6	Elastic secondary tangential in-plane stresses around an elliptic opening in a	
	homogenous, isotropic medium	320
Appene	dix B: Some mechanical properties of rocks	321
B.1	Tensile strength	321
	B.1.1 Johnston (1985)	
	B.1.2 Kluckner (2012)	
	B.1.3 Rostami et al. (2016)	
B.2	Dilation angle	
	B.2.1 Terminology	
	B.2.2 Kluckner (2012)	
B.3	Poisson's ratio	326
B.4	Young's modulus	326
A	dia C. Stiff black most to accounting (2D). Dominator of the	220
C.1	dix C: Stiff block next to excavation (2D): Parametric study Numerical model setup	329
0.1	C.1.1 Evaluation of constitutive model for matrix material	
	C.1.2 Evaluation of minimum in-plane model size	
	C.1.3 Evaluation of solve limit	337
	C.1.4 Evaluation of excavation method	342
C.2	Numerical input parameters	343
0.2	C.2.1 Mechanical properties of model features	343
	C.2.2 Evaluation of interface stiffnesses	350
C.3	Results: Details	355
	C.3.1 In-plane block-matrix interface slip	355
	C.3.2 Shear strain increment	370
	C.3.3 Block deformation: Bending	385
	C.3.4 Block deformation: Change in the block height	391
	C.3.5 Block deformation: Change in the block width	393
	C.3.6 Block displacement	396
	C.3.7 Path of the largest secondary in-plane major principal stresses	400
	C.3.8 Shear strain increment along tunnel periphery	405
	C.3.9 Displacement of the tunnel periphery	411
	C.3.10 Yielded zones	425
	C.3.11 Block failure	438

CONTENTS	xix
C.3.12 In-plane stresses	457
C.3.13 Orientation of in-plane stresses	472

C.3.14 Elastic work	485
Appendix D: Fibre optic monitoring section: Data evaluation	497

Chapter 3

Some properties of rocks and rock masses

The studies in Chapter 6 (p. 81) and Chapter 7 (p. 159) simulate a tunnel drive through a weak zone of matrix material comprising one stiff block next to the tunnel. This chapter here reports about information from literature on geometric properties of blocks and mechanical properties of block and matrix material. Since the studies aim to consider for a wide range of material parameter combinations existing in nature, many sections below cite properties and parameter relationships not relating to bimrock but to rocks in general. Because some fault zone material is soil-like, also some soil parameters are listed. The parameter relationships help to identify reasonable parameter combinations for the parametric study in Chapter 6.

The information on material properties cited in this chapter is limited to results from tests under drained conditions. Because the thesis focusses on scenarios where the block is stronger and stiffer than the matrix material, data from contrary cases (i.e., matrix material is stronger and stiffer than the block; cf., e.g., [9]) is not considered here. And this chapter does also not describe the overall strength and stiffness of bimrock and related determinants (e.g., volumetric block proportion), because here, it is all about a single-block scenario. For the former, refer to, e.g., [306] and literature cited therein.

Section 3.1 lists information on the geometric properties of bimrock blocks. And Section 3.2 (p. 22) identifies ranges of some mechanical properties of rocks and rock masses.

3.1 Geometric properties of bimrock blocks

The following subsections give some information on the shape, location and orientation, and size of blocks of block-in-matrix rocks (bimrocks).

3.1.1 Block shape

The more competent, less strained rock bodies embedded within a matrix often show an ellipsoidal, lenticular, or prolate shape ([114, p. 184], [254, p. 264]). Such a rock body (i.e., block) forms when shears of various types link with each other ([114, p. 184]; cf. also Section 2.2 on p. 14). In subsequent shear movements, the block may wear and round off. If it has been detached from the host rock, during further shearing it may also translate and rotate within the matrix.

Which block shape eventually results probably depends on many factors, some of which might be: initial shape defined by the shears, stress conditions, thickness and structure of the zone within which the block is embedded (determines, e.g., the degree of freedom regarding a block rotation), and location of concentrated shear within the zone. Some of these factors vary in time. Hence, depending on the history a block has experienced, many shapes seem possible. [250, p. 22], for example, report that large blocks in Franciscan mélange can feature a smoothly ellipsoidal but also an irregular shape. Random shape of blocks (with typically rounded edges) in serpentinite bimrock was reported by [127, p. 55]. The two examples of bimrocks different in scale given in Fig. 3.1 highlight the variability in the block shapes within each imaged bimrock zone ranging from compact to elongated.

In case of Franciscan mélange, the aspect ratio (i.e., major axis length to minor axis length) of some mapped large blocks ranges from 1 to 3, and is 2 on average ([255, p. 74]). [255, Fig. 3.12, p. 74] determined a similar average ratio for some blocks in sheared serpentinite. [317, p. 23] reports an average aspect ratio of 3.6 of blocks in phyllitic matrix mapped at the north tube of the tunnel *Spital* between chainage 933.4 m and 1094.7 m (cf. Fig. 3.2). Blocks with an initially larger aspect ratio most probably fail during the fault zone's evolution due to bending. In line, [227] (cited in [255, p. 74]) fabricated blocks with an aspect ratio of 2 to 3 for his tests on artificial bimrock specimens; [306, p. 54] used ellipsoids with a ratio of 2.3 to 2.5 for his laboratory tests; and [23] modelled ellipsoids with a ratio of 2 in their two-dimensional numerical studies.¹



Figure 3.1: Images of exemplary bimrocks: (a) Transition from blocky rock mass into bimrock (central part of picture); mesoscale (from [324, Fig. 7, p. 18]). (b) Franciscan mélange showing anisotropic fabric of elongated blocks entrained within sheared shale matrix; scale bar is 1.5 m (from [255] graphed in [253, Fig. 1, p. 600]).

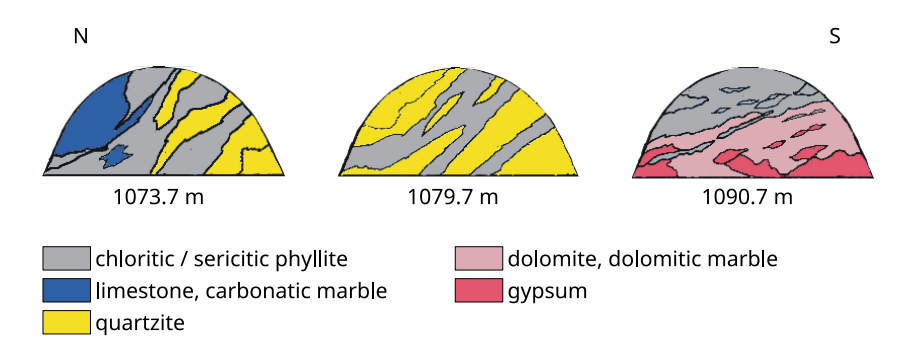


Figure 3.2: Sketches of the observed geological conditions at tunnel faces at chainage 1073.9 m, 1079.7 m, and 1090.7 m of the north tube of the tunnel *Spital*, Austria (modified from [317, Fig. 10, p. 13]). In the graphs, the phyllites (coloured in grey) are the weak matrix material.

¹In [255, p. B-6], the major axis is the longest line that can be drawn within the block, and the minor axis is the longest line that can be drawn normal to the major axis. [317, p. 23] fitted ellipsoids to the mapped rock blocks. So, the authors used different approaches to determine the block size and shape. Thus, given aspect ratios cannot be compared directly.

3.1.2 Block location and orientation

The incorporation of competent blocks (i.e., rock fragments or lenses) into the fault zone can happen when progressing faults (through the host rock) link at dilational jogs² and form relays³ (cf. also previous subsection). These relays then surround blocks of relatively undeformed protolith. [420, p. 9]

Relays are shears that accommodated much displacement and comprise fault gouges or other highly strained fault rocks ([420, p. 9]). Commonly, blocks entrained within the shears are oriented subparallel to these ([254, p. 268], [88] in [227, p. 4]). Shears can cross through a fault zone in a tortuous way ([254, p. 268]). For example, because of linkage with other shears, or because the path along which they progress changes at a tectonic event different in its characteristics to a previous one. Hence, considering the complexity a fault zone can have, the orientation of blocks can change abruptly from one place to another within the fault zone ([254, p. 268]). If the matrix features a well-developed foliation, traces of fault systems and related shear zones, and, therefore, blocks embedded in those systems or zones, may align sub-parallel to the foliation planes (c.f., e.g., [317, p. 12ff, 23]).

Depending on the fault zone's evolutionary history, the block may be still next to the host rock walls or far away from them closer to the damage zone or fault core centre.

3.1.3 Block size

Block sizes in fault zones can range between millimetres and hundreds of metres. The block size distribution in brittle faults is often fractal (i.e., conforming to negative power laws; [254, p. 266]). That means that at a specific scale, a fault or a fault zone comprises "relatively few large blocks and increasing numbers of ever diminishing smaller blocks". [324, p. 17f]

At a different scale, a similar picture results. Hence, block size distributions are scale-independent (probably between some natural upper and lower fractal limits), showing a self-repeating pattern at different scales: small blocks at one scale of interest are part of the matrix at the smaller scale ([254, p. 265f]). [256, p. 911] report about the scale-independency of Franciscan mélange over seven orders of magnitude regardless of the scale of measurement or the nature of the mélange's fabric.

According to [255], because of the scale-independency of block size distributions, for each engineering problem dealing with bimrocks, a scale of interest must be specified. For this purpose, he introduced the characteristic engineering dimension, ced, being, for example, the length of a straight line through an object or space, or the square root of an area of interest, \sqrt{A} . Depending on the problem at hand, this can be the slope height, the size of the yield zone around openings, or the dimensions of laboratory test specimens ([255, p. 3]). Now, to discriminate between matrix material, blocks, and blocky rock mass for a given zone, [255] further introduced two threshold values for the block size:

- $d_{max} < 0.75 \cdot ced$: Blocks with a size below this threshold are treated as single blocks of the bimrock. Is the block larger, then the block takes up almost the entire area (or volume) of interest, and the zone should be treated as blocky rock mass with matrix-filled joints.
- $d_{min} > 0.05 \cdot ced$: Blocks with a size below this threshold can be seen as part of the matrix

²Jogs (or bends, or ramps) are curved parts of a continuous fault trace that connect two noncoplanar but approximately parallel segments of faults ([397, p. 86, 193]). Such jogs can be of compressional or dilational nature (cf. Fig. 5b in [373, p. 1035]).

³Along relays (a fault, or a zone) displacement (or slip) is *transferred* from the end of one fault to an adjacent parallel fault ([397, p. 86]).

material. They may represent up to 95% of the total number of blocks but less than 1% of the total volume of blocks and, therefore, contribute little to the strength of the bimrock ([255, p. 31]). Larger blocks are treated as single blocks of the bimrock.

Here, d_{max} is the size⁴ of the largest geotechnically significant block in the given population, and d_{min} is the size of the smallest block. One can imagine that at a laboratory test sample with, for example, a maximum dimension of 15 cm, a block with contrasting mechanical properties but a size of less than $0.05 \cdot 15 = 0.75$ cm may not alter the overall behaviour of the sample much during testing. However, a block with a size of 5 cm will. And in case the block features a size of greater than $0.75 \cdot 15 = 11.25$ cm (maximum observed dimension at the test sample; d_{mod} in [255]), it makes up almost the whole sample and one cannot talk about a block-in-matrix structure here anymore. Similar considerations apply to a tunnel surrounded by a yielded zone. Note that depending on the scale of interest, e.g., a rock boulder⁵ or a sand grain⁶ can be declared as a block. According to [254, p. 267, 274], "the most conservative block-matrix threshold that can be justified should be selected"; and for the characteristic engineering dimension, ced, it is the area or dimension within which most likely the critical mode of failure will occur. Note that the selected thresholds for the block size then decide upon the number of blocks the investigation rock or fault zone mass comprises.

[255] identified the threshold values above analysing outcrops and geological maps of several Franciscan mélanges with the measurement areas ranging from 0.01 m² to 1000 km² (cf. Fig. 2.8 in [255, p. 27]). Considering that other bimrocks also exhibit scale-independent (or self-similar) block size distributions—e.g., fault gouges ([338] in [254, p. 266]), Italian olistostromes ([79] in [254, p. 265]), or carbonate and quartzite blocks within phyllitic matrix ([317, p. 61])—the threshold values probably apply to them as well.

3.2 Mechanical properties of rocks and rock masses

Since block-in-matrix rocks (bimrocks) comprise blocks (strong rock) and matrix material (weak rock or rock mass), the following subsections cite some general information on the mechanical properties of rocks and rock masses, and some specifics on bimrock. The information is required to identify suitable material parameters for the numerical studies.

Note that more information is available on fault rocks and fault-zone masses than on bimrock. Anyway, depending on the scale of interest, the former can make up the matrix material of a bimrock. Because the parametric study relates the block strength and stiffness to the matrix strength and stiffness, attention is paid on the matrix material and on general parameter relationships.

If not state otherwise, parameters cited below refer to rock and not to rock mass. Bimrock is a rock mass. Its constituents, the block and the matrix, are rocks. Fault zone material is also considered as rock, unless it is homogenised with, e.g., more competent fault zone features.

3.2.1 Shear strength of the matrix material

This section lists strength parameters of the weaker matrix material of bimrocks, but also of weak fault zone material that is not characterised as bimrock. A fault zone that mainly comprises such weak fault zone material still can feature single stiff blocks even if not encountered, e.g., with investigation drillings or during tunnelling.

⁴Diameter or any other characteristic dimension of the block (cf. [255, p. xvii]). Cf. also Footnote 1 (p. 20).

⁵A particle is classified as a boulder if it features a length of 256 . . . 4096 mm (cf., e.g., [40, Fig. 2, p. 8]).

⁶A particle is classified as a *grain* if it features a length of 0.063 . . . 2 mm (cf., e.g., [40, Fig. 2, p. 8]).

[106] compiled and re-analysed published laboratory data about shear strength properties of shear zone materials in crystalline rocks. Fig. 3.3 compares the cohesion and the friction angle (peak shear strength) of different shear zone material. Most of the values for the internal angle of friction range from 22° to 36° with $\varphi_{min} \approx 16^{\circ}$ and $\varphi_{max} \approx 42^{\circ}$. The cohesion ranges from 0 MPa to approx. 1.8 MPa. From the graph it seems that at least for the schist kakirite there is a negative relationship: a material sample with a high friction angle shows a lower cohesion than a material sample with a lower friction angle. The material samples then may be at a different stage of evolution regarding shearing. Consider that the cementation of $(intact)^7$ rock material is gradually destroyed with shearing, reducing the cohesive strength (softening of cohesion) and transforming the material to a granular one eventually featuring frictional hardening only ([410, p. 37]). But, during shearing also composites of bonded particles break apart. Those fragments now involved in the shearing process feature an angular shape contributing to an increase in the internal angle of friction (for more details, refer to Section 3.2.10 on p. 40; there, it is also described in which case the friction angle decreases with increasing shearing). Anyhow, when trying to identify relationships one has to keep in mind that test results strongly depend on the sample preparation and test settings (e.g., loading sequence).

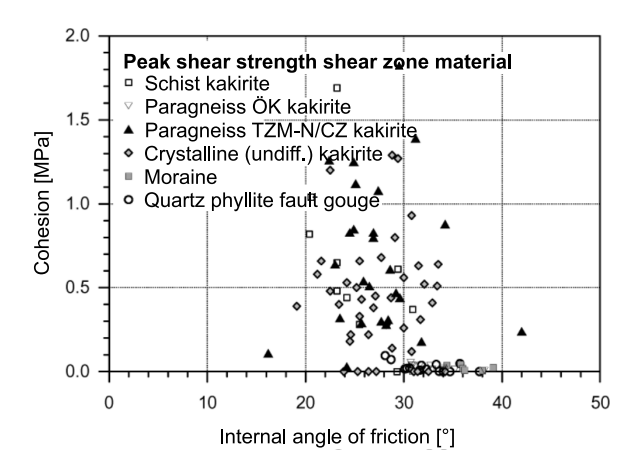


Figure 3.3: Peak shear strength of shear zone materials in crystalline rocks (modified from [106, Fig. 7, p. 70]; modification: translation). For results of linear regression of this data, cf. Fig. 3.4. ÖK ... Ötztal Kristallin (crystalline), TZM-N ... northern Tavetscher Zwischenmassiv (intermediate massif), CZ ... Clavaniev zone.

The tests on shear zone material from which [106] have reviewed the results (triaxial compression, direct shear, and ring shear tests; cf. text above), have been performed under different stress conditions. The Mohr-Coulomb parameters, i.e., the internal angle of friction, φ , and the cohesion, c, are fitting parameters and depend on the stress range within which the fit is performed. Thus, the authors decided to do the linear regression analysis on the normal stress, σ_n , and shear stress, τ , data pairs rather than on the Mohr-Coulomb parameters. From the

⁷In this context, *intact* relates to a pre-peak state of a particular rock (or rock mass) volume for a given stress state. If the material reaches its final residual (post-peak) state after intense shearing, and, for whatever reason, the stress state changes (e.g., confinement increases), it might regain a pre-peak state capable of resisting additional load. This is probably not an infinite process. At high temperature and pressure, depending on the characteristics of elements present (e.g., fluids, gases), chemical reactions may take place (e.g., metamorphose, recrystallisation, or cementation). In geotechnics, *intact* also relates to the state a material exhibits prior to additional straining because of natural (e.g., earthquake) or man-made events (e.g., tunnel excavation). As material inevitably gets disturbed at recovery (e.g., damage during cutting or drilling, unloading), transportation or preparation, the amount of which is often unknown or indefinable, the term *intact* generally relates to the material state prior testing (laboratory or in situ). Moreover, in rock mechanics, the term *intact* is often used to differentiate between (intact) rock and (imperfect) rock mass. The former does not feature a persistent plane of weakness. Few or many persistent or non-persistent discontinuities cross the latter, splitting it into a volume comprising several connected or unconnected (intact) rock pieces. It is apparent that this all is a question of scale.

fits, they then determined average values for the Mohr-Coulomb parameters. By introducing the requirement that the maximum value for φ can only relate to the minimum value for c, and vice versa (cf. negative relationship in text above), they could identify a region of confidence. The requirement somehow attempts to satisfy the fact that for most rocks the shape of failure envelopes (here, the trend of normal stress and shear stress data pairs) is between straight and parabolic (i.e., the envelope curves downward with decreasing normal stress) ([165, 180] in [130, p. 87]). Fig. 3.4 graphs some results of the fitting processes. Even though it compares the strengths of different shear zone material, it indicates the problem regarding the stress-dependency of the Mohr-Coulomb parameters: at low normal-stress levels, high friction angles and low values for the cohesion result; at high normal-stress levels, low friction angles and high values for the cohesion result. Depending on the geotechnical problem at hand and on the stress state and its temporal evolution, using the standard Mohr-Coulomb model (like in this thesis) with a fixed set of Mohr-Coulomb parameters, the rock strength may either get over- or underestimated. However, the characteristics of this relationship probably depend on the maturity of the shear zone material (e.g., level of decomposition). Fig. 3.15 (p. 42) compares peak and residual strengths from shear tests on joints in weak phyllites. It is not a strong sign, but the scatter of the residual strengths (represented by the error bars) is less than of the peak strengths. Thus, the influence of the difference in the stress level may be smaller.

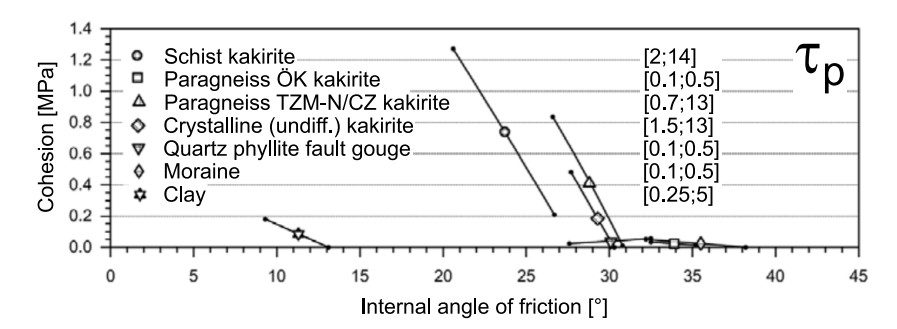


Figure 3.4: Peak shear strength, τ_p , of different crystalline shear zone material (from [106, Fig. 10, p. 75]; translated, and information on the range of normal stress, σ_n , from Tab. 1 in [106, p. 74] constituting the limits for the individual regression analysis has been added). Symbols constitute average values from linear regression of normal stress, σ_n , and shear stress, τ , data pairs from triaxial compression and shear tests. Inclination of error bars (90% confidence level) indicate the influence of uncertainties of the internal angle of friction or cohesion on the shear strength. ÖK ... Ötztal Kristallin (crystalline), TZM-N ... northern Tavetscher Zwischenmassiv (intermediate massif), CZ ... Clavaniev zone.

Fig. 3.5 shows the change in shear strength—from peak to residual strength—of some initially intact but weak rock samples from the Semmering Base Tunnel project subjected to direct shear tests (for details on the tests, refer to Section B.2.2 on p. 325 in the appendix). In most cases, φ and c are lower in the residual state (arrows point to the left and downwards). Section 3.2.10 (p. 40) details why strength can also increase with shearing. By normalising the change in shear strength to the peak shear strength, i.e.,

$$(\varphi - \varphi_r)/\varphi$$
 and (3.1)

$$\left(c - c_r\right)/c,\tag{3.2}$$

the graph in Fig. 3.6 results. In 26 of 35 cases, φ reduces by up to 20% and c by 50% to 100%. Tab. 3.1 lists some statistical parameters of the normalised changes in strength graphed in Fig. 3.6.

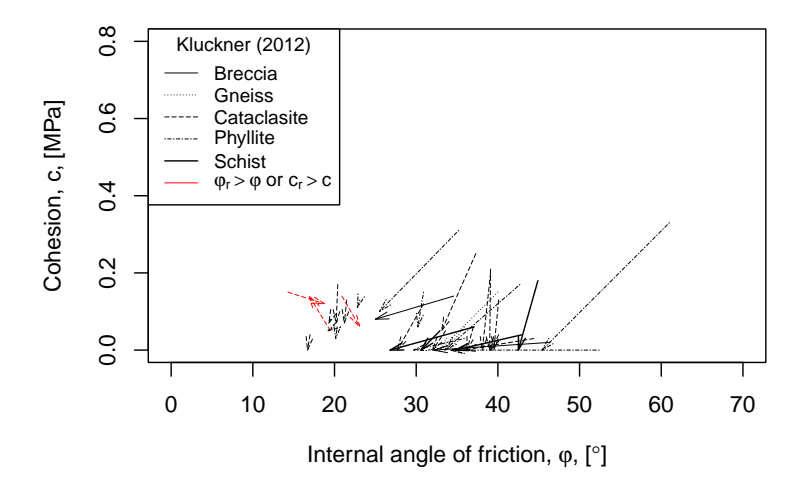


Figure 3.5: Shear strengths (in terms of internal angle of friction, φ , and cohesion, c, data pairs) from direct shear tests on intact rock specimens under constant normal stiffness (CNS) or constant normal load (CNL) conditions: Change from peak to residual strength. Orientation of weakness planes (e.g., foliation planes; if present) relative to shear direction not considered here. Rear end of arrows: peak shear strength (φ , c); arrowhead: residual shear strength (φ_r , c_r). Data from Kluckner (2012) [199]. CNS: n=23, $\tau_{max}=[0.24;2.83]$ (in mega-pascal), $s(\tau=\tau_{max})=[0.21;18.35]$ (in millimetres); for more details, cf. Section B.2.2 (p. 325) in the appendix. CNL: n=12; multistage test; phyllites, schists, or phyllite or schist cataclasites. Data also plotted in Fig. 3.6.

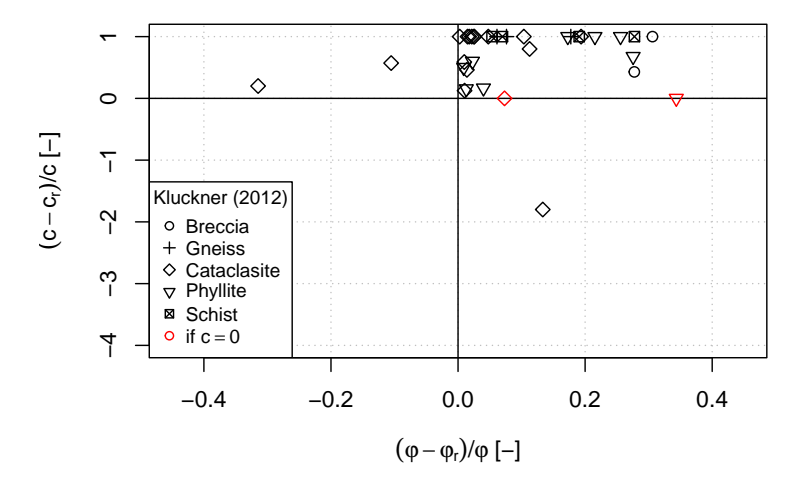


Figure 3.6: Shear strengths from direct shear tests on intact rock specimens: Normalised change in strength (from peak strength $\{\varphi;c\}$ to residual strength $\{\varphi_r;c_r\}$). Same data as for Fig. 3.5. Corrections (marked in the graph with a different colour): $c=0 \land c_r=0 \Rightarrow (c-c_r)/c=0$; $c=0 \land c_r\neq 0 \Rightarrow (c-c_r)/c=-4$.

SD...standard deviation

Ratio	Statistical parameter	Shear test on intact rocks (cf. Fig. 3.6) [199]
$(\varphi - \varphi_r)/\varphi$	Median Average SD	0.06 0.10 0.10
$(c-c_r)/c$	Median Average SD	1 0.82 0.29

Table 3.1: Shear strengths from direct shear tests on intact rock specimens: Statistics on normalised change in strength (cf. Fig. 3.6).

In 2016, the Swiss Geological Survey published the final report on the geological, geotechnical, and hydrogeological conditions of the *Gotthard Base Tunnel* project ([145]). Tab. 3.2 lists some rock parameters of fault gouge from fault zones given in the report. Here, the friction angle ranges from 21° to 37°, and the cohesion from 0.3 MPa to 2.7 MPa.

Table 3.2: Rock parameters of fault gouge from the *Gotthard Base Tunnel* project ([145, Tab. 5.3–5.5, p. 56f]).

Rock type	$arphi^{ m a}$	c^{a}	$E^{ m a,b}$				
<u>, , , , , , , , , , , , , , , , , , , </u>	[°]	[MPa]	[GPa]				
Prognosis for the construction project from literature, technical reports, and in situ and laboratory tests							
Kakirite (gneiss, schist, phyllite)	25 – 34	0.4 – 0.5	-				
Triaxial compression tests on samples recovered from exploratory drillings							
Kakirite (CZ): strongly sheared, >30% ^c	30.1	0.5	1.4/3.9				
Kakirite (TZM N): strongly sheared, >30% ^c	24.9	0.5	0.8/2.9				
Kakirite (TZM N): sheared, crumbled, 10–30% ^c	24.6	0.4	0.9/2.9				
Kakirite (TZM N): sheared, crushed, $<10\%^{c}$	27.4	0.5	1.2/3.6				
Triaxial compression tests on samples recovered from core drillings performed at the tunnel							
level during construction							
Kakirite (CZ)	25.8-29.0	0.3 – 0.4	-/2.7-3.5				
Kakirite (TZM N)	20.8 – 36.5	0.3 – 2.7	3.2 – 5.5				

 $^{{\}rm CZ}\dots {\it Clavaniev}$ zone; TZM N \dots northern ${\it Tavetscher Zwischenmassiv}$ (intermediate massif); both zones mainly comprise chloritic two-mica gneiss to schist and chlorite-sericite schist with biotite

Tab. 3.3 summarises the representative design rock parameters (engineering judgement based on literature, technical reports, and in situ and laboratory test results) of five fault rock types from the Semmering Base Tunnel project. For the fault rock parameters, $\varphi = [23; 40]$ (in degrees) and c = [0.06; 0.2] (in mega-pascal). And for the fault-zone mass parameters it is $\varphi = [23; 36]$ (in degrees) and c = [0.06; 0.8] (in mega-pascal).

^a Single value (e.g., 30.1) ... average value; range of values (e.g., 0.4–0.5)

^b Values depending on the lateral pressure, σ_3 , at the triaxial compression tests (e.g., 1.4/3.9): left value: $\sigma_3 = 1...2$ MPa; right value: $\sigma_3 = 9...12$ MPa

^c Content of fines

Table 3.3: Fault rock parameters and fault-zone mass parameters (in parentheses; homogenisation of fault rock and less disturbed zones) from the *Semmering Base Tunnel* project ([380, p. 30–34]). For a brief description of the fault rock types, refer to, e.g., Tab. 2 in [114, p. 192].

Rock type	φ [°]	c [MPa]	E [GPa]	ν [-]
Carbonate cataclasites, silty/sandy/gravelly, <30% or >30% a	25-36 (27–33)	<0.2 (0.2–0.8)	0.3-1 $(0.75-3)$	NA (0.2–0.3)
Quartzite cataclasites, sandy/gravelly	25–40 (27–36)	<0.1 (0.3–0.7)	<3 (1–8)	NA (0.2–0.3)
Phyllosilicate-rich cataclasites (schist, phyllite), silty/sandy/gravelly, <30% or >30% a	$\begin{array}{c} 23-27 \\ \parallel (23-27) \\ \perp (25-30) \end{array}$	0.06-0.15 (0.06-0.15) 	$0.16-1.63^{b}$ $\parallel (2-10)^{b}$ $\perp (0.4-2)^{b}$	≈ 0.3 $(0.25-0.3)$
Phyllosilicate-rich cataclasites (schist, phyllite), silty/sandy, >30% ^a	23–27 rm=r	0.06-0.15 rm=r	0.18-0.43 ^b rm=r	≈ 0.3 $(0.25-0.35)$
Phyllosilicate-rich cataclasites (sericite phyllite), silty, >50% ^a	23–25 rm=r	0.1-0.15 rm=r	0.16–0.37 ^b rm=r	≈ 0.3 $(0.25-0.35)$

without parentheses: fault rock parameters; with parentheses: fault-zone mass parameters; \parallel ... parallel to cataclastic layers; \perp ... perpendicular to cataclastic layers; rm ... rock mass; r ... rock; NA ... not available

[127] report about serpentinite bimrock material making up parts of the foundation of a gravity dam in Indonesia. They performed uniaxial and multistage triaxial compression tests on intact matrix specimens. The average cohesion results to c=3.7 MPa, and the average friction angle to $\varphi=36^\circ$ ([127, Tab. 2, p. 56]). [418] performed in situ direct shear tests on soil-rock mixtures at the Xiazanri slope in China. The mixture comprises limestone blocks (selected thresholds for the block size: 2 cm and 30 cm; maximum observed dimension) and a clayey matrix. From a test on a specimen with no blocks (i.e., matrix material only), they determined a cohesion of c=4.3 kPa and a friction angle of $\varphi=25.6^\circ$ ([418, Fig. 15, p. 1245]). [426] also analysed a soil-rock mixture of sedimentary origin. They performed triaxial compression tests on specimens different in block content (selected lower threshold for the block size: 5 mm; grain size). The material was recovered from the Tangjiashan Barrier Dam in China. From a test on a specimen comprising no blocks, they determined a cohesion of c=25.9 kPa and a friction angle of $\varphi=33.1^\circ$ ([426, Tab. 2, p. 50]).

The data listed above suggests a lower bound for the friction angle of approx. 20° . In contrast, [254, p. 269] report that a sheared matrix material in Franciscan mélange (matrix often composed of sheared shale, argillite, siltstone, serpentinite, or sandstone) can feature an effective friction angle of $<10^{\circ}$ (and low to zero cohesion). However, such a low friction angle seems to be extraordinary and not representative for the material usually encountered at tunnelling projects. The friction angle of the fault gouge at the section of the *Galgenberg* tunnel where the collapse occurred ranged from 12° to 14° (cf. Section 1.1 on p. 1).

 $^{^{\}rm a}$ Content of fine grains (fraction ${<}63~\mu{\rm m})$

^b Oedometer modulus; values refer to virgin loading; values valid for $5 \le \sigma_1 \le 20$ (in mega-pascal)

3.2.2 Uniaxial compressive strength of the matrix material

With the Mohr-Coulomb strength criterion (cf. Eq. 6.3 on p. 96), the equivalent uniaxial compressive strengths, σ_c , of two exemplarily selected specimens (both Paragneiss TZM-N/CZ kakirite) plotted in Fig. 3.3 (p. 23) are approx. 0.27 MPa (with $c \approx 0.1$ MPa and $\varphi \approx 16^{\circ}$) and approx. 6.2 MPa (with $c \approx 1.8$ MPa and $\varphi \approx 29.7^{\circ}$). Applying the same approach, it is approx. 14.5 MPa for the matrix material investigated by [127], approx. 0.01 MPa for the one from [418], and approx. 0.1 MPa for the one from [426] (cf. Section 3.2.1 on p. 22 for [127, 418, 426]). Anyway, σ_c of matrix material can be much higher:

- [378, Tab. 1, p. 555]: volcaniclastic Ankara agglomerate (matrix: tuff; blocks: andesite) with $\sigma_c = [6.4; 14.4]$ (in mega-pascal) for the matrix material;
- [185, Tab. 1, p. 1472]: strongly cemented Misis fault breccia (matrix: claystone; blocks: dolomitic limestone) with $\sigma_c = [40.2; 76.0]$ (in mega-pascal) for the matrix material.

Both the lower and upper bound values cited above are close to or within the range of strength values for fault zone material reported by [339] (cf. list on p. 39).

3.2.3 Shear strength of the block material

According to [255, p. 29], the friction angle contrast $(\tan \varphi_b/\tan \varphi_m)$ between (the weakest) block and matrix material must be at least 1.5–2.0 to discriminate the components. Then, failure surfaces propagate around the blocks as observed at the laboratory tests of [227] rather than through the blocks (i.e., if contrast is too low and strength matrix \sim strength block).

The matrix material of the mélange below the foundation of the Scott Dam (California), for example, features an average friction angle of 29°. It is 54° for the blocks within the mélange. The frictional strength contrast results to 2.48. [412] in [255, p. 29]

A similar ratio exists at chainage 282.3 m of the access tunnel *Göstritz* of the *Semmering Base Tunnel* project.⁸ Fig. 3.7 shows a sketch of the geological situation observed at the tunnel face. Here, weak cataclasites (zones A–C) surround a strong shear body of gypsum dolomite breccia (zone D). The frictional strength contrast ranges from 1.7 to 2.8 (based on the intact rock properties) and from 1.3 to 2.3 (based on the homogenised rock mass properties) (cf. Tab. 3.4).

[255, p. 28f] suggests that not only the friction angle can be used to identify a minimum contrast, but also the cohesion, or the uniaxial compressive strength (cf. Section 3.2.4). No threshold is given for the cohesion. For the bimrock given in Tab. 3.4, the contrast in cohesion ranges from 6 to 417.

3.2.4 Uniaxial compressive strength of the block material

Highlighted by [254, p. 268], in terms of the Mohr-Coulomb failure criterion, the rock strength is not only determined by the internal angle of friction but also by the cohesion. Thus, to discriminate between rock mixtures where larger blocks have negligible influence on the overall behaviour of the mixture, and bimrocks comprising significant blocks, a strength-contrast concept can be utilised rather than a friction angle-contrast concept (cf. Section 3.2.3). After a personal communication with Prof. Harun Sönmez in 2009, [254, p. 268] propose that the uniaxial compressive strength of the block should be greater than 1.5 times the uniaxial compressive strength of the matrix material (i.e., $\sigma_{c,b} > 1.5 \cdot \sigma_{c,m}$).

⁸The thesis uses the tunnel section this chainage is in as validation case (cf. Chapter 10 on p. 243).

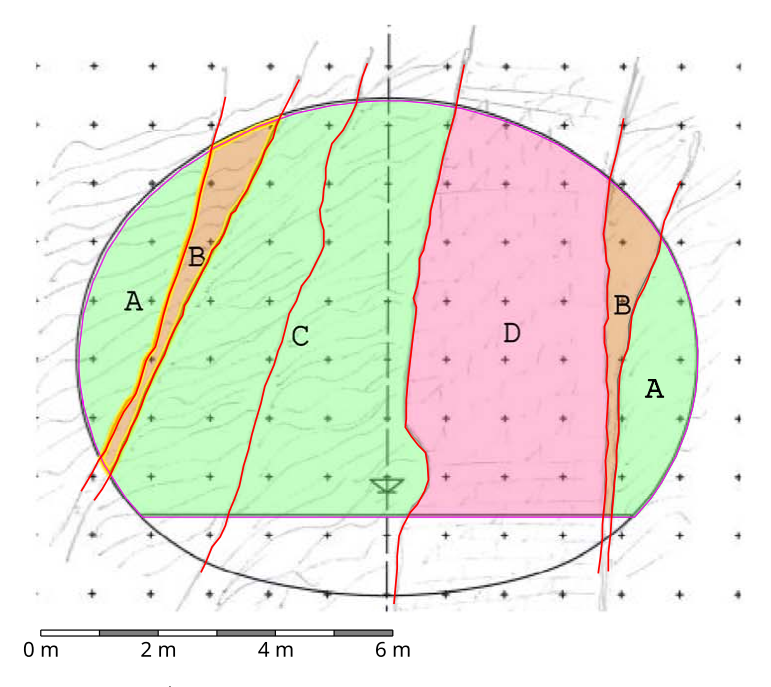


Figure 3.7: Sketch of the top/bench-heading tunnel face at chainage 282.3 m of the access tunnel Göstritz (construction lot SBT 1.1) of the Semmering Base Tunnel project (from [152]). Area A: cataclasite (sericite phyllite); area B: cataclasite (calcareous clay schist); area C: cataclasite (sericite phyllite); area D: gypsum dolomite breccia. Tab. 3.4 lists some strength parameters.

Table 3.4: Design values for the friction angle and cohesion of intact rocks and rock masses encountered at chainage 282.3 m of the access tunnel *Göstritz* (construction lot SBT 1.1) of the *Semmering Base Tunnel* project ([380, p. 25, 32, 34]). Note that the values given are design values and do not account for the actual composition of each zone observed at site (e.g., actual share of fault rocks and less disturbed zones within fault-zone masses). Fig. 3.7 graphs the sketch of the tunnel face.

Zone	bimrock component		φ [°]	c [MPa]	$\tan \varphi_b / \tan \varphi_m$ [-]		c_b/c_m [-]	
					min.	max.	min.	max.
A, B	matrix		23 - 27	0.06 – 0.15	1.7	2.8	113	417
			(23-27)	(0.06-0.15)	(1.4)	(2.3)	33	250
		\perp	(25-30)	(0.4 – 0.8)	(1.3)	(2.1)	6	38
С	matrix		23 - 25	0.10 – 0.15	1.8	2.8	113	250
			rm=r	rm=r	(1.6)	(2.3)	33	150
D	block		40 – 50	17 - 25	-	-	-	-
			(36-44)	(5-15)	-	-	-	-

without parentheses: intact rock parameters; with parentheses: rock mass parameters; $\parallel \dots$ parallel to cataclastic layers; $\perp \dots$ perpendicular to cataclastic layers; rm ...rock mass; r ...rock

[378, p. 555] reports a strength contrast between the block and the matrix material of Ankara Agglomerate of up to $\sigma_{c,b}/\sigma_{c,m} = 18.7$. Utilising Eq. 6.3 (p. 96) and the values for friction angle and cohesion of each component of the soil-rock mixture at the Longpan landslide (China; matrix: clay; blocks: sandstones, slate; [417, p. 753, 759]), the strength contrast results to approx. 11.1. The strength contrast between the cement-based matrix and block materials prepared by [306] for laboratory direct shear tests on artificial bimrocks is approx. 13.4 after a curing period of 28 days.

3.2.5 Tensile strength

Because tensile tests are far less often executed than, e.g., uniaxial compression tests, few tensile strength values exist in literature. If no data is available, engineers often assume the uniaxial peak tensile strength, σ_t , of intact rock to be one-tenth of the uniaxial peak compressive strength, σ_c . Literature quotes this approximation being valid for common rocks (cf., e.g., [181, p. 94], or [113] in [329, p. 147]).

Many authors have analysed the σ_c to σ_t ratio and tried to identify a general correlation. However, usually the correlation relates to the splitting tensile strength, $\sigma_{t,sp}$, since more often Brazilian tests are selected over direct tensile tests; most probably because of a lack in a direct tensile test apparatus.

[329, Tab. 1, p. 148] have listed some correlations published between 1955 and 2013, most of which are linear or have an exponential form (tensile strength from Brazilian tests). The strength ratios vary between 1.9 and 176.6 ([329, p. 147]). The ratios of some rock specimens [130, Tab. 3.1, p. 61] reports about vary between 10.0 and 167.6 (tensile strength from point load or Brazilian tests). And also ratios reported by [213] (cited in [183, p. 742]) range from 1 to well over 100.9

Fig. 3.8 plots pairs of uniaxial compressive and tensile strengths from [199] and correlations between the two strengths identified by [183] and [329]. Note that it is the splitting tensile strength, $\sigma_{t,sp}$, in case of [199, 329], and the uniaxial peak tensile strength, σ_{t} , in case of [183]. Section B.1 (p. 321) in the appendix lists some details on the rock types tested, on the fittings, and on criteria checking the suitability of tests to be considered.

Neither [183] nor [329] mention in any way the sizes and shapes of the specimens from the tests of which they used the results for their fittings. For example, for both the uniaxial compression test and the Brazilian test, the maximum load applicable to the test specimen (reflecting the specimen's strength) commonly decreases with increasing specimen height to diameter ratio (cf. Fig.6.5a on p. 92 in the appendix; [392, p. 171]). In contrast, in literature, conclusions on the influence of the specimen size (i.e., volume) on the test results are inconsistent. Fig. 6.8 (p. 99) in the appendix suggests that the uniaxial compressive strength decreases with increasing specimen size. At other studies, the specimen size had little or no effect on the test results (e.g., Brazilian test: [392, p. 172]; uniaxial compression test: [392, p. 172], [162, 286] in [166, p. 155]). Anyway, many other factors affect the specimen's behaviour during testing and cause scatter in correlation plots: moisture content, loading rate, rock foliation resulting in anisotropy ([329, p. 149]), included defects or zones of weakness ([183, p. 742, 744]), etc.

In Fig. 3.8, all fitted correlations from [183] show an increase in the σ_t to σ_c ratio if σ_c decreases (inclination of lines in the graph is less than 45°). This applies also to the fittings

⁹[183, p. 732] already warned the reader that quality and reliability of test results published in literature varies. He, for example, examined the results published by [213] and doubts some of them because he either missed relevant information on applied techniques or involved failure modes, or he identified involved failure modes non-typical for particular test types ([183, p. 744]).

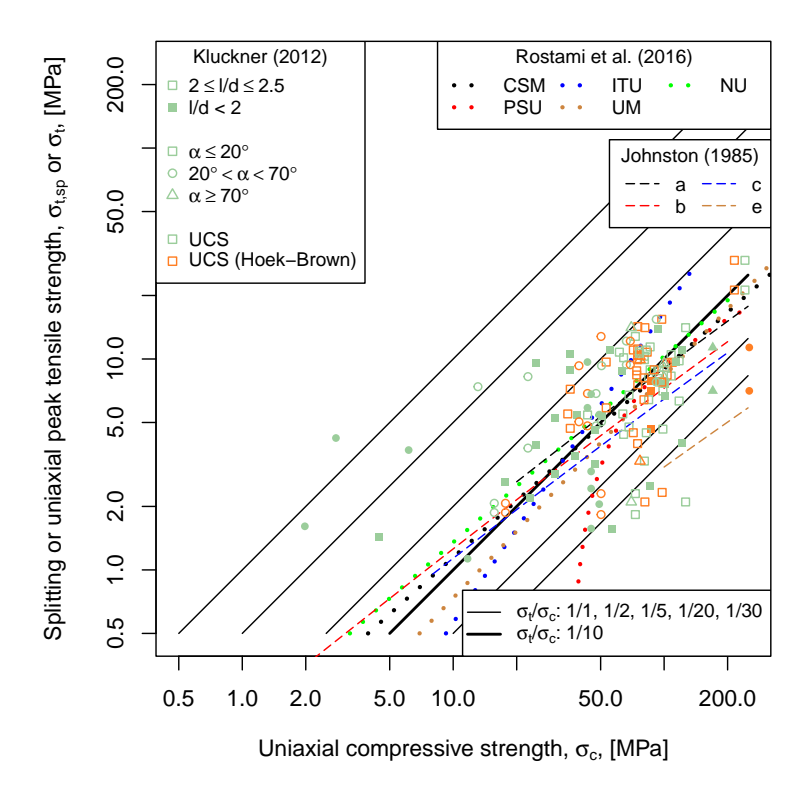


Figure 3.8: Relationship between splitting tensile strength, $\sigma_{t,sp}$, or uniaxial peak tensile strength, σ_{t} , and uniaxial peak compressive strength, σ_{c} , of rocks. Log-log plot. Johnston (1985) [183]: σ_{t} ; carbonate (a), argillaceous (b), arenaceous (c), and igneous and metamorphic (e) materials; for details, cf. Section B.1.1 (p. 321). Kluckner (2012) [199]: $\sigma_{t,sp}$; data from the Semmering Base Tunnel project; dolomite, gneiss, limestone, phyllite, and schist; l/d ... specimen length to specimen diameter ratio, α ... dip of weakness planes (if existing; if not: $\alpha = 0^{\circ}$), UCS ... σ_{c} from uniaxial compression test, UCS (Hoek-Brown) ... σ_{c} from triaxial compression test utilising the Hoek-Brown criterion; for details, cf. Section B.1.2 (p. 322). Rostami et al. (2016) [329] (rock types not differentiated): $\sigma_{t,sp}$; data from Colorado School of Mines (CSM), Pennsylvania State University (PSU), Istanbul Technical University (ITU), University of Melbourne (UM), and Nidge University (NU); for details, cf. Section B.1.3 (p. 324).

of the CSM and NU data by [329], and to the data by [199]. Skipping test results from [199] with l/d < 2, this increase cannot be observed anymore. A contrary picture results for the fittings of the ITU, PSU and UM data. Here, the ratio decreases with decreasing σ_c . Note that there might be some discrepancies in the fittings of [329] as the authors did not differentiate between rock types. Also, the dominance of anisotropic or isotropic rocks determines the best fits which the authors recognised themselves (cf. [329, p. 150]). They did not differentiate between isotropic and anisotropic specimens, nor between anisotropic specimens with different orientations of the weakness planes relative to the loading direction (for a brief introduction on the orientation's influence, refer to Section B.1.2 on p. 322 in the appendix). The adverse effect of varying anisotropy on the best fits by [183] is probably less because the fitting procedure considers several tests of different types (e.g., triaxial compression, Brazilian) on the same rock type (cf. Fig. B.1 on p. 322 in the appendix.).

[130, p. 65] reports that tensile strengths obtained with Brazilian tests are generally higher than those from direct tensile strengths. According to [394] (cited in [130, p. 65]), the splitting tensile strength exceeds the uniaxial peak tensile strength by a factor of >1 up to over 10.¹⁰

¹⁰For comparison: A factor of 1 is to be assumed for concrete if no information on the correlation between the two strengths is available (cf. [121, p. 78, 199]).

Now, considering this, in Fig. 3.8, data pairs from [199] and correlation lines from [329] need to be shifted downwards a little (e.g., from being close to the 1/5 line to then being closer to the 1/10 line) to get the σ_t to σ_c ratio instead of the $\sigma_{t,sp}$ to σ_c ratio. Then, $\sigma_t/\sigma_c = 1/5$ seems to be a good approximation of the upper bound. And $\sigma_t/\sigma_c = 1/10$ is still a good approximation of the mean, especially for rocks with a low to moderate compressive strength. Considering the shift described above, for rocks with a high compressive strength, a ratio of 1/10 is then more of an upper bound. Even if the data from [183, 329] comprise rocks with a strength below 2 MPa, the major part of the evaluated rocks feature a higher strength. Thus, correlations in Fig. 3.8 are to be treated with caution for low-strength rocks.

3.2.6 Dilation angle (zone failure, disintegration)

If uncemented or cemented granular material (e.g., sand, rock, concrete) experiences deviatoric deformation (i.e., shearing), it usually changes its volume. This process is termed dilatancy.¹¹ Whether the volume remains more or less constant, decreases (contraction), or increases (dilation), depends on the material characteristics and state. Determining factors are, e.g., the properties of the material's constituents (e.g., shape, size), the constituents share and arrangement within the composition (e.g., state of packing, void space), the bonding between each of the constituents, and the experienced shear distortion so far. In general, if a specimen is loaded (compression, or shear), it first contracts by rearranging its constituents (if possible), closing cracks and other voids (if present), and deforms elastically. At a particular load level, the formation of new cracks and crack propagation initiates, and with that void spaces start to enlarge because some constituents slip over others (frictional sliding). From that moment on, both contraction and dilation take place simultaneously. For a dilatant material and if the confining stress is not too high (cf. text below), at any one time when deformation increases, the share of dilation exceeds the share of contraction and the test specimen features a larger volume than prior to testing ([130, p. 70]). Volume increase associated with plastic deformation is a pervasive phenomenon for granular material subjected to compression ([82] in [427, p. 369]) and can be verified theoretically based on plastic work considerations ([161] in [427, p. 368]). After a large deformation, the specimen or a particular zone within the rock mass reaches a state at which subsequent loading does not change the volume anymore. Further deformations are then localised in narrow shear bands. [410]

Note that the dilation described here refers to the increase in volume of a soil, rock, or rock mass zone with all its weaknesses because of zone failure upon loading. In rock mechanics, it differs from the increase in volume because of shear movement along a single rock fracture. At the latter, the mean aperture typically increases, since "the asperities of one fracture surface must by necessity ride up in order to move past those of the other surface" ([181, p. 375]). This is also termed dilation. In both cases, sliding along rock surfaces—either of rock fragments, or of rock asperities—causes the volume to increase. Anyway, the former refers to shear failure of a zone and zone disintegration, but the latter refers to shear failure of a rock fracture (cf. Section 3.2.10 on p. 40).

Classical continuum mechanics utilises the dilation angle, ψ , to record dilation ([427, p. 368]). For simple shear, it is the arcsine of the ratio of plastic volume change over plastic shear strain ([410, p. 7, 19f]). For triaxial compression and plane strain conditions, [410, Eq. 3.2, p. 13] propose a formula considering the plastic volume change and the uniaxial plastic strain.

The onset and amount of dilation strongly depends on the confining stress. At higher confining

 $^{^{11}}$ Literature review disclosed the variety of how differently terms like dilatancy or dilation are used. Section B.2.1 (p. 325) in the appendix briefly list some uses and how it is understood for working out this thesis.

stress, dilation gets delayed, and dilation rate and peak dilation are lower ([427, p. 370]). Studying evaluations of triaxial test results in [427, Fig. 8, p. 375] shows that already low confining stress can restrain dilation significantly. In case of very high confining stress, dilation vanishes ([410, p. 14] with data from [395]).

According to [410, p. 16, 60], the dilation angle is always lower than the angle of internal friction, at least by 20° (i.e., $\varphi - \psi \ge 20^{\circ}$). Typical values for soils and rocks are ([410, p. 13f]):

- very dense sand: $\psi = 15^{\circ}$ (data from [160]);
- loose sand: $\psi = \text{just a few degrees};$
- normally consolidated clay: $\psi = 0^{\circ}$;
- granular (high porosity: 4.6%) to intact (low porosity: 0.45%) marble: $\psi = [12; 20]$ (in degrees), which reduces to $\psi = [6; 9]$ (in degrees) at very high confining pressure (200 MPa) (data from [262]).

In line, [95, p. 15] generally suggests $\psi < \varphi$ (non-associated plasticity), and $\psi = \varphi - 30^{\circ}$ for $\varphi \ge 30^{\circ}$ or $\psi = 0^{\circ}$ for $\varphi < 30^{\circ}$ in case no information is available from experiments. [95, p. 15] further suggests that after a certain plastic shear strain reaching a critical volume increase or a critical void ratio, $\psi = 0^{\circ}$. According to [244], these recommendations by [95] relate more to soils than to rocks.

Somewhat contrary, [293] (cited in [427, p. 371]) concluded based on numerical modelling that for most geological materials, particularly brittle ones, the dilation angle can be greater than the internal angle of friction. And [163] (cited in [427, p. 371]) suggest using a constant dilation angle with the value depending on the rock mass quality (very good: $\psi \approx \varphi/4$; average: $\psi \approx \varphi/8$; poor: $\psi \approx 0$; in degrees). Data from [199] (detailed in Section B.2.2 on p. 325 in the appendix) on weak rock material show a dilation angle of below 11°; and $(\varphi - \psi)_{min} = 23.8^{\circ}$, which complies with the statement by [410, p. 60] (cf. text above).

3.2.7 Poisson's ratio

At compression tests, the Poisson's ratio, ν , is the negative of the ratio of the absolute transverse (or lateral) strain to the absolute axial strain, $-|\varepsilon_l|/|\varepsilon_a|$, ([181, p. 84, 108], [130, p. 67]). Upon the theory of elasticity, $-1 < \nu < 0.5$, where usually only man-made materials feature negative values and a value of 0.5 refers to an incompressible material ([181, p. 110f], [241, p. 165]). $0 < \nu < 0.5$ applies to most real materials ([334, p. 92]). 12

For a mere linear elastic material, ν is independent of the stress state ([181, p. 84]) and a constant of proportionality ([130, p. 67]). This is also true for rock material subjected to a load at which it deforms approximately elastically. At compression tests, that is

- at the virgin loading after pre-existing cracks have closed upon loading but prior to when pre-existing cracks grow and new ones initiate (i.e., from point A to point B in Fig. 3.9a), and
- at unloading-reloading loops (cf. Fig. 3.10a).

Performing unloading-reloading loops prior and beyond peak load at different material states, the development of the Poisson's ratio can be evaluated (cf. dashed line in Fig. 3.10c). It is not

¹²In this context, it must be noted that the Poisson effect is not to be confused with dilatancy both being a measure for volume change. The former only concerns the elastic (i.e., recoverable) part of deformations of a material upon loading or unloading. The latter refers to plastic deformations upon loading only (cf. Section 3.2.6).

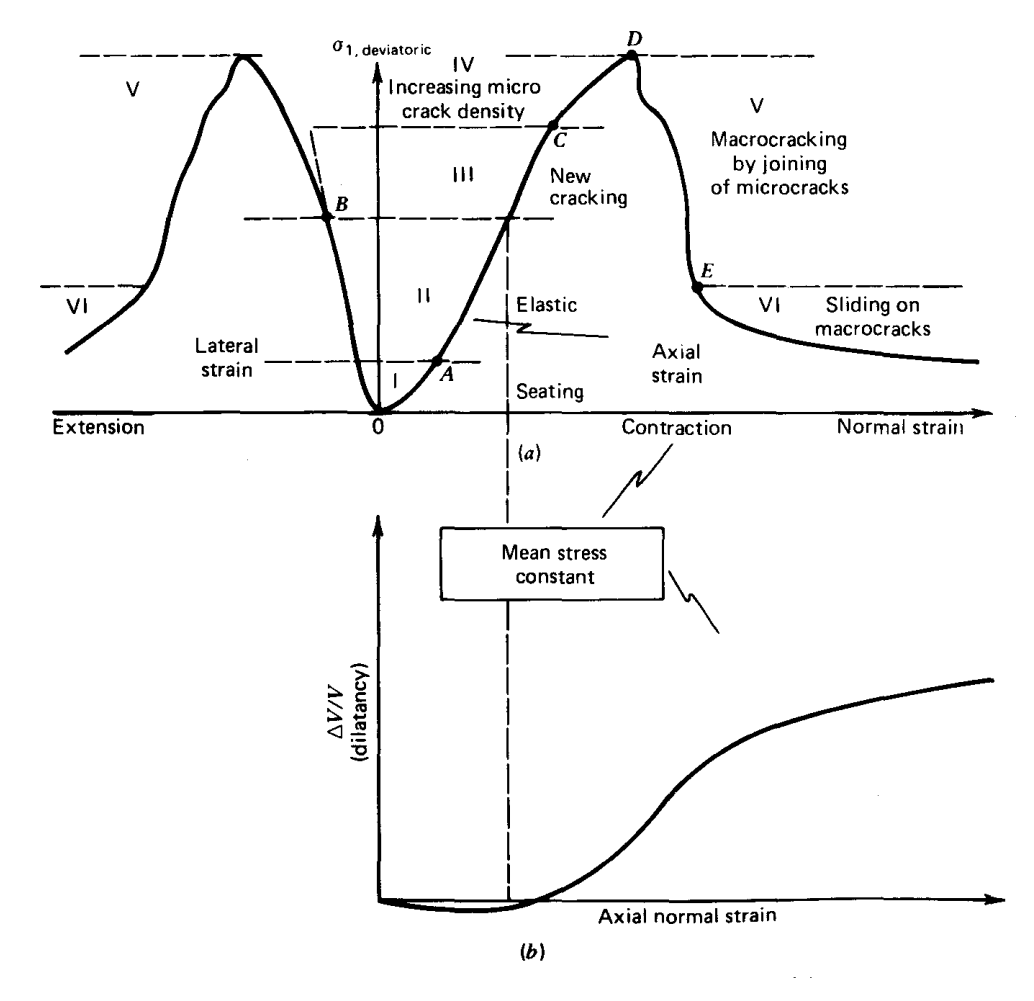


Figure 3.9: Triaxial compression test: Deformation under increasing deviatoric stress, with constant mean stress (hypothetical curves) (from [130, Fig. 3.7, p. 70]). (a) Axial and lateral normal strain with increasing deviatoric axial stress; (b) volumetric strain with increasing axial normal strain (dilatancy).

constant but increases with increasing deformation. According to [241, p. 178], the Poisson's ratio not only depends on the differential (i.e., deviatoric) stress, but also on the effective mean stress (i.e., hydrostatic or non-deviatoric). It generally increases with increasing confining or differential stress ([241, p. 165]). This stress-dependency is because of internal changes of pore space in a dry rock upon external load ([241, p. 171]). Thus, considering all that but also specimen characteristics not addressed here (e.g., anisotropy), a single value for the Poisson's ratio (e.g., given in a technical report or publication) should be understood as a mean value (cf. [241, p. 178]).

Typical values for rock range between 0.1 and 0.3 ([181, p. 149, 291], [241, p. 165]). Except for shale, all average values given in the labels of the y-axis in Fig. 3.11 fall into this range. Fig. B.3 (p. 327) in the appendix graphs data from [130, 199] aiming to find a trend between the Poisson's ratio, ν , and the Young's modulus, E, or the uniaxial peak compressive strength, σ_c . The data plotted covers a wide range of rock stiffness and strength. Most values for the Poisson's ratio are below 0.3. For a rock with a higher stiffness, usually a lower Poisson's ratio is determined ([241, p. 349, 179]). However, such a trend cannot be identified in Fig. B.3b/d. And considering the criteria detailed in Section B.3 (p. 326) limiting the comparison of data, no other trend is to be constructed either.

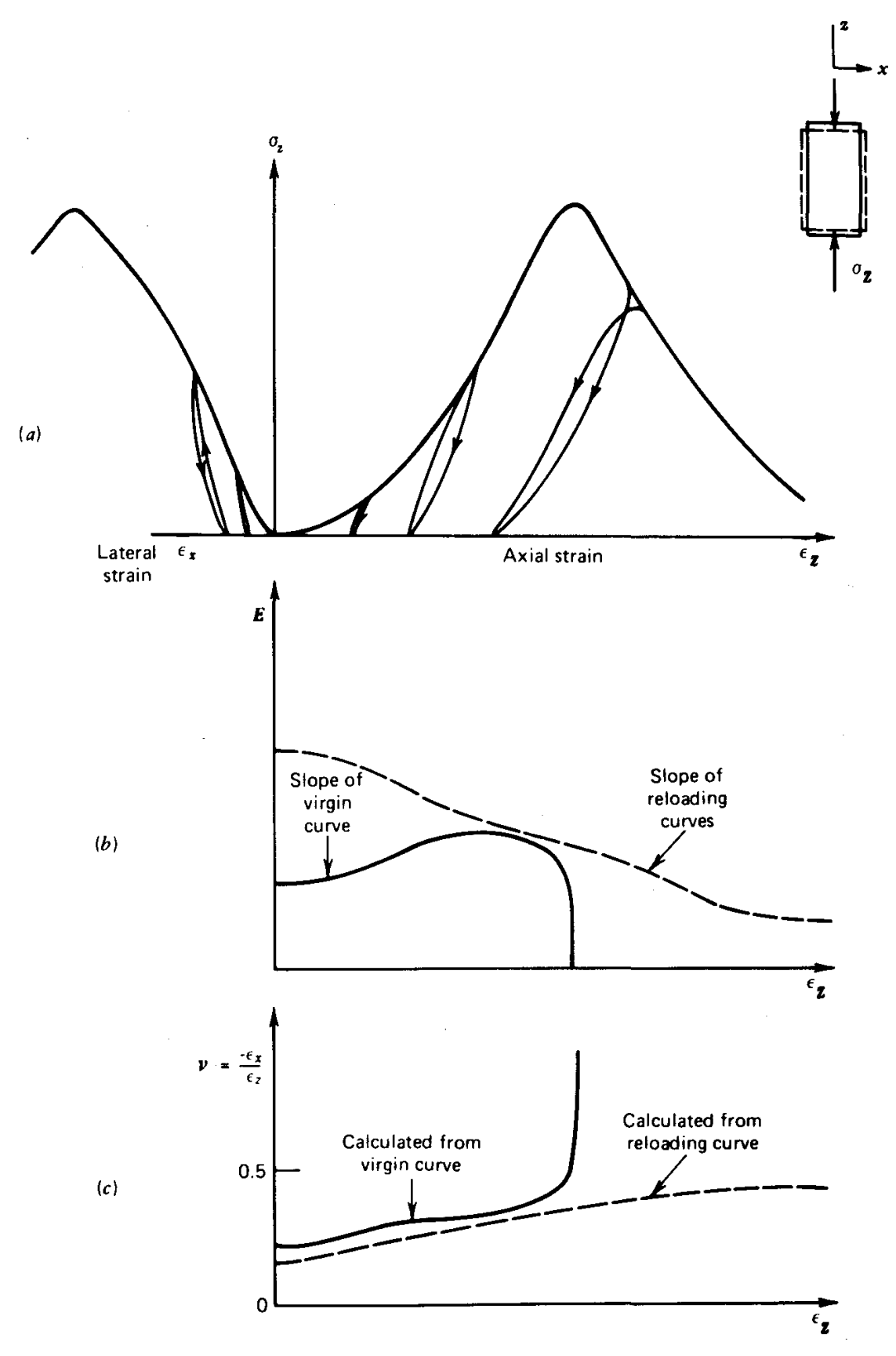


Figure 3.10: Uniaxial compression test: Variation of the modulus of elasticity, E, (tangent modulus) and the Poisson's ratio, ν , with axial strain (from [130, Fig. 6.3, p. 185]). (a) Development of axial strain, ϵ_z , and lateral strain, ϵ_x , with increasing axial stress, σ_z ; (b) variation of E with increasing ϵ_z ; (c) variation of ν with increasing ϵ_z .

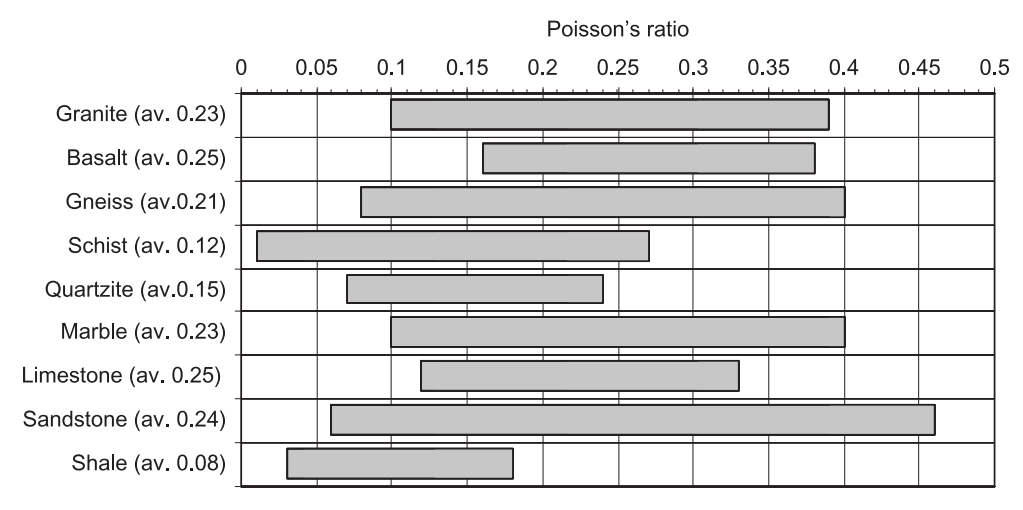


Figure 3.11: Poisson's ratio: Average (av.) and value range for common rock types (from [357, Fig. 7.8, p. 277] after [182]). For related values and value ranges for the Young's modulus, refer to Fig. 6.9 (p. 101); and for the uniaxial peak compressive strength, refer to Fig. 6.7 (p. 98).

3.2.8 Density

A material comprising more open cracks and other empty spaces and, thus, less solid constituents, necessarily features a lower density and stiffness than a similar material with less empty spaces; for at least as long as those spaces have not closed upon loading.¹³ Accordingly, from two specimens of the same rock type but different in the density, the denser one must feature a higher stiffness. [377] identified such a positive correlation for Ankara agglomerate (not shown).

Now, a stiffer rock material usually also features a higher strength (cf. Section 3.2.9). Thus, rock density must increase with increasing rock strength. [298], for example, identified this positive correlation for limestone to be of an exponential form (not shown). They have analysed results from tests on 1150 samples from 220 different limestones.

Considering the above statements, it is safe to assume that for a particular bimrock zone, the weak matrix material features a lower density than the stronger block material. The following examples of published data verify this assumption ($\rho \dots$ density):

- [185, Tab. 1, p. 1472]: strongly cemented Misis fault breccia (matrix: claystone; blocks: dolomitic limestone) with $\rho_m = 2.44 \text{ g/cm}^3$ and $\rho_b = 2.68 \text{ g/cm}^3$;
- [378, Tab. 1, p. 555]: volcanoclastic Ankara agglomerate (matrix: tuff; blocks: andesite) with $\rho_m = 1.72 \text{ g/cm}^3$ and $\rho_b = [2.31; 2.48]$ (in g/cm³);
- [417, Tab. 2, p. 759]: soil-rock mixture (matrix: clay; blocks: sandstones, slate) with $\rho_m = 1.80 \text{ g/cm}^3$ and $\rho_b = 2.41 \text{ g/cm}^3$.

3.2.9 Young's modulus

Similar as for the strength, [254] demand for a minimum contrast between the stiffness of the block and matrix material so that blocks have a significant influence on the ground behaviour. They suggest a value of 2. The same value was utilised by [227] (cited in [254, p. 268]) for his experimental studies.

Because the parametric study of this thesis determines the material stiffnesses from relationships with the material strengths, such relationships are researched. In rock mechanics, the

¹³The differences depend also on the properties of the substances the spaces are filled with. That can be gases, fluids, or other solids being weaker or even stronger.

non-dimensional ratio of the Young's modulus, E, to the uniaxial peak compressive strength, σ_c , is known as modulus ratio, MR, (or modulus reduction; cf. [93, p. 138] and [164, p. 209]). For the determination of MR, the original formulation utilises the tangent modulus, $E_{t,50}$, at the virgin loading curve at 50% of the peak strength (cf. [93, p. 138]). [93, p. 136f] considered MR for his rock classification (cf. Fig. 3.12), which depends on σ_c (strength classes A to E) and on MR (high for MR > 500, average for $200 \le MR \le 500$, and low for MR < 200).

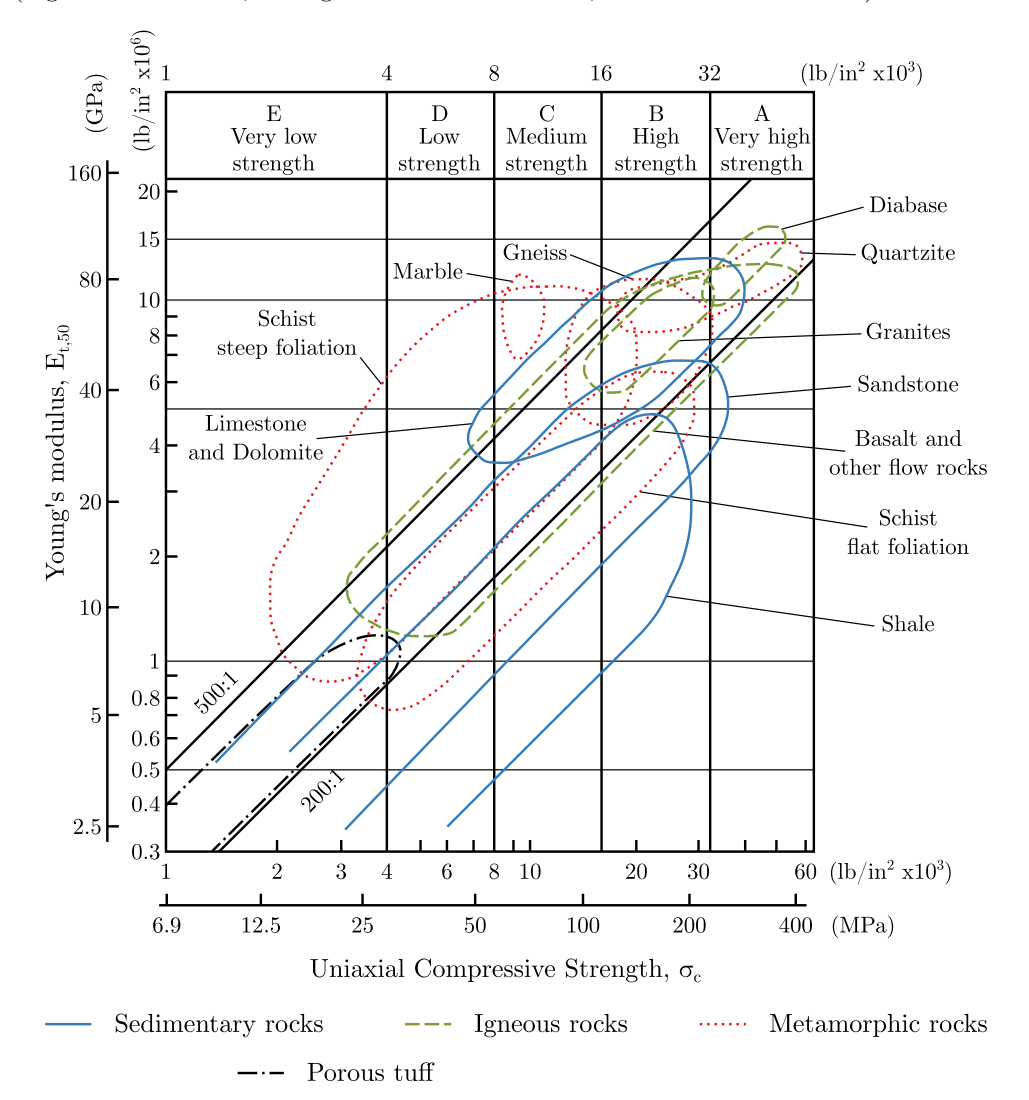


Figure 3.12: Relationships between the Young's modulus, $E_{t,50}$, (tangent modulus at 50% of peak strength) and the uniaxial peak compressive strength, σ_c , of intact rocks. Log-log plot. This graph combines Fig. 6.1, Fig. 6.2, and Fig. 6.3 from [331, p. 151–153]. All those figures originate from [94], but have been modified. The envelope for porous tuff in Fig. 6.12 in [94, p. 154] is added to the graph here. Each envelope covers 75% of all data from tests on specimens of the particular rock type (e.g., data from tests on shale specimens). Total data: 193 sedimentary rocks, 176 igneous rocks, 167 metamorphic rocks, and 44 porous tuff. Straight inclined solid lines represent a modulus ratio of $MR = \{200; 500\}$ (non-dimensional). lb ... pound ≈ 0.45 kg, in ... inch = 25.4 mm.

The values for MR covered by all the envelopes in Fig. 3.12 range from approx. 60 (shale) to approx. 1700 (schist with a steep foliation).¹⁴ Values given in [164, Tab. 3, p. 210] (not shown) base on [93, 297] and range from 150 for shales and marls to 1100 for schists. [130, p. 184] refers

The extrema cited in [94] but being outside the envelopes are: approx. 35 for hard shale ($E_{t,50} \approx 6.2$ GPa, $\sigma_c \approx 179.3$ MPa; cf. Fig. 6.11 on p. 152 in the reference), and approx. 2500 for schist with a steep foliation ($E_{t,50} \approx 51.7$ GPa, $\sigma_c \approx 20.7$ MPa; cf. Fig. 6.17 on p. 159 in the reference).

also to [93] and states that for most rocks MR ranges "from 200 to 500 but extreme values range as widely as 100 to about 1200." Some other published ranges are: from 84 for schists to 1157 for sandstones ([398, Tab. 1, p. 4])¹⁵; and from 80 for flysch sandstone to 760 for peridotite ([245, Tab. 3, p. 1263]).

The scatter of published MR values is large. There is no clear trend showing that lower-strength rocks generally feature either a lower or a higher value than rocks with a relatively higher strength. Reasons for the scatter are manifold. Every process a rock volume undergoes, starting at the recovery, transportation, storage, and preparation and, eventually, ending at testing, changes its state. The stress relaxation of a rock volume when recovered from depth, for example, already damages it because of initiation and propagation of microcracks ([164, p. 209]). From the same altered rock volume, however, later a specimen for testing will be prepared (accompanied by further altering) and the test results will then be used to characterise the non-altered (i.e., undisturbed; as long as the man-made construction is outside the range of influence; cf. Footnote 7 on p. 23) in situ rock and rock mass. Here, different characterisations result depending on the way laboratory test results are evaluated (often not cited in publications). Fig. 3.13 shows possible ways to determine the rock mass deformability from in situ plate jacking tests. Similarly, different values for the rock deformability can be obtained from laboratory compression tests (for more details refer to, e.g., [238]).

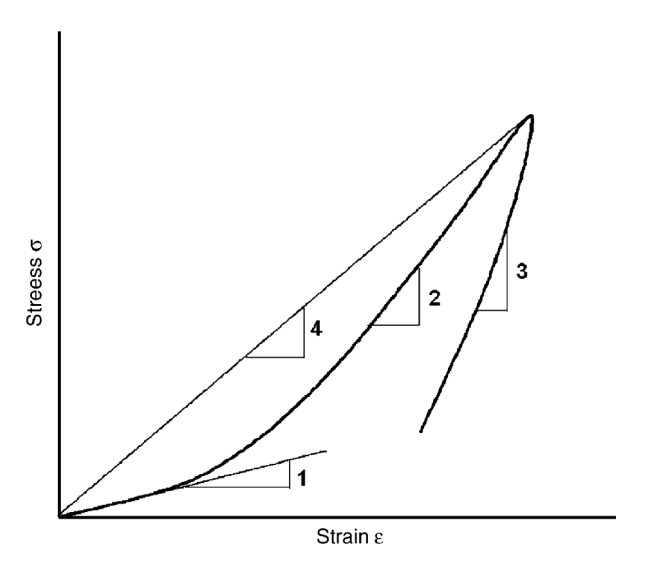


Figure 3.13: Alternative definitions for the deformability of a rock mass (from [164, Fig. 4, p. 205]). (1) Initial tangent modulus, (2) elastic tangent modulus (or modulus of elasticity), (3) recovery modulus, and (4) (secant) modulus of deformation. Note that the peak in the graph does not represent the moment of failure. It is just the point where the direction of loading gets reversed (from loading to unloading).

Thus, depending on how the rock deformability is determined, a different value for MR results for the particular rock specimen (or rock mass zone) tested. The identification of a true value is even more difficult since this in-the-course-of- and post-recovery damage of the specimen has a greater impact on its deformability than on its strength (cf. [164, p. 209]). In addition, the orientation of weakness planes (if present) relative to the loading direction also determines MR. It will be higher if the rock specimen gets loaded parallel to its weakness planes, and lower if loaded perpendicular to them ([164, Note a, Tab. 3, p. 210]).

The graph in Fig. 3.14 (p. 42) shows some published relationships between and data pairs

¹⁵Somehow inconsistent in [398, p. 3f]: the maximum value of 1157 given in Tab. 1 in the reference is much lower than the maximum value of approx. 3985 plotted in Fig. 1 in the reference.

of the Young's modulus, E, and the uniaxial peak compressive strength, σ_c . Note that in this section (especially regarding labels in graphs), Young's modulus is synonymous with all alternative pre-peak moduli of which some are illustrated in Fig. 3.13. Otherwise, the Young's modulus relates to the secant modulus from an unloading-reloading loop as it represents the true modulus of elasticity quite well ([272, p. 826], [130, p. 184]).

Fig. 3.14 plots the data from [199] two times: first, σ_c relates to E with E determined as a secant modulus at the unloading-reloading loop (unfilled circles); and second, it relates to the deformation modulus, V, determined as a secant modulus at the virgin loading curve (filled circles). Section B.4 (p. 326) in the appendix describes the same data from [199] in more detail. Using V, lower values for MR result. Differences are often quite large, e.g., $MR_E = 1336$ vs. $MR_V = 245$ for a rock with $\sigma_c = 6.25$ MPa, E = 8.35 GPa, and V = 1.53 GPa. This highlights the difficulty of comparing data from various sources and the identification of valid MR values, especially when no information is available on the method of test result interpretation. Considering all data from [199] plotted in Fig. 3.14, $MR_E = [191; 2580]$ and $MR_V = [137; 1404]$.

Most data pairs in Fig. 3.14, especially those of moderate- to high-strength rock, fall within the upper bound for sedimentary rocks (MR = 2500) and the lower bound for metamorphic rocks (MR = 85) (both relationships are from [398]). An exception is the data of low-strength rock from [274], where many of the pairs are below the lower bound. But this data may be faulty (cf. caption of Fig. 3.14). Anyway, the graph somehow agrees with the statement by [93] (cited in [130, p. 184]) that clastic rocks (here data from [274, 403] generally feature a lower MR than crystalline rocks (here most of the other data pairs; cf. also Fig. B.4 on p. 328 in the appendix). The linear relationships for sandstone, siltstone, conglomerate, limestone, and peridotite cited in [245] (not plotted; data of rocks with 2 MPa $< \sigma_c < 110$ MPa) all fall within the range MR = [130; 430] (non-dimensional). Considering only $\sigma_c < 50$ MPa in Fig. 3.14, the non-linear relationships by [298, 377, 398] indicate a higher MR for rocks with a lower strength (inclination of the lines in the graph $< 45^{\circ}$).

The following list comprises MR values of fault rocks¹⁶ and have been estimated from Fig. 4 in [339, p. 161]:

- Cohesionless kakirites, fault breccias (primary phyllitic structure):
 - Dolomite kakirite (sand- to gravel-size): E = 0.1 GPa, $\sigma_c \approx 0.12$ MPa, MR = 833;
- Cohesive kakirites, fault gouge (no internal structure visible anymore, soil-like):
 - Phyllite kakirite: E = 0.24 GPa, $\sigma_c \approx 1.3$ MPa, MR = 185;
 - Shale kakirite: E = 0.1 GPa, $\sigma_c \approx 0.7$ MPa, MR = 143;
- Intact rocks and cataclasites (cohesive):
 - Bedded limestone: E = 47 GPa, $\sigma_c \approx 71.5$ MPa, MR = 657;
 - Carbonate cataclasite (well-cemented fault breccia): E = 48 GPa, $\sigma_c \approx 87$ MPa, MR = 552; observed ranges are E = [32; 66] (in giga-pascal) and $\sigma_c = [63; 139]$ (in mega-pascal) ([339, p. 165]).

For some stiffness values for fault rocks and fault-zone masses from the *Gotthard Base Tunnel* project and the *Semmering Base Tunnel* project, refer to Tab. 3.2 (p. 26) and Tab. 3.3 (p. 27), respectively.

¹⁶It is assumed that the bedded limestones (intact rock) in the list make up the host rock or larger blocks embedded in the fault zone.

3.2.10 Block-matrix contacts

This study focuses on brittlely formed bimrocks with competent blocks, a weak matrix, and even weaker block-matrix contacts (cf. Section 2.2 on p. 14). Since the contact surface between a block and the surrounding matrix material constitutes a plane of weakness, this subsection lists some mechanical properties from joints in weak rock material. However, results and conclusions to some extent may also apply to welded or cemented bimrocks with competent blocks, a weak matrix, and block-matrix contacts which are at least as competent as the matrix material. For the latter, if numerical models do not consider interfaces between blocks and the matrix, because of deformation incompatibility and resulting stress concentrations along the block's surfaces (cf. Section 2.2), zones of the weak matrix will fail first around the blocks. Eventually, distinct shears will border the blocks. Some results and conclusions may apply to a bimsoil only if the matrix of this composite soil is cohesive. In case of a purely granular matrix possessing no cohesion (cf. [33, p. 14]), rearrangement of clasts will dominate the deformation behaviour rather than brittle failure mechanisms.

Fig. 3.15 plots the results of fittings done by [106] on data from shear tests on weakness planes in three different groups of weak phyllites (cf. Section 3.2.1 on p. 22 for some information on the fitting approach). In the figure, the filled symbols refer to the peak strength of the joints (labelled with joint // cleav. peak), and the unfilled symbols to the residual strength of the same joints but now comprising shear products (labelled with kak. res.). One can observe that the shear products of the quartz and limestone phyllites formed during the shearing along joints parallel to the cleavage feature a lower friction angle and a lower cohesion than was obtained for the unfilled joints. However, for the group of undifferentiated phyllites (labelled with Phyl. joint), the cohesion decreases but the friction angle increases.

Consider that if rock gets sheared (intact rock, joint walls, or joint fillings), bonds between individual rock fragments or minerals break. This reduces the cohesive strength. Whether frictional strength increases or decreases with additional shear depends on a few factors. If the constituents within the shear zone (i.e., those which are involved in the shearing process, e.g., broken off from the joint walls) mainly feature a round shape, turbulent rolling mechanisms will dominate and prevent platy or elongate constituents to align in a preferred direction (i.e., parallel to the shear direction) ([106, p. 66]). Because rolling friction (macroscopic friction of granulate) generally is higher than sliding friction (contact between particles) ([146, 237, 391] in [106, p. 78]), frictional strength increases when the mechanisms during shear change from pure sliding along the asperities on a joint surface or along a smooth joint surface to partly rolling of shear products ([106, p. 78], [62, p. 92]). A low joint normal stress promotes rolling of shear products (once formed) ([62, p. 81]) as it allows for some dilation and particles to roll over others. At high normal stresses, dilation and roll-over get restricted and rather a discrete sliding shear plane forms through the shear zone. In contrast, if the rock (or shear zone) comprises much platy or elongate constituents (e.g., phyllosilicates), those constituents align parallel to the shear direction and promote laminar sliding mechanisms ([106, p. 66]). Here, the frictional strength decreases with additional shear and alignment of constituents. But also the mineral composition affects the evolution of the shear strength. For example, shear zones in rocks comprising a significant amount of quartz or other competent minerals still may feature some cohesive strength and (an increased) frictional strength in the residual state ([106, p. 78]). To some extent, the competent minerals prevent sliding along phyllosilicates ([234, 375] in [106, p. 78]). They will not align themselves parallel to the shear direction as phyllosilicates do, and they serve as essentials for rolling friction as soon as they break off from the joint walls. If the rock lacks competent

minerals, in the residual state, the shear zone may feature no cohesion at all (i.e., purely frictional material) and a lower frictional strength than a shear zone material rich in competent minerals ([106, p. 78]).

[127, Tab. 1, p. 56] reports about the shear strength of surfaces of weakness in the matrix material of serpentinite bimrock. Here, the cohesion reduces from the initial to the residual state: $c = [0.22; 0.64] \rightarrow c_r = [0; 0.24]$ (in mega-pascal). In contrast, the range of the friction angle in the residual state is larger than in the initial state, indicating that for some joints the friction angle decreases but for others it increases: $\varphi = [21; 23.1] \rightarrow \varphi_r = [18.5; 24.2]$ (in degrees).

Fig. 3.16 graphs the alteration of the shear strength from its initial state (peak strength) to its residual state (residual strength) of joints in different rocks. The data is from direct shear tests performed under constant normal stiffness (CNS) conditions with the external stiffness $K \approx \infty$ (i.e., suppression of any vertical displacement). In the residual state, the rock joints necessarily comprise shear products (cf. text above). In almost all cases, the friction angle, φ , and the cohesion, c, are lower in the residual state than in the initial state (arrows point to the left and downwards). Fig. 3.17 plots the normalised strength (cf. Eq. 3.1 and Eq. 3.2 on p. 24). In 43 of 64 cases, the normalised change in φ ranges between 0 and 0.2. And it is 0.5 to 1 for the normalised change in c in 55 of 64 cases. The dilation angles of the joints of which the Mohr-Coulomb parameters are plotted in Fig. 3.16 range from 1.2° to 25°.

Tab. 3.5 lists some statistical parameters of the normalised changes in strength graphed in Fig. 3.17.

Table 3.5: Shear strengths from direct shear tests on rock discontinuities: Statistics on normalised change in strength (cf. Fig. 3.17).

Ratio	Statistical parameter	Shear test on discontinuities (cf. Fig. 3.17)	
		[199]	[62]
	Median	0.13	0.15
$(\varphi - \varphi_r)/\varphi$	Average	0.15	0.14
	SD	0.10	0.08
$(c-c_r)/c$	Median	1	0.97
	Average	0.95	0.90
	SD	0.12	0.19

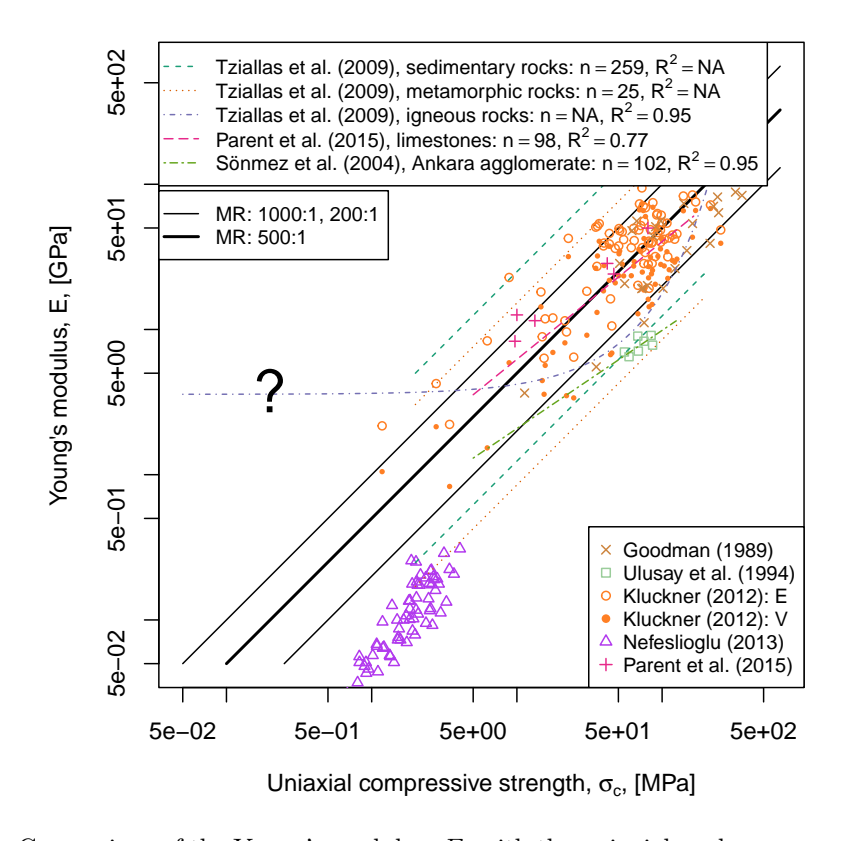


Figure 3.14: Comparison of the Young's modulus, E, with the uniaxial peak compressive strength, σ_c , of some rock specimens, and some relationships between the two parameters. Log-log plot. Data from: Tziallas et al. (2009) [398], tangent modulus; Parent et al. (2015) [298], secant modulus from unloading-reloading loop; Sönmez et al. (2004) [377], tangent modulus from virgin loading curve; Goodman (1989) [130], tangent modulus from virgin loading curve; Ulusay et al. (1994) [403], secant modulus; Kluckner (2012) [199], secant modulus from virgin loading curve (V) and from unloading-reloading loop (E); Nefeslioglu (2013) [274], type of modulus unknown. The stress level for the determination of the modulus is mostly unknown; for [199], cf. Fig. B.4; [298]: between 33% of the estimated failure load and 1 MPa. [130]: sandstone, siltstone, limestone, dolomite, shale, gneiss, schist, quartzite, marble, granite, tonalite, diabase, basalt, and tuff. [403]: medium-grained litharenite sandstone with low porosity, loading perpendicular to bedding planes (i.e., $\alpha = 90^{\circ}$). [199]: cf. Fig. B.4. [274]: claystone and mudstone; caution is recommended when interpreting data as Fig. 2 in [274, p. 12] suggests poor deformation measurement. [298]: limestones with a porosity ranging from 4.5% to 36.2%. Relationships of [398] for sedimentary and metamorphic rocks represent fitted boundaries of analysed data pairs. Range of σ_c for fitting by [398] for igneous rocks is unknown (marked with? in the graph). NA... not available.

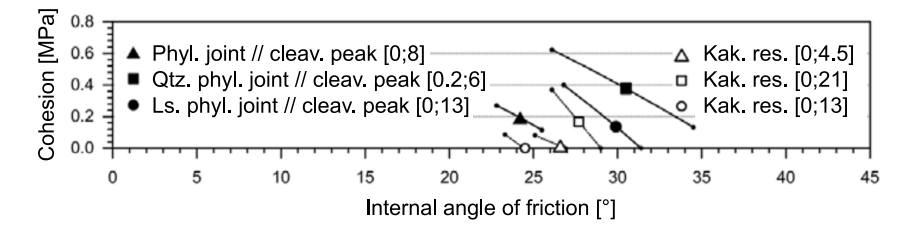


Figure 3.15: Peak shear strength (shear tests on unfilled joints parallel to cleavage) and residual shear strength (same joints but now filled with kakirites formed during shearing) of phyllites (from [106, Fig. 14, p. 75]; translated; abbreviations used: cleavage (cleav.), kakirite (kak.), limestone (ls.), phyllite (phyl.), quartz (qtz.), residual (res.)). Regarding symbols and error bars refer to Fig. 3.4. [106] used data from [62] some of which are also used in Fig. 3.16.

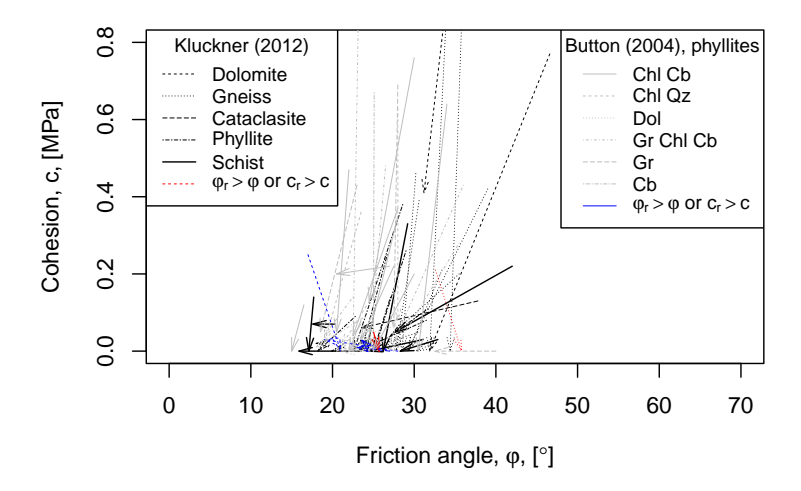


Figure 3.16: Shear strengths (in terms of friction angle, φ , and cohesion, c, data pairs) from direct shear tests on rock discontinuities (pre-existing joints or open cleavage planes) under constant normal stiffness conditions: Change from peak to residual strength. Rear end of arrows: peak shear strength with $\{\varphi;c\}$; arrowhead: residual shear strength with $\{\varphi_r;c_r\}$. Data from Kluckner (2012) [199]: $n=33, \ \psi=[1.2;25]$ (in degrees), $\tau_{max}=[0.38;10.79]$ (in mega-pascal), $s(\tau=\tau_{max})=[0.32;16.2]$ (in millimetres). Data from Button (2004) [62, Tab. 7, p. 88]: phyllites comprising mainly following minerals (or mineral groups): chlorite (Chl), carbonate (Cb), quartzite (Qz), dolomite (Dol), graphite (Gr); $\tau_{max}=[0.4;6.9]$ (in mega-pascal), $s(\tau=\tau_{max})=[0.27;19.16]$ (in millimetres), $\sigma_{n,max}=[0.94;14.98]$ (in mega-pascal), $s(\sigma_n=\sigma_{n,max})=[0.75;22.01]$ (in millimetres). Data also plotted in Fig. 3.17 (p. 43).

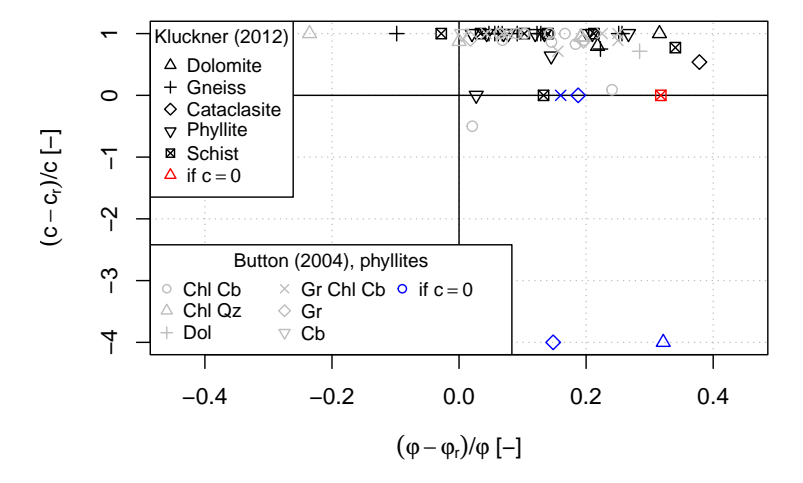


Figure 3.17: Shear strengths from direct shear tests on rock discontinuities: Normalised change in strength (from peak strength $\{\varphi;c\}$ to residual strength $\{\varphi_r;c_r\}$). Same data as for Fig. 3.16. Corrections (marked in the graph with different colours): $c=0 \land c_r=0 \Rightarrow (c-c_r)/c=0$; $c=0 \land c_r\neq 0 \Rightarrow (c-c_r)/c=-4$.

Bibliography

- [1] Abler, P. Einflüsse auf das Verformungsverhalten von jungem Spritzbeton im Tunnelbau. Diploma thesis, University of Innsbruck, Innsbruck, Austria, 1992.
- [2] ACI. ACI Manual of Concrete Practice. Technical report, American Concrete Institute (ACI), 1978.
- [3] ACI Committee 209. 209R-92. Prediction of Creep, Shrinkage, and Temperature Effects in Concrete Structures. Technical report, American Concrete Institute (ACI), March 1992. Reapproved 1997.
- [4] ACI Committee 209. 209.1R-05. Report on Factors Affecting Shrinkage and Creep of Hardened Concrete. Technical report, American Concrete Institute (ACI), July 2005.
- [5] ACI Committee 209. 209.2R-08. Guide for Modeling and Calculating Shrinkage and Creep in Hardened Concrete. Technical report, American Concrete Institute (ACI), May 2008.
- [6] Acker, P. Comportement mécanique du béton: Apports de l'approche physico-chimique (Mechanical behavior of concrete: A physico-chemical approach). PhD thesis, Ecole Nationale des Ponts et Chaussées, Paris, France, 1988.
- [7] Acker, P. Micromechanical Analysis of Creep and Shrinkage Mechanisms. In Ulm, F.-J., Bažant, Z. P., and Wittmann, F. H., editors, Creep, Shrinkage and Durability Mechanics of Concrete and other Quasi-brittle Materials. Proceedings of the 6th International Conference CONCREEP@MIT, pages 15–26, Cambridge, USA, August 2001. Elsevier: Amsterdam.
- [8] Adhikary, D. P. Shortcomings in the standard continuum based implicit joint model of layered rocks. *Journal of Geology and Mining Research*, 2(2):23–28, May 2010.
- [9] Alber, M. and Kahraman, S. Predicting the uniaxial compressive strength and elastic modulus of a fault breccia from texture coefficient. *Rock Mechanics and Rock Engineering*, 42(1):117–127, January 2009.
- [10] Aldrian, W. Beitrag zum Materialverhalten von früh belastetem Spritzbeton. PhD thesis, Montanuniversität Leoben, Leoben, Austria, May 1991.
- [11] Allaby, M., editor. A Dictionary of Geology and Earth Sciences. Oxford University Press, 4th edition, January 2013.
- [12] Allmendinger, R. W. Stereonet, September 2020. URL https://www.rickallmendinger.net/stereonet. Last access: 26.09.2020.
- [13] Allmendinger, R. W., Cardozo, N., and Fisher, D. M. Structural Geology Algorithms: Vectors and Tensors. Cambridge University Press, December 2011.

BIBLIOGRAPHY 288 of 498

[14] ASTM. D5607-02. Standard Test Method for Performing Laboratory Direct Shear Strength Tests of Rock Specimens Under Constant Normal Force. Standard, 2002.

- [15] ASTM. D7012-10. Test Methods for Compressive Strength and Elastic Moduli of Intact Rock Core Specimens under Varying States of Stress and Temperatures. Standard, 2010.
- [16] Atkins, P., Jones, L., and Laverman, L. Chemical principles. W. H. Freeman and Company, 6th edition, 2013.
- [17] Atzl, G., Brandtner, M., Selan, V., and Moritz, B. Numerical analyses of deep tunnels driven through massive faults. In Schubert, W. and Kluckner, A., editors, *Proceedings of the ISRM Regional Symposium EUROCK 2015 & 64th Geomechanics Colloquium–Future Development of Rock Mechanics*, pages 877–882, Salzburg, Austria, October 2015. Austrian Society for Geomechanics.
- [18] Austin, S. A. and Robins, P. J., editors. Sprayed Concrete: Properties, Design and Application. Whittles Publishing, 1995.
- [19] Austrian Standards Institute. ÖNORM EN 14487-1-1:2006. Spritzbeton: Teil 1: Begriffe, Festlegungen und Konformität. Standard, May 2006.
- [20] Austrian Standards Institute. ÖNORM EN 1992-1-1:2015. Eurocode 2: Bemessung und Konstruktion von Stahlbeton- und Spannbetontragwerken Teil 1-1: Allgemeine Bemessungsregeln und Regeln für den Hochbau (konsolidierte Fassung). Standard, February 2015.
- [21] Aydan, O., Sezaki, M., and Kawamoto, T. Mechanical and numerical modelling of shotcrete. In Pande, G. N. and Pietruszczak, S., editors, Proceedings of the Fourth International Symposium on Numerical Models in Geomechanics (NUMOG IV), pages 757–764, Swansea, Wales, August 1992. Taylor & Francis, London.
- [22] Bandis, S. C., Lumsden, A. C., and Barton, N. R. Fundamentals of rock joint deformation. International Journal of Rock Mechanics and Mining Sciences & Geomechanics Abstracts, 20(6):249–268, December 1983.
- [23] Barbero, M., Bonini, M., and Borri-Brunetto, M. Numerical modelling of the mechanical behaviour of bimrock. In Ribeiro e Sousa, L., Olalla, C., and Grossmann, N., editors, Proceedings of the 11th Congress of the International Society for Rock Mechanics—The Second Half Century of Rock Mechanics, volume 1 & 2, pages 377–380, Lisbon, Portugal, July 2007. Taylor & Francis Group, London.
- [24] Barbero, M., Bonini, M., and Borri-Brunetto, M. Three-Dimensional Finite Element Simulations of Compression Tests on Bimrock. In Proceedings of the 12th International Conference of International Association for Computer Methods and Advances in Geomechanics (IACMAG), pages 631–637, Goa, India, October 2008.
- [25] Bažant, Z. P., editor. Mathematical Modelling of Creep and Shrinkage in Concrete. Wiley & Sons Ltd, New York, 1988.
- [26] Bažant, Z. P. Creep and thermal effects in concrete structures: a conceptus of some new developments. In Mang, H. A., Bicanic, N., and de Borst, R., editors, *Proceedings of the* Int. Conf. EURO-C "Computational Modelling of Concrete Structures", pages 461–480, Swansea, Wales, 1994. Pineridge Press.

BIBLIOGRAPHY 289 of 498

[27] Bažant, Z. P. Materials Science of Concrete IV, chapter Creep and Damage in Concrete, pages 335–389. American Ceramic Society, Westerville, USA, 1995.

- [28] Bažant, Z. P. and Panula, L. Practical prediction of time-dependent deformations of concrete. *Matériaux et Constructions*, 11(5):317–328, September 1978.
- [29] Bažant, Z. P. and Prasannan, S. Solidification Theory for Concrete Creep. I: Formulation. Journal of Engineering Mechanics, 115(8):1691–1703, 1989.
- [30] Bažant, Z. P. and Wittmann, F. H., editors. Creep and Shrinkage in Concrete Structures. John Wiley & Sons Ltd, Chichester, 1982.
- [31] Bažant, Z. P., Hauggaard, A. B., and Baweja, S. Microprestress solidification theory for concrete creep. II: Algorithm and verification. *Journal of Engineering Mechanics*, 123(11): 1195–1201, November 1997.
- [32] Bažant, Z. P., Hauggaard, A. B., Baweja, S., and Ulm, F.-J. Microprestress solidification theory for concrete creep. I: Aging and drying effects. *Journal of Engineering Mechanics*, 123(11):1188–1194, 1997.
- [33] Bell, F. G. Engineering Properties of Soils and Rocks. Butterworth-Heinemann Ltd: Oxford, 3rd edition, 1992.
- [34] Benz, T., Vermeer, P. A., and Schwab, R. A small-strain overlay model. International Journal for Numerical and Analytical Methods in Geomechanics, 33(1):25–44, January 2009.
- [35] Benz, T. Small-strain stiffness of soils and its numerical consequences. PhD thesis, University of Stuttgart, 2007.
- [36] Bergmair, M., Harer, G., Riedmüller, G., and Stadlmann, T. Die Baugeologie des Galgenbergtunnels. Felsbau, 14(1):15–21, 1996.
- [37] Biscoping, M. and Kampen, R. Zusammensetzung von Normalbeton Mischungsberechnung, February 2017. URL https://mitglieder.vdz-online.de/fileadmin/gruppen/vdz/3LiteraturRecherche/Zementmerkblaetter/ZM_B20_2017_2.pdf. Zement-Merkblatt Betontechnik B 20; last access: December 16th, 2022.
- [38] Bjureland, W., Johansson, F., Sjölander, A., Spross, J., and Larsson, S. Probability distributions of shotcrete parameters for reliability-based analyses of rock tunnel support. *Tunnelling and Underground Space Technology*, 87:15–26, May 2019.
- [39] Bjurström, S. Shear strength of hard rock joints reinforced by grouted untensioned bolts. In Proceedings of the 3rd Congress of the International Society for Rock Mechanics (ISRM), pages 1194–1199, Denver, Colorado, USA, September 1974.
- [40] Blair, T. C. and McPherson, J. G. Grain-size and textural classification of coarse sedimentary particles. *Journal of Sedimentary Research*, 69(1):6–19, January 1999.
- [41] Blümel, M. Personal communication, November 2020.
- [42] Boos, P. and Dietermann, M. Wet Shotcrete Performance—Laboratory Test Methods and influencing Factors in Practice. *Tunnel*, 29(6):31–41, 2010.

BIBLIOGRAPHY 290 of 498

[43] Bossart, P., Meier, P. M., Moeri, A., Trick, T., and Mayor, J.-C. Geological and hydraulic characterisation of the excavation disturbed zone in the Opalinus Clay of the Mont Terri Rock Laboratory. *Engineering Geology*, 66(1–2):19–38, October 2002.

- [44] Boumiz, A., Vernet, C., and Tenoudji, F. C. Mechanical properties of cement pastes and mortars at early ages. *Advanced Cement Based Materials*, 3(3-4):94–106, April 1996.
- [45] Brady, B. H. G. and Brown, E. T. Rock Mechanics for underground mining. Springer Netherlands, 3rd edition, 2004.
- [46] Brandtner, M. Numerical Analysis of Fault Zones—Coming Closer to a Solution. In Schubert, W., Kluckner, A., and Pilgerstorfer, T., editors, *Proceedings of the Workshop "Characterization of Fault Zones" as part of the 62nd Geomechanics Colloquium*, pages 60–63, Salzburg, Austria, October 2013. Austrian Society for Geomechanics.
- [47] Brandtner, M. Personal communication, June 2020.
- [48] Brandtner, M. Personal communication, April 2022.
- [49] Brandtner, M. Personal communication, May 2022.
- [50] Brandtner, M. and Lenz, G. Checking the system behaviour using a numerical model. Geomechanics and Tunnelling, 10(4):353–365, August 2017.
- [51] Bray, J. W. Unpublished note. 1977.
- [52] BRITE-EURAM. BRE-CT92-0231. new Materials, Design and Construction Techniques for Underground Structures in Soft Rock and Clay Media. Technical report, Mott MacDonald Ltd (project coordinator), 1998. Research project funded by EU (programme: FP3-BRITE/EURAM 2).
- [53] Brodie, K., Fettes, D., Harte, B., and Schmid, R. Towards a unified nomenclature of metamorphic petrology: 5. structural terms including fault rock terms. PDF, November 2004. URL https://www.ugr.es/~agcasco/personal/IUGS/pdf-IUGS/scmr_struc2_structuraltermsincludingfaultrockterms.pdf. Recommendations by the IUGS Subcommission on the Systematics of Metamorphic Rocks. Last access: 07.01.2023.
- [54] Brosch, F.-J. and Pischinger, G. Small- to meso-scale brittle rock structures and the estimation of "paleostress" axes—A case study from the Koralm region (Styria/Carinthia). Austrian Journal of Earth Sciences, 107(2):37–59, 2014.
- [55] Brown, E. T. and Gonano, L. P. Improved compression test technique for soft rock. *Journal of the Geotechnical Engineering Division*, 100(2):196–199, 1974.
- [56] Brugg Kabel AG. Datasheet: BRUsens strain V3 (LLK-BSST V3 7.2 mm). Version: 2012/09/12 Rev. 02 TH. Technical report, Brugg, Switzerland, 2012.
- [57] Bryne, L. E. Time Dependent Material Properties of Shotcrete for Hard Rock Tunnelling. PhD thesis, KTH Royal Institute of Technology, Stockholm, Sweden, May 2014.
- [58] Buchmayer, F., Monsberger, C. M., and Lienhart, W. Advantages of tunnel monitoring using distributed fibre optic sensing. *Journal of Applied Geodesy*, 15(1):1–12, December 2020.

BIBLIOGRAPHY 291 of 498

[59] Budil, A. Längsverschiebungen beim Tunnelvortrieb. PhD thesis, Graz University of Technology, Graz, Austria, May 1996.

- [60] Bürgi, C. Cataclastic fault rocks in underground excavations A geological characterisation. Phd thesis, École Polytechnique Fédérale de Lausanne, Lausanne, Switzerland, 1999.
- [61] Burgstaller, M., Goricki, A., and Vanek, R. Semmering Base Tunnel new—Tender documents: Report on the geotechnical ground characterisation. Project document (in german), Austrian Federal Railways, April 2014.
- [62] Button, E. A. A Contribution to the Characterization of Phyllitic and Schistose Rock Masses for Tunnelling. PhD thesis, Graz University of Technology, Graz, Austria, 2004.
- [63] Byfors, J. Plain concrete at early ages. Technical report, Swedish Cement and Concrete Research Institute, Stockholm, Sweden, 1980.
- [64] Candappa, D. C., Sanjayan, J. G., and Setunge, S. Complete Triaxial Stress-Strain Curves of High-Strength Concrete. *Journal of Materials in Civil Engineering*, 13(3):209–215, June 2001.
- [65] Cardozo, N. and Allmendinger, R. W. Spherical projections with OSXStereonet. Computers & Geosciences, 51:193–205, February 2013.
- [66] Çengel, Y. A., Boles, M. A., and Kanoğlu, M. Thermodynamics: an engineering approach. McGraw-Hill Education, New York, USA, 9th edition, 2019.
- [67] CEB. International System of Unified Standard Codes of Practice for Structures—Volume 2: CEB-FIP Model Code for Concrete Structures. In CEB Bulletins d'information, number 124. Comité Euro-International du Béton (CEB), 1978.
- [68] CEB. CEB-FIP Model Code 90: Design Code. Technical report, Comité Euro-International du Béton (CEB), 1993.
- [69] Cervera, M., Oliver, J., and Prato, T. Thermo-Chemo-Mechanical Model for Concrete. I: Hydration and Aging. *Journal of Engineering Mechanics*, 125(9):1018–1027, September 1999.
- [70] Cervera, M., Oliver, J., and Prato, T. Thermo-Chemo-Mechanical Model for Concrete. II: Damage and Creep. Journal of Engineering Mechanics, 125(9):1028–1039, September 1999.
- [71] Chang, Y. Tunnel support with shotcrete in weak rock—a rock mechanics study. PhD thesis, KTH Royal Institute of Technology, Stockholm, Sweden, 1994.
- [72] Chen, A. C. T. and Chen, W.-F. Constitutive Relations for Concrete. *Journal of the Engineering Mechanics Division*, 101(4):465–481, August 1975.
- [73] Chen, G., Kemeny, J. M., and Harpalani, S. Fracture propagation and coalescence in marble plates with pre-cut notches under compression. In Myer, L. R., Cook, N. G. W., Goodman, R. E., and Tsang, S. F., editors, *Proceedings of the International Symposium on Fractured and Jointed Rock Masses*, pages 443–448, Lake Tahoe, California, USA, June 1992. A.A. Balkema.
- [74] Chen, W.-F. Plasticity in Reinforced Concrete. McGraw-Hill, New York, 1982.

BIBLIOGRAPHY 292 of 498

[75] Cheng, C. Influence of discontinuities on post-peak behavior of rock in uniaxial compressive test by numerical study. In Farag, A. A., editor, *Proceedings of the 2nd International Conference on Multimedia Technology (ICMT 2011)*, pages 6406–6409, Hangzhou, China, July 2011. Institute of Electrical and Electronics Engineers.

- [76] Cheng, Z. and Detournay, C. Plastic hardening model I: Implementation in FLAC3D. In Gómez, P., Detournay, C., Hart, R., and Nelson, M., editors, *Proceedings of the 4th Itasca Symposium on Applied Numerical Modeling*, pages 267–276, Lima, Perú, March 2016. Itasca International Inc., Minneapolis.
- [77] Cheng, Z. and Lucarelli, A. Plastic hardening model II: Calibration and validation. In Gómez, P., Detournay, C., Hart, R., and Nelson, M., editors, *Proceedings of the 4th Itasca Symposium on Applied Numerical Modeling*, pages 393–402, Lima, Perú, March 2016. Itasca International Inc., Minneapolis.
- [78] Codegone, G., Festa, A., and Dilek, Y. Formation of Taconic mélanges and broken formations in the Hamburg Klippe, Central Appalachian Orogenic Belt, Eastern Pennsylvania. Tectonophysics, 568-569:215–229, September 2012.
- [79] Coli, N., Berry, P., and Boldini, D. Analysis of the block-size distribution in the Shale-Limestone Chaotic Complex (Tuscany, Italy). In Wilson, S., Ewy, R., and Tutuncu, A., editors, Proceedings of the 42nd US Rock Mechanics Symposium and 2nd U.S.-Canada Rock Mechanics Symposium, pages 1–7, San Francisco, California, 29 June–2 July, 2008. American Rock Mechanics Association (ARMA): Alexandria. ARMA 08-233.
- [80] Coli, N., Boldini, D., and Bandini, A. Modeling of complex geological rock mixtures under triaxial testing conditions. In *Proceedings of the 2012 Regional Symposium of the International Society for Rock Mechanics (EUROCK 2012)—Rock Engineering and Technology for Sustainable Underground Construction*, pages 1–12, Stockholm, Sweden, May 2012.
- [81] Cook, N. G. W. The application of seismic techniques to problems in rock mechanics. International Journal of Rock Mechanics and Mining Sciences & Geomechanics Abstracts, 1(2):169–179, March 1964.
- [82] Cook, N. G. W. An experiment proving that dilatancy is a pervasive volumetric property of brittle rock loaded to failure. *Rock Mechanics*, 2(4):181–188, December 1970.
- [83] Cook, N. G. W., Hoek, E., Pretorius, J. P. G., Ortlepp, W. D., and Salamon, M. D. G. Rock mechanics applied to the study of rockbursts. *Journal of the South African Institute* of Mining and Metallurgy, 66:436–528, 1966.
- [84] Cordes, T., Weifner, T., Unteregger, D., and Bergmeister, K. Interaction between deep tunnel drives and an existing tunnel in fault zones-Modelling against reality. *Geomechanics* and Tunnelling, 12(6):641-650, December 2019.
- [85] Cornejo-Malm, G. Schwinden von Spritzbeton. Research report, ETH Zurich, 1995.
- [86] Coussy, O. Mechanics of Porous Continua. Wiley: Chichester, United Kingdom, 1995.
- [87] Coussy, O. Mechanics and physics of porous solids. John Wiley & Sons, Ltd: Chichester, United Kingdom, 1st edition, 2010.

BIBLIOGRAPHY 293 of 498

[88] Cowan, D. S. Structural styles in Mesozoic and Cenozoic mélanges in the western Cordillera of North America. *GSA Bulletin*, 96(4):451–462, April 1985.

- [89] Cudny, M. and Truty, A. Refinement of the Hardening Soil model within the small strain range. *Acta Geotechnica*, 15(8):2031–2051, March 2020.
- [90] Daller, J., Atzl, G., and Blümel, M. Festschrift zum 60. Geburtstag von Wulf Schubert, chapter Bestimmung von Gesteinskennwerten an Störungsmaterial, pages 50–58. Institute of Rock Mechanics and Tunnelling, Graz University of Technology, Graz, Austria, 2010.
- [91] Dassault Systèmes Simulia Corp. Abaqus/CAE 2017 documentation.
- [92] Davila Mendez, J. M. Displacements Analysis in Layered Rock Masses. PhD thesis, Graz University of Technology, Graz, Austria, January 2016.
- [93] Deere, D. U. Rock Mechanics in Engineering Practice, chapter Geological considerations, pages 1–20. Wiley, New York, 1968. Chapter 1.
- [94] Deere, D. U. and Miller, R. P. Engineering classification and index properties for intact rock. Technical report AFWL-TR-65-116, Air Force Weapons Laboratory, Kirtland Air Force Base, New Mexico, USA, December 1966.
- [95] Deutsche Gesellschaft für Geotechnik e.V. (DGGT). Empfehlungen des Arbeitskreises "Numerik in der Geotechnik"–EANG. Wilhelm Ernst & Sohn, Verlag für Architektur und technische Wissenschaften GmbH & Co. KG, Berlin, Germany, February 2014.
- [96] Dickmann, T. Personal communication, July 2021.
- [97] Diederichs, M. S., Carvalho, J. L., and Carter, T. G. A Modified Approach For Prediction of Strength And Post Yield Behaviour For High GSI Rockmasses In Strong, Brittle Ground. In Eberhardt, E., Stead, D., and Morrison, T., editors, Proceedings of the 1st Canada-US Rock Mechanics Symposium: Rock Mechanics: Meeting Society's Challenges and Demands, pages 249–257, Vancouver, Canada, April 2007. ARMA-07-031.
- [98] Ding, Y. Technologische Eigenschaften von jungem Stahlfaserbeton und Stahlfaserspritzbeton. PhD thesis, University of Innsbruck, Innsbruck, Austria, 1998.
- [99] Dorfmann, E. M. Zugkriechen von Beton in Abhängigkeit der Spannungsgeschichte. Master's thesis, Graz University of Technology, Graz, Austria, June 2017.
- [100] Eberhardt, E. Numerical modelling of three-dimension stress rotation ahead of an advancing tunnel face. *International Journal of Rock Mechanics and Mining Sciences*, 38(4):499–518, June 2001.
- [101] Eberly, D. Approximating an Ellipse by Circular Arcs, April 2016. URL https://www.geometrictools.com/Documentation/ApproximateEllipse.pdf. Last access: 26.09.2020.
- [102] Egger, P. Einfluss des Post-Failure Verhaltens von Fels auf den Tunnelausbau unter besonderer Berücksichtigung des Ankerausbaus. PhD thesis, Universität Karlsruhe, Karlsruhe, Germany, 1973.
- [103] Ekici, Z. Semmering Base Tunnel, construction lot SBT 1.1, tunnel Gloggnitz—Tender documents: Calculation values. Project document (in german), Austrian Federal Railways, 2014.

BIBLIOGRAPHY 294 of 498

[104] Engels, S., Wieselthaler, F., Pischinger, G., and Holzer, R. Semmering Base Tunnel, construction lot SBT 1.1, tunnel Gloggnitz, track 1—Engineering geological documentation. Project document (in german), Austrian Federal Railways, 2016.

- [105] Engels, S., Wieselthaler, F., and Holzer, R. Semmering Base Tunnel, construction lot SBT 1.1, tunnel Gloggnitz, track 1—Geotechnical horizontal and longitudinal section. Project document (in german), Austrian Federal Railways, 2017.
- [106] Engl, D. A., Fellin, W., and Zangerl, C. Scherfestigkeiten von Scherzonengesteinen—Ein Beitrag zur geotechnischen Bewertung von tektonischen Störungszonen und Gleitzonen von Massenbewegungen. Bulletin für Angewandte Geologie, 13(2):63–81, 2008.
- [107] England, G. L. and Illston, J. M. Methods of computing stress in concrete from a history of measured strain. *Civil Engineering and Public Works Review*, 60(1–3):513–517, 692–694, 846–847, April, May, June 1965.
- [108] Entfellner, M. Prediction of Displacements and Shotcrete Lining Utilization—Decision strategy for a timely application of ductile support systems in conventional tunnelling. Master's thesis, Graz University of Technology, Graz, Austria, August 2017.
- [109] Entfellner, M., Schubert, W., and Moritz, B. A. Early warning of overbreaks in tunnels. In Proceedings of the 2022 Regional Symposium of the International Society for Rock Mechanics (EUROCK 2022)–Rock and Fracture Mechanics in Rock Engineering and Mining, pages 1–8, Espoo, Finland, September 2022.
- [110] European Committee for Standardization. EN 1992-1-1:2004. Eurocode 2: Design of concrete structures Part 1-1: General rules and rules for buildings. Standard, December 2004.
- [111] Fairhurst, C. E. and Hudson, J. Draft ISRM suggested method for the complete stress-strain curve for intact rock in uniaxial compression. *International Journal of Rock Mechanics and Mining Sciences & Geomechanics Abstracts*, 36:279–289, 1999.
- [112] Farmer, I. W. Stress distribution along a resin grouted rock anchor. *International Journal of Rock Mechanics and Mining Sciences & Geomechanics Abstracts*, 12(11):347–351, November 1975.
- [113] Farmer, I. W. Engineering Behaviour of Rocks. Springer Netherlands, 1st edition, 1983.
- [114] Fasching, F. and Vanek, R. Engineering geological characterisation of fault rocks and fault zones. *Geomechanics and Tunnelling*, 4(3):181–194, June 2011.
- [115] Faulkner, D. R., Lewis, A. C., and Rutter, E. H. On the internal structure and mechanics of large strike-slip fault zones: field observations of the Carboneras fault in southeastern Spain. *Tectonophysics*, 367(3-4):235–251, June 2003.
- [116] Faulkner, D. R., Jackson, C. A. L., Lunn, R. J., Schlische, R. W., Shipton, Z. K., Wibberley, C. A. J., and Withjack, M. O. A review of recent developments concerning the structure, mechanics and fluid flow properties of fault zones. *Journal of Structural Geology*, 32(11): 1557–1575, November 2010.
- [117] Feder, G. and Arwanitakis, M. Zur Gebirgsmechanik ausbruchsnaher Bereiche tiefliegender Hohlraumbauten (unter zentralsymmetrischer Belastung). Berg- und Hüttenmännische Monatshefte, 121(4):103–117, 1976.

BIBLIOGRAPHY 295 of 498

[118] Feenstra, P. H. and de Borst, R. Aspects of Robust Computational Models for Plain and Reinforced Concrete. *HERON*, 38(4):1–76, 1993.

- [119] Feynman, R. P., Leighton, R. B., and Sands, M. The Feynman Lectures on Physics, volume I: Mainly Mechanics, Radiation, and Heat. Basic Books, 2010.
- [120] fib. Structural Concrete: Textbook on Behaviour, Design and Performance: Updated knowledge of the CEB/FIP Model Code 1990. Technical report, fédération internationale du béton (fib), Lausanne, Switzerland, July 2000.
- [121] fib. CEB-FIP Model Code for Concrete Structures 2010. Technical report, fédération internationale du béton (fib), 2013.
- [122] Fischnaller, G. Untersuchungen zum Verformungsverhalten von jungem Spritzbeton im Tunnelbau—Grundlagen und Versuche. Master's thesis, University of Innsbruck, Innsbruck, Austria, 1992.
- [123] Fjellström, P. Measurement and Modelling of Young Concrete Properties. Licentiate thesis, Luleå University of Technology, Luleå, Sweden, 2013.
- [124] Forth, J. P. Predicting the tensile creep of concrete. Cement and Concrete Composites, 55: 70–80, January 2015.
- [125] Fossen, H. Structural Geology. Cambridge University Press, 2nd edition, 2016.
- [126] GEOKON. Instruction Manual: Model 4200 Series, Vibrating Wire Strain Gauges. Version: 11/08/2019 (revision DD). Technical report, Lebanon, New Hampshire, USA, 2019.
- [127] Glawe, U. and Upreti, B. N. Better Understanding the Strengths of Serpentinite Bimrock and Homogeneous Serpentinite. *Felsbau*, 22(5):53–60, 2004.
- [128] Golser, J., Schubert, P., and Rabensteiner, K. A new concept for evaluation of loading in shotcrete linings. In *Proceedings of the International Congress on Progress and Innovation* in *Tunnelling*, volume I, pages 79–85, Toronto, Canada, September 1989.
- [129] Golser, J., Rabensteiner, K., Sigl, O., Aldrian, W., Wedenig, H., Brandl, J., and Maier, C. Materialgesetz für Spritzbeton. Technical report, Bundesministerium für wirtschaftliche Angelegenheiten: Straßenforschung, 1990.
- [130] Goodman, R. E. Introduction to Rock Mechanics. John Wiley & Sons, 2nd edition, 1989.
- [131] Goodman, R. E. Engineering geology: rock in engineering construction. John Wiley & Sons, Inc., 1993.
- [132] Goricki, A. and Pimentel, E. Triaxial Tests on Cataclasites. Rock Mechanics and Rock Engineering, 48(5):2167–2171, November 2014.
- [133] Granet, I., Alvarado, J. L., and Bluestein, M. Thermodynamics and Heat Power. CRC Press, Boca Raton, USA, 9th edition, 2021.
- [134] Grassl, P. and Jirásek, M. Damage-plastic model for concrete failure. *International Journal of Solids and Structures*, 43(22-23):7166–7196, November 2006.
- [135] Graziani, A., Boldini, D., and Ribacchi, R. Practical Estimate of Deformations and Stress Relief Factors for Deep Tunnels Supported by Shotcrete. *Rock Mechanics and Rock Engineering*, 38(5):345–372, June 2005.

BIBLIOGRAPHY 296 of 498

[136] Green, S. J. and Swanson, S. R. Static constitutive relations for concrete. Technical report AFWL-TR-72-244, Air Force Weapons Laboratory, Kirtland Air Force Base, New Mexico, USA, April 1973.

- [137] Groshong, R. H. j. Low-temperature deformation mechanisms and their interpretation. Geological Society of America Bulletin, 100(9):1329–1360, September 1988.
- [138] Gross, D., Hauger, W., and Wriggers, P. Technische Mechanik 4: Hydromechanik, Elemente der Höheren Mechanik, Numerische Methoden. Springer Berlin Heidelberg, 7th edition, 2009.
- [139] Großauer, K. Tunnelling in Heterogeneous Ground—Numerical Investigation of Stresses and Displacements. Diploma thesis, Graz University of Technology, Graz, Austria, October 2001.
- [140] Großauer, K. Expert System Development for the Evaluation and Interpretation of Displacement Monitoring Data in Tunnelling. PhD thesis, Graz University of Technology, Graz, Austria, February 2009.
- [141] Grübl, P., Weigler, H., and Karl, S. Beton—Arten, Herstellung und Eigenschaften. Ernst & Sohn Verlag, Berlin, 2nd edition, 2001.
- [142] Gruppe TUNNEL:Monitor. TUNNEL:monitor (v2021.1.4). URL https://igt-engineering.com/de/forschung-und-entwicklung/tunnelmonitor/. Last access: 15.11.2022.
- [143] Gschwandtner, G. G. Analytische Berechnungsansätze zum Kennlinienverfahren. Master's thesis, Montanuniversität Leoben, Leoben, Austria, January 2010.
- [144] Gudmundsson, A., Simmenes, T. H., Larsen, B., and Philipp, S. L. Effects of internal structure and local stresses on fracture propagation, deflection, and arrest in fault zones. *Journal of Structural Geology*, 32(11):1643–1655, November 2010.
- [145] Guntli, P., Keller, F., Lucchini, R., and Rust, S. Gotthard-Basistunnel: Geologie, Geotechnik, Hydrologie zusammenfassender Schlussbericht. Technical report 7, Landesgeologie, 2016.
- [146] Guo, P. and Su, X. Shear strength, interparticle locking, and dilatancy of granular materials. Canadian Geotechnical Journal, 44(5):579–591, May 2007.
- [147] Harer, G., Prein, R., Schwab, P., and Wehr, H. Tunnelling in Poor Ground Conditions Case History Galgenbergtunnel. *Felsbau*, 14(2):82–86, 1996.
- [148] Hartog, A. H. An Introduction to Distributed Optical Fibre Sensors. CRC Press, May 2017.
- [149] Hauggaard-Nielsen, A. B. Mathematical Modelling and Experimental Analysis of Early Age Concrete. PhD thesis, Technical University of Denmark, Lyngby, Denmark, October 1997.
- [150] Havlásek, P., Šmilauer, V., Hájková, K., and Baquerizo, L. Thermo-mechanical simulations of early-age concrete cracking with durability predictions. In *IOP Conference Series:*Materials Science and Engineering, volume 236, pages 1–7. IOP Publishing, September 2017.
- [151] Heinisch, M., Mayr, B., Millen, B., and Holzer, R. Semmering Base Tunnel, construction lot SBT 1.1, access tunnel Göstritz—Geotechnical horizontal and longitudinal section. Project document (in german), 2016.

BIBLIOGRAPHY 297 of 498

[152] Heinisch, M., Mayr, B., Millen, B., and Holzer, R. Semmering Base Tunnel, construction lot SBT 1.1, access tunnel Göstritz—Engineering geological documentation. Project document (in german), Austrian Federal Railways, 2016.

- [153] Heinrich, P. J. Effiziente Erfassung viskoelastischer Eigenschaften bei der Spannungsermittlung von gezwängten Betonbauteilen. PhD thesis, Graz University of Technology, Graz, Austria, November 2018.
- [154] Hellmich, C. Shotcrete as part of the New Austrian Tunneling Method: From Thermochemomechanical Material Modeling to Structural Analysis and Safety Assessment of Tunnels. PhD thesis, Vienna University of Technology, Vienna, Austria, 1999.
- [155] Hellmich, C., Ulm, F.-J., and Mang, H. A. Multisurface Chemoplasticity. I: Material Model for Shotcrete. *Journal of Engineering Mechanics*, 125(6):692–701, 1999.
- [156] Hellmich, C., Ulm, F.-J., and Mang, H. A. Multisurface Chemoplasticity. II: Numerical Studies on NATM Tunneling. *Journal of Engineering Mechanics*, 125(6):702–713, 1999.
- [157] Hellmich, C., Sercombe, J., Ulm, F.-J., and Mang, H. A. Modeling of Early-Age Creep of Shotcrete. II: Application to Tunneling. *Journal of Engineering Mechanics*, 126(3):292–299, 2000.
- [158] Hellmich, C., Mang, H. A., and Ulm, F.-J. Hybrid method for quantification of stress states in shotcrete tunnel shells: combination of 3D in situ displacement measurements and thermochemoplastic material law. *Computers & Structures*, 79(22):2103–2115, 2001.
- [159] Henzinger, M. R., Schachinger, T., Lienhart, W., Buchmayer, F., Weilinger, W., Stefaner, R., Haberler-Weber, M., Haller, E.-M., Steiner, M., and Schubert, W. Fibre-optic supported measurement methods for monitoring rock pressure. *Geomechanics and Tunnelling*, 11(3): 251–263, June 2018.
- [160] Hettler, A. and Vardoulakis, I. Behaviour of dry sand tested in a large triaxial apparatus. Géotechnique, 34(2):183–197, June 1984.
- [161] Hill, R. The mathematical theory of plasticity. The Clarendon Press, Oxford, 1951.
- [162] Hodgson, K. and Cook, N. G. W. The effects of size and stress gradient on the strength of rock. In Proceedings of the 2nd Congress of the International Society for Rock Mechanics, volume 2, pages 31–34, Belgrade, Serbia, September 1970.
- [163] Hoek, E. and Brown, E. T. Practical estimates of rock mass strength. *International Journal of Rock Mechanics and Mining Sciences*, 34(8):1165–1186, December 1997.
- [164] Hoek, E. and Diederichs, M. S. Empirical estimation of rock mass modulus. *International Journal of Rock Mechanics and Mining Sciences*, 43(2):203–215, February 2006.
- [165] Hoek, E. Brittle failure of rock. Rock Mechanics in Engineering Practice. Wiley: New York, 1968.
- [166] Hoek, E. and Brown, E. T. *Underground Excavations in Rock*. CRC Press, 1st edition, 1980.
- [167] Hoek, E. and Brown, E. T. Empirical Strength Criterion for Rock Masses. *Journal of the Geotechnical Engineering Division*, 106(9):1013–1035, September 1980.

BIBLIOGRAPHY 298 of 498

[168] Holt, E. E. Early age autogeneous shrinkage of concrete. Vtt publications 446, Technical Research Centre of Finland, Espoo, Finland, 2001.

- [169] Holter, K. G. Properties of waterproof sprayed concrete tunnel linings: A study of EVAbased sprayed membranes for waterproofing of rail and road tunnels in hard rock and cold climate. PhD thesis, Norwegian University of Science and Technology, Trondheim, Norway, December 2015.
- [170] Holzer, R. Personal communication, September 2022.
- [171] Holzer, R., Prall, K., Wagner, O. K., and Gobiet, G. Semmering Base Tunnel Tunnelling in challenging geotechnical and geological conditions in major fault zones. *Geomechanics* and *Tunnelling*, 13(5):509–518, October 2020.
- [172] Hösthagen, A. Thermal Crack Risk Estimation and Material Properties of Young Concrete. Licentiate thesis, Luleå University of Technology, Luleå, Sweden, 2017.
- [173] Huber, H. Untersuchungen zum Verformungsverhalten von jungem Spritzbeton im Tunnelbau. Master's thesis, University of Innsbruck, Innsbruck, Austria, 1991.
- [174] Ikumi, T., Salvador, R. P., and Aguado, A. Mix proportioning of sprayed concrete: A systematic literature review. *Tunnelling and Underground Space Technology*, 124(104456): 12, June 2022.
- [175] Itasca Consultants S.A.S. Dynamic Analysis in FLAC3D. Electronical, 2020. URL https://www.itasca.fr/software/dynamic-analysis-in-flac3d. Last access: 23.12.2020.
- [176] Itasca Consulting Group, Inc. UDEC 5.0 documentation, 2011.
- [177] Itasca Consulting Group, Inc. FLAC3D 6.0 documentation, 2017.
- [178] Itasca Consulting Group, Inc. FLAC3D 7.0 documentation, 2019.
- [179] Itasca Consulting Group, Inc. Learning Itasca Educational Partnership. Electronical, 2023. URL https://www.itascainternational.com/learning/iep/iep-research-program. Last access: 05.01.2023.
- [180] Jaeger, J. C. and Cook, N. G. W. Fundamentals of Rock Mechanics. Chapman & Hall: London, 3rd edition, 1979.
- [181] Jaeger, J. C., Cook, N. G. W., and Zimmerman, R. W. Fundamentals of Rock Mechanics. Blackwell Publishing, 4th edition, 2007.
- [182] Johnson, R. B. and DeGraff, J. V. Principles of Engineering Geology. John Wiley & Sons, Inc., 1988.
- [183] Johnston, I. W. Strength of Intact Geomechanical Materials. *Journal of Geotechnical Engineering*, 111(6):730–749, June 1985.
- [184] Kahraman, S. and Alber, M. Estimating unconfined compressive strength and elastic modulus of a fault breccia mixture of weak blocks and strong matrix. *International Journal of Rock Mechanics and Mining Sciences*, 43(8):1277–1287, December 2006.

BIBLIOGRAPHY 299 of 498

[185] Kahraman, S., Alber, M., Fener, M., and Gunaydin, O. Evaluating the geomechanical properties of Misis fault breccia (Turkey). *International Journal of Rock Mechanics and Mining Sciences*, 45(8):1469–1479, December 2008.

- [186] Kahraman, S., Gunaydin, O., Alber, M., and Fener, M. Evaluating the strength and deformability properties of Misis fault breccia using artificial neural networks. *Expert Systems with Applications*, 36(3):6874–6878, April 2009.
- [187] Kainrath-Reumayer, S., Gschwandtner, G., Schuller, E., and Galler, R. Beitrag zur Anwendung des Kennlinienverfahrens. *Berg- und Hüttenmännische Monatshefte*, 155(2): 83–89, February 2010.
- [188] Kainrath-Reumayer, S., Neugebauer, E., Charette, F., Plouffe, M., and Galler, R. Ankerung im Untertagebau - Entwicklungen in Theorie und Praxis. Geomechanik und Tunnelbau, 1 (5):345–351, October 2008.
- [189] Kaiser, P. K. and Kim, B. H. Rock mechanics challenges of underground constructions and mining. In *Proceedings of the Korean Rock Mechanics Symposium*, pages 1–16, Seoul, South Korea, 2008. Korean Society for Rock Mechanics.
- [190] Kaiser, P. K. and Tannant, D. D. The Role of Shotcrete in Hard Rock Mines. In Hustrulid, W. A. and Bullock, R. L., editors, *Underground Mining Methods—Engineering Fundamentals* and International Case Studies, chapter 67, pages 579–592. Society for Mining, Metallurgy, and Exploration, Inc. (SME), 2001.
- [191] Kaiser, P. K., Diederichs, M. S., Martin, C. D., Sharp, J., and Steiner, W. Underground Works In Hard Rock Tunnelling And Mining. In *Proceedings of the International Conference on Geotechnical & Geological Engineering (GeoEng2000)*, ISRM International Symposium, pages 841–926, Melbourne, Australia, November 2000. Technomic Publishing Co.
- [192] Kaiser, P. K., Amann, F., and Steiner, W. How Highly Stressed Brittle Rock Failure Impacts Tunnel Design. In Proceedings of the 2010 Regional Symposium of the International Society for Rock Mechanics (EUROCK 2010), pages 1–12, Lausanne, Switzerland, June 2010. ISRM-EUROCK-2010-003.
- [193] Kalender, A., Sönmez, H., Medley, E. W., Tunusluoglu, C., and Kasapoglu, K. E. An approach to predicting the overall strengths of unwelded bimrocks and bimsoils. *Engineering Geology*, 183:65–79, December 2014.
- [194] Kastner, H. Statik des Tunnel- und Stollenbaues: auf der Grundlage geomechanischer Erkenntnisse. Springer Berlin Heidelberg, 1962.
- [195] Kettunen Linder, M. and Kilic, O. En studie av sprutbetongförstärkningen i Citybanan -Norrströmstunneln. Master's thesis, KTH Royal Insitute of Technology, Stockholm, Sweden, March 2011. Examensarbete 326.
- [196] Kim, Y.-S., Peacock, D. C. P., and Sanderson, D. J. Fault damage zones. *Journal of Structural Geology*, 26(3):503–517, March 2004.
- [197] Kirsch, G. Die Theorie der Elastizität und die Bedürfnisse der Festigkeitslehre. Zeitschrift des Vereines Deutscher Ingenieure, 42(29):797–807, 1898.

BIBLIOGRAPHY 300 of 498

[198] Klein, C. and Philpotts, A. R. Earth materials: introduction to mineralogy and petrology. Cambridge University Press, 1st edition, 2013.

- [199] Kluckner, A. Aspekte der Gebirgscharakterisierung im Tunnelbau. Master's thesis, Graz University of Technology, Graz, Austria, October 2012.
- [200] Kluckner, A. and Schubert, W. Study on the Anisotropic Displacement Pattern at a Conventional Tunnel Drive. In *Proceedings of the 5th ISRM Young Scholars' Symposium on Rock Mechanics and International Symposiumon Rock Engineering for Innovative Future (YSRM2019 & REIF2019)*, pages 1–6, Okinawa, Japan, December 2019.
- [201] Knipe, R. J. Deformation mechanism path diagrams for sediments undergoing lithification. Structural Fabric in Deep Sea Drilling Project Cores From Forearcs, Memoir 166:151–160, 1986.
- [202] Kovler, K. Why sealed concrete swells. ACI Materials Journal, 93(4):334-340, 1996.
- [203] Kropik, C. and Mang, H. A. Computational mechanics of the excavation of tunnels. Engineering Computations, 13(7):49–69, November 1996.
- [204] Kulhawy, F. H. Stress deformation properties of rock and rock discontinuities. *Engineering Geology*, 9(4):327–350, December 1975.
- [205] Kusterle, W. Qualitätsverbesserungen beim Spritzbeton durch technologische Massnahmen, durch den Einsatz neuer Materialien und auf Grund der Erfassung von Spritzbetoneigenschaften. Habilitation dissertation, University of Innsbruck, Innsbruck, Austria, 1992.
- [206] Kusterle, W. Comparison of shrinkage behaviour and creep properties under different compressive stress levels for wet-mix sprayed concrete from ten hours up to two weeks. Technical report, Morgan Tunnelling, 1999.
- [207] Kusterle, W. and Lukas, W. Spritzbeton hoher Güte für die einschalige Spritzbetonbauweise. In Tagungsband der 3. Internationalen Fachtagung Spritzbeton-Technologie, Innsbruck, Austria, pages 29–40, 1990.
- [208] Kusterle, W., Jäger, J., John, M., Neumann, C., and Röck, R. Spritzbeton im Tunnelbau. In Bergmeister, K., Fingerloos, F., and Wörner, J.-D., editors, Beton-Kalender 2014: Unterirdisches Bauen, Grundbau, Eurocode 7, chapter IX, pages 303–390. Ernst & Sohn GmbH & Co. KG., 2014.
- [209] Kuwajima, F. M. Early Age Properties of Shotcrete. In Celestino, T. B. and Parker, H. W., editors, Proceedings of the Eighth International Conference on Shotcrete for Underground Support, São Paulo, Brazil, April 1999. American Society of Civil Engineers.
- [210] Lackner, R. and Mang, H. A. Cracking in shotcrete tunnel shells. *Engineering Fracture Mechanics*, 70(7–8):1047–1068, May 2003.
- [211] Lackner, R., Hellmich, C., and Mang, H. A. Constitutive modeling of cementitious materials in the framework of chemoplasticity. *International Journal for Numerical Methods in Engineering*, 53(10):2357–2388, 2002.
- [212] Lackner, R., Macht, J., Hellmich, C., and Mang, H. A. Hybrid Method for Analysis of Segmented Shotcrete Tunnel Linings. *Journal of Geotechnical and Geoenvironmental Engineering*, 128(4):298–308, April 2002.

BIBLIOGRAPHY 301 of 498

[213] Lama, R. D. and Vutukuri, V. S. *Handbook on Mechanical Properties of Rocks*, volume 2 of *Series on Rock and Soil Mechanics*. Trans Tech Publications, Clausthal, Germany, 1978.

- [214] Laplante, P. Propriétés mécaniques des bétons durcissants: analyse comparée des bétons classiques et à très hautes performances [Mechanical properties of hardening concrete: a comparative analysis of classical and high strength concretes]. PhD thesis, Ecole Nationale des Ponts et Chaussées, Paris, France, 1993.
- [215] Laplante, P. and Boulay, C. Evolution du coefficient de dilatation thermique du béton en fonction de sa maturité aux tout premiers âges. *Materials and Structures*, 27(10):596–605, December 1994.
- [216] Leber, C. Einfluss der Primärspannungsorientierung auf die Verschiebungscharakteristik. Master's thesis, Graz University of Technology, Graz, Austria, March 2009.
- [217] Lebschy, D. Investigation of the influence of the tunnel lining on the displacement development. Master's thesis, Graz University of Technology, Graz, Austria, September 2014.
- [218] Lenz, G. Displacement monitoring data in tunnelling—Development of a semiautomatic evaluation system. Diploma thesis, Graz University of Technology, Graz, Austria, April 2007.
- [219] Lenz, G. Characterization of ground and system behaviour in water-bearing fault zones. PhD thesis, Graz University of Technology, Graz, Austria, July 2020.
- [220] Lenz, G. Personal communication, May 2022.
- [221] Lenz, G. Personal communication, July 2022.
- [222] Lenz, G. Personal communication, November 2022.
- [223] Lepique, M. Empfehlung Nr. 10 des Arbeitskreises 3.3 "Versuchstechnik Fels" der Deutschen Gesellschaft für Geotechnik e. V.: Indirekter Zugversuch an Gesteinsproben Spaltzugversuch. Bautechnik, 85(9):623–627, September 2008.
- [224] Lienhart, W., Schubert, W., Henzinger, M. R., Buchmayer, F., Weilinger, W., and Stefaner, R. Faseroptisch unterstützte Messmethoden zur Beobachtung von Gebirgsdruck. Research report, Federal Ministry Republic of Austria, Climate Action, Environment, Energy, Mobility, Innovation and Technology, Vienna, Austria, October 2018.
- [225] Lindlar, B., Jahn, M., and Schlumpf, J. Sika Sprayed Concrete Handbook. Sika AG, 2020. URL https://www.sika.com/content/dam/dms/corporate/n/glo-sprayed-concrete-handbook-2021.pdf. Last access: 14.01.2023.
- [226] Lindquist, E. S. and Goodman, R. E. Strength and deformation properties of a physical model melange. In Nelson, P. P. and Laubach, S. E., editors, Rock Mechanics - Models and Measurements - Challenges from Industry: Proceedings of the 1st North American Rock Mechanics Symposium (NARMS), pages 843–850. The University of Texas at Austin, A.A. Balkema: Rotterdam, June 1994.
- [227] Lindquist, E. S. The Strength and Deformation Properties of Melange. PhD thesis, University of California, Berkeley, California, USA, 1994.

BIBLIOGRAPHY 302 of 498

[228] Lockner, D. A. Rock Physics and Phase Relations: A Handbook of Physical Constants, volume 3 of AGU Reference Shelf, chapter Rock Failure, pages 127–147. American Geophysical Union, Washington, D.C., USA, 1st edition, January 1995.

- [229] Logan, J. M., Friedmann, M., Higgs, N., Dengo, C., and Shimamoto, T. Experimental studies of simulated gouge and their application to studies of natural fault zones. In Proceedings of Conference VIII—Analysis of Actual Fault Zones in Bedrock, pages 305—343, Menlo Park, California, USA, April 1979. United States Department of the Interior, Geological Survey, Office of Earthquake Studies. Open-file report 79-1239.
- [230] Lu, T. Autogenous shrinkage of early age cement paste and mortar. PhD thesis, Delft University of Technology, Delft, Netherlands, 2019.
- [231] Lucarelli, A. Personal communication, June 2022.
- [232] Luna Innovations Inc. Datasheet: Luna Optical Backscatter Reflectometer (OBR) Model 4600. Version: LTOBR4600 REV. 004 02/13/2014. Technical report, Blacksburg, Virginia, USA, 2014.
- [233] Luna Innovations Inc. Datasheet: Luna Optical Backscatter Reflectometer (OBR) Model 4600. Version: LTOBR4600 REV. 006 03/09/2018. Technical report, Blacksburg, Virginia, USA, 2018.
- [234] Lupini, J. F., Skinner, A. E., and Vaughan, P. R. The drained residual strength of cohesive soils. *Géotechnique*, 31(2):181–213, June 1981.
- [235] Ma, J. Faserfreier Ultrahochfester Beton—Entwicklung und Materialeigenschaften. PhD thesis, Leipzig University, Leipzig, Germany, 2010.
- [236] Macht, J. Hybrid Analysis of Shotcrete Tunnel Linings: Assessment and Online Monitoring of the Level of Loading. PhD thesis, Vienna University of Technology, Vienna, Austria, 2002.
- [237] Mair, K., Frye, K. M., and Marone, C. Influence of grain characteristics on the friction of granular shear zones. *Journal of Geophysical Research: Solid Earth*, 107(B10):ECV 4–1–ECV 4–9, October 2002.
- [238] Małkowski, P., Ostrowski, L., and Brodny, J. Analysis of Young's modulus for Carboniferous sedimentary rocks and its relationship with uniaxial compressive strength using different methods of modulus determination. *Journal of Sustainable Mining*, 17(3):145–157, 2018.
- [239] Mandl, G. Discontinuous fault zones. *Journal of Structural Geology*, 9(1):105–110, January 1987.
- [240] Mandl, G. Mechanics of Tectonic Faulting: Models and Basic Concepts. Developments in Structural Geology, 1. Elsevier Science Publishers B.V.: Amsterdam, 1988.
- [241] Mandl, G. Faulting in Brittle Rocks: An Introduction to the Mechanics of Tectonic Faults. Springer Berlin Heidelberg, 1st edition, 2000.
- [242] Mang, H. A. and Hofstetter, G. Festigkeitslehre. Springer Berlin Heidelberg, 5th edition, 2018.

BIBLIOGRAPHY 303 of 498

[243] Manton, N. and Mee, N. *The Physical World*. Oxford University Press, 1st edition, April 2017.

- [244] Marcher, T. Personal communication, January 2021.
- [245] Marinos, P. V. and Tsiambaos, G. Strength and Deformability of Specific Sedimentary and Ophiolithic Rocks. *Bulletin of the Geological Society of Greece*, 43(3):1259–1266, January 2010.
- [246] Marshak, S. Earth: portrait of a planet. New York: W.W. Norton & Company, 6th edition, 2019.
- [247] Martin, J. Back-analysis of rock mass parameters at the Semmering Base Tunnel based on the convergence confinement method. Master's thesis, Graz University of Technology, Graz, Austria, December 2022.
- [248] Medley, E. W. Using stereological methods to estimate the volumetric proportions of blocks in melanges and similar block-in-matrix rocks (bimrocks). In Oliveira, R., Rodrigues, L. F., Coelho, A. G., and Cunha, A. P., editors, *Proceedings of the 7th International Congress of the International Association of Engineering Geology (IAEG)*, pages 1031–1040. A.A. Balkema: Rotterdam, September 1994.
- [249] Medley, E. W. Systematic Characterization of Melange Bimrocks and Other Chaotic Soil/Rock Mixtures. Felsbau, 17(3):152–162, 1999.
- [250] Medley, E. W. Orderly Characterization of Chaotic Franciscan Melanges. *Felsbau*, 19(4): 20–33, 2001.
- [251] Medley, E. W. Observations on Tortuous Failure Surfaces in Bimrocks. *Felsbau*, 22(5): 35–43, 2004.
- [252] Medley, E. Tunneling Through Fault Zones and Melanges. Lecture slides of lecture 4 of the short course "Anticipating and addressing the characterization, design and construction problems of fault rocks, melanges and other bimrocks", Geological Engineering Department, Hacettepe University, Ankara, Turkey, June 2004.
- [253] Medley, E. W. Estimating Block Size Distributions of Melanges and Similar Block-in-Matrix Rocks (Bimrocks). In Hammah, R., Bawden, W., Curran, J., and Telesnicki, M., editors, Proceedings of 5th North American Rock Mechanics Symposium (NARMS), pages 599–606, Toronto, Canada, July 2002. University of Toronto Press.
- [254] Medley, E. W. and Zekkos, D. Geopractitioner approaches to working with antisocial mélanges. In Mélanges: Processes of Formation and Societal Significance, number 480, pages 261–277. The Geological Society of America, 2011.
- [255] Medley, E. W. The Engineering Characterization of Melanges and Similar Block-in-Matrix Rocks (Bimrocks). PhD thesis, University of California, Berkeley, California, USA, 1994.
- [256] Medley, E. W. and Lindquist, E. S. The engineering significance of the scale-independence of some Franciscan melanges in California, USA. In Daemen, J. J. K. and Schultz, R. A., editors, *Proceedings of the 35th U.S. Symposium on Rock Mechanics*, pages 907–914. A.A. Balkema, Rotterdam, 1995.

BIBLIOGRAPHY 304 of 498

[257] Meixner, T. Trigger Values for tunnel monitoring in SCL shallow tunnels. Master's thesis, Graz University of Technology, Graz, Austria, September 2016.

- [258] Menétrey, P. and Willam, K. J. Triaxial Failure Criterion for Concrete and its Generalization. ACI Structural Journal, 92(3):311–318, 1995.
- [259] Merriam-Webster, Inc. Dictionary: Autogenous. Electronical, 2020. URL https://www.merriam-webster.com/dictionary/autogenous. Last access: 23.06.2020.
- [260] Meschke, G. Consideration of aging of shotcrete in the context of a 3-D viscoplastic material model. *International Journal for Numerical Methods in Engineering*, 39:3123–3143, 1996.
- [261] Meschke, G., Kropik, C., and Mang, H. A. Numerical analyses of tunnel linings by means of a viscoplastic material model for shotcrete. *International Journal for Numerical Methods* in Engineering, 39:3145–3162, 1996.
- [262] Michelis, P. N. Work-softening and hardening behaviour of granular rocks. *Rock Mechanics*, 14(3):187–200, December 1981.
- [263] Mindess, S., Young, J. F., and Lawrence, F. V. Creep and drying shrinkage of calcium silicate pastes I. Specimen preparation and mechanical properties. *Cement and Concrete Research*, 8(5):591–600, 1978.
- [264] Mitchell, T. M. and Faulkner, D. R. The nature and origin of off-fault damage surrounding strike-slip fault zones with a wide range of displacements: A field study from the Atacama fault system, northern Chile. *Journal of Structural Geology*, 31(8):802–816, August 2009.
- [265] Mödlhammer, H. *Spritzbeton: In situ Versuche*. Bachelor's thesis, Montanuniversität Leoben, Leoben, Austria, April 2008.
- [266] Monsberger, C. M., Lienhart, W., Kluckner, A., Wagner, L., and Schubert, W. Continuous strain measurements in a shotcrete tunnel lining using distributed fibre optic sensing. In *Proceedings of the 9th European Workshop on Structural Health Monitoring*, pages 1–13, Manchester, United Kingdom, July 2018.
- [267] Monsberger, C. M., Lienhart, W., Kluckner, A., and Schubert, W. In-situ assessment of distributed strain and curvature characteristics in shotcrete tunnel linings based on fiber optic strain sensing. In *Proceedings of the 14th International Congress on Rock Mechanics* and Rock Engineering, pages 1–8, Foz do Iguassu, Brazil, September 2019.
- [268] Monsberger, C. M. and Lienhart, W. Distributed fiber optic shape sensing along shotcrete tunnel linings: Methodology, field applications, and monitoring results. *Journal of Civil* Structural Health Monitoring, 11(2):337–350, January 2021.
- [269] Monsberger, C. M., Bauer, P., Buchmayer, F., and Lienhart, W. Large-scale distributed fiber optic sensing network for short and long-term integrity monitoring of tunnel linings. *Journal of Civil Structural Health Monitoring*, 12(6):1317–1327, March 2022.
- [270] Moritz, B., Grossauer, K., and Schubert, W. Short Term Prediction of System Behaviour of Shallow Tunnels in Heterogeneous Ground. *Felsbau*, 22(5):44–52, 2004.
- [271] Müller, M. Kriechversuche an jungen Spritzbetonen zur Ermittlung der Parameter für Materialgesetze. mathesis, Montanuniversität Leoben, Leoben, Austria, October 2001.

BIBLIOGRAPHY 305 of 498

[272] Mutschler, T. Neufassung der Empfehlung Nr. 1 des Arbeitskreises "Versuchstechnik Fels" der Deutschen Gesellschaft für Geotechnik e. V.: Einaxiale Druckversuche an zylindrischen Gesteinsprüfkörpern. *Bautechnik*, 81(10):825–834, October 2004.

- [273] Naylor, M. A., Mandl, G., and Supesteijn, C. H. K. Fault geometries in basement-induced wrench faulting under different initial stress states. *Journal of Structural Geology*, 8(7): 737–752, January 1986.
- [274] Nefeslioglu, H. A. Evaluation of geo-mechanical properties of very weak and weak rock materials by using non-destructive techniques: Ultrasonic pulse velocity measurements and reflectance spectroscopy. *Engineering Geology*, 160:8–20, June 2013.
- [275] Neuner, M., Cordes, T., Drexel, M., and Hofstetter, G. Time-Dependent Material Properties of Shotcrete: Experimental and Numerical Study. *Materials*, 10(9):1067, September 2017.
- [276] Neuner, M., Gamnitzer, P., and Hofstetter, G. An Extended Damage Plasticity Model for Shotcrete: Formulation and Comparison with Other Shotcrete Models. *Materials*, 10(1): 1–22, January 2017.
- [277] Neuner, M., Schreter, M., Unteregger, D., and Hofstetter, G. Influence of the Constitutive Model for Shotcrete on the Predicted Structural Behavior of the Shotcrete Shell of a Deep Tunnel. *Materials*, 10(6):1–17, May 2017.
- [278] Neuner, M., Gamnitzer, P., and Hofstetter, G. Correction: An Extended Damage Plasticity Model for Shotcrete: Formulation and Comparison with Other Shotcrete Models. *Materials*, 11(1):135, January 2018.
- [279] Neville, A. M. Properties of Concrete. Prentice Hall, 4th edition, 1995.
- [280] Neville, A. M., Dilger, W. H., and Brooks, J. J. Creep of plain and structural concrete. Construction Press (Longman), Harlow, UK, 1983.
- [281] Nielsen, L. F. Composite creep analysis of concrete: A rational, incremental stress-strain approach. Byg Rapport R-178, Technical University of Denmark, Lyngby, Denmark, 2007.
- [282] Nilsson, M. Restraint Forces and Partial Coefficients for Crack Risk Analyses of Early Age Concrete Structures. PhD thesis, Luleå University of Technology, Luleå, Sweden, 2003.
- [283] Nübel, K. and Huang, W. A study of localized deformation pattern in granular media. Computer Methods in Applied Mechanics and Engineering, 193(27-29):2719–2743, July 2004.
- [284] Oberdörfer, W. Auswirkung von unterschiedlichen Betonnachbehandlungsmassnahmen auf die Qualit\u00e4t des Nassspritzbetons. Master's thesis, University of Innsbruck, Innsbruck, Austria, 1996.
- [285] Obert, L. and Duvall, W. I. Rock Mechanics and the Design of Structures in Rock. John Wiley & Sons, New York, 1967.
- [286] Obert, L., Windes, S. L., and Duvall, W. I. Standardized tests for determining the physical properties of mine rock. Report of Investigations 3891, United States Department of the Interior-Bureau of Mines, August 1946.

BIBLIOGRAPHY 306 of 498

[287] Obrzud, R. F. and Truty, A. The Hardening Soil Model-A practical guidebook (Z_Soil.PC 100701 report, revised 21.10.2018). Zace Services Ltd, October 2018.

- [288] ÖBV. Spritzbeton: Teil 1—Anwendung. Guideline, Österreichischer Betonverein (ÖBV), 1989.
- [289] ÖBV. Sprayed Concrete. Guideline, Österreichische Bautechnik Vereinigung (ÖBV), April 2013.
- [290] ÖGG. Guideline for the Geotechnical Design of Underground Structures with Conventional Excavation. Guideline, Austrian Society for Geomechanics (ÖGG), Salzburg, Austria, 2010. Translated from German version 2.1.
- [291] ÖGG. Geotechnical Monitoring in Conventional Tunnelling. Austrian Society for Geomechanics (ÖGG), Salzburg, Austria, 2014.
- [292] Oluokun, F. A., Burdette, E. G., and Deatherage, J. H. Splitting Tensile Strength and Compressive Strength Relationships at Early Ages. ACI Materials Journal, 88(2):115–121, 1991.
- [293] Ord, A. Deformation of rock: A pressure-sensitive, dilatant material. *Pure and Applied Geophysics (PAGEOPH)*, 137(4):337–366, 1991.
- [294] Oreste, P. P. A Procedure for Determining the Reaction Curve of Shotcrete Lining Considering Transient Conditions. Rock Mechanics and Rock Engineering, 36(3):209–236, June 2003.
- [295] Oreste, P., Spagnoli, G., and Ceravolo, L. A. A numerical model to assess the creep of shotcrete linings. Proceedings of the Institution of Civil Engineers - Geotechnical Engineering, 172(4):344–354, August 2019.
- [296] Palkovic, S. D., Brommer, D. B., Kupwade-Patil, K., Masic, A., Buehler, M. J., and
 Büyüköztürk, O. Roadmap across the mesoscale for durable and sustainable cement paste
 A bioinspired approach. Construction and Building Materials, 115:13-31, July 2016.
- [297] Palmström, A. and Singh, R. The deformation modulus of rock masses comparisons between in situ tests and indirect estimates. *Tunnelling and Underground Space Technology*, 16(2):115–131, April 2001.
- [298] Parent, T., Domede, N., Sellier, A., and Mouatt, L. Mechanical characterization of limestone from sound velocity measurement. *International Journal of Rock Mechanics and Mining* Sciences, 79:149–156, October 2015.
- [299] Passchier, C. W. and Trouw, R. A. J. Microtectonics. Springer Verlag, Berlin, 1996.
- [300] Paulini, P. Reaction mechanisms of concrete admixtures. Cement and Concrete Research, 20(6):910–918, November 1990.
- [301] Peacock, D. C. P., Dimmen, V., Rotevatn, A., and Sanderson, D. J. A broader classification of damage zones. *Journal of Structural Geology*, 102:179–192, 2017.
- [302] Pichler, B. and Hellmich, C. Hybrid methods for shotcrete and segmental linings tunnel shells Combining displacement and rotation measurements with computational multiscale mechanics. *Geomechanics and Tunnelling*, 11(3):226–235, June 2018.

BIBLIOGRAPHY 307 of 498

[303] Pichler, B., Hellmich, C., and Eberhardsteiner, J. Spherical and acicular representation of hydrates in a micromechanical model for cement paste: prediction of early-age elasticity and strength. *Acta Mechanica*, 203(3-4):137–162, June 2008.

- [304] Pichler, B., Hellmich, C., and Eberhardsteiner, J. Reaktionskinetik und Kriecheigenschaften des Spritzbetons, der im Zuge des Vortriebs des Koralmtunnels (Baulos KAT2) verwendet wird. Technical report (preliminary), Institute for Mechanics of Materials and Struttures, Vienna University of Technology, Vienna, Austria, December 2011.
- [305] Pilgerstorfer, T. Prediction of displacement development using closed form solutions. Diploma thesis, Graz University of Technology, Graz, Austria, May 2008.
- [306] Pilgerstorfer, T. Mechanical Characterization of Fault Zones. PhD thesis, Graz University of Technology, Graz, Austria, 2014.
- [307] Pilgerstorfer, T. Personal communication, January 2022.
- [308] Pilgerstorfer, T., Radončić, N., Moritz, B., and Goricki, A. Evaluation and interpretation of monitoring data in the test adit EKT Paierdorf. Geomechanics and Tunnelling, 4(5): 423–434, October 2011.
- [309] Pittino, G., Galler, R., Bonin, K., and Bezler, J. Experiences with polymer-modified shotcrete. In Amberg, F. and Knut, F. G., editors, *Proceedings of the 11th Conference on Shotcrete for Underground Support*, pages 1–18, Davos, Switzerland, June 2009. Engineering Conferences International (ECI).
- [310] Pötsch, M. The analysis of rotational and sliding modes of failure for slopes, foundations, and underground structures in blocky, hard rock. PhD thesis, Graz University of Technology, Graz, Austria, March 2011.
- [311] Potts, D. M. and Zdravković, L. Finite element analysis in geotechnical engineering: theory. Thomas Telford Ltd, London, 1999.
- [312] Poturovic, S., Schubert, W., and Blümel, M. Comparison of Constant Normal Load (CNL) and Constant Normal Stiffness (CNS) Direct Shear Tests. In Schubert, W. and Kluckner, A., editors, *Proceedings of the ISRM Regional Symposium EUROCK 2015 & 64th Geomechanics Colloquium—Future Development of Rock Mechanics*, pages 1–6, Salzburg, Austria, October 2015. Austrian Society for Geomechanics.
- [313] Powers, T. C. Causes and Control of Volume Change. *Journal of the PCA Research and Development Laboratories*, pages 30–39, January 1959. Portland Cement Association (PCA).
- [314] Powers, T. C. and Brownyard, T. L. Studies of the Physical Properties of Hardened Portland Cement Paste. In *Bulletin No. 22*, pages 1–342. Portland Cement Association (PCA), March 1948.
- [315] Probst, B. Entwicklung einer Langzeitdruckversuchsanlage für den Baustellenbetrieb zur Bestimmung des Materialverhaltens von jungem Spritzbeton. Diploma thesis, Montanuniversität Leoben, Leoben, Austria, 1999.
- [316] Pusch, R. Alteration of the Hydraulic Conductivity of Rock by Tunnel Excavation.

 International Journal of Rock Mechanics and Mining Sciences & Geomechanics Abstracts,
 26(1):79–83, January 1989.

BIBLIOGRAPHY 308 of 498

[317] Püstow, H. Tunnelling in a tectonic melange of high structural complexity. mathesis, Aachen University of Technology, Aachen, Germany, 2001.

- [318] R Core Team. R: A Language and Environment for Statistical Computing. R Foundation for Statistical Computing, Vienna, Austria, 2022. URL https://www.R-project.org/. Last access: 14.01.2023.
- [319] Radončić, N. Tunnel design and prediction of systembehaviour in weak ground. PhD thesis, Graz University of Technology, Graz, Austria, March 2011.
- [320] Rastrup, E. Heat of hydration in concrete. *Magazine of Concrete Research*, 6(17):79–92, September 1954.
- [321] Raymond, L. A. Classification of melanges. In Raymond, L. A., editor, *Melanges: Their Nature, Origin, and Significance*, pages 7–20. The Geological Society of America, 1984.
- [322] Reyes, O. and Einstein, H. H. Failure Mechanisms of Fractured Rock—A Fracture Coalescence Model. In Wittke, W., editor, *Proceedings of the 7th International ISRM Congress*, pages 333–339, Aachen, Germany, September 1991. A.A. Balkema.
- [323] Riedmüller, G. and Schubert, W. Tunnelling in Fault Zones Innovative Approaches. In Proceedings of the 4th North American Rock Mechanics Symposium (NARMS 2000): Rock Around The Rim, pages 1–12, Seattle, Washington, USA, July 2000. Balkema: Rotterdam. ARMA-2000-0113.
- [324] Riedmüller, G., Brosch, F. J., Klima, K., and Medley, E. W. Engineering Geological Characterization of Brittle Faults and Classification of Fault Rocks. *Felsbau*, 19(4):13–19, 2001.
- [325] Rokahr, R. B. and Lux, K. H. Einfluß des rheologischen Verhaltens des Spritzbetons auf den Ausbauwiderstand. *Felsbau*, 5(1):11–18, 1987.
- [326] Rombach, G. Spannbetonbau. Wiley-VCH Verlag GmbH, April 2010.
- [327] Roscoe, K. H. The Influence of Strains in Soil Mechanics. *Géotechnique*, 20(2):129–170, June 1970.
- [328] Rosso, R. S. A comparison of joint stiffness measurements in direct shear, triaxial compression, and In Situ. *International Journal of Rock Mechanics and Mining Sciences & Geomechanics Abstracts*, 13(6):167–172, June 1976.
- [329] Rostami, J., Kahraman, S., Yu, X., Copur, H., Balci, C., Bamford, W., and Asbury, B. The relation between uniaxial compressive and Brazilian tensile strength. In Ulusay, R., Aydan, O., Gercek, H., and Hindistan, M. A., editors, Proceedings of the 2016 Regional Symposium of the International Society for Rock Mechanics (EUROCK 2016)—Rock Mechanics and Rock Engineering: From the Past to the Future, volume 1, pages 147–152, Ürgüp, Cappadocia Region, Turkey, August 2016. Turkish National Society for Rock Mechanics, CRC Press.
- [330] Rowe, P. W. The stress-dilatancy relation for static equilibrium of an assembly of particles in contact. *Proceedings of the Royal Society of London. Series A. Mathematical and Physical Sciences*, 269(1339):500–527, October 1962.
- [331] Rowe, R. K., editor. Geotechnical and geoenvironmental engineering handbook. Springer US, 2001.

BIBLIOGRAPHY 309 of 498

[332] Ruetz, W. Das Kriechen des Zementsteins im Beton und seine Beeinflussung durch gleichzeitiges Schwinden. In *Deutscher Ausschuss für Stahlbeton*, number 183. Wilhelm Ernst & Sohn, Berlin, 1966.

- [333] Rust, W. Nichtlineare Finite-Elemente-Berechnungen. Springer Fachmedien Wiesbaden, 3rd edition, 2016.
- [334] Sadd, M. Elasticity. Academic Press, 3rd edition, 2014.
- [335] Sainsbury, B. L. and Sainsbury, D. P. Practical Use of the Ubiquitous-Joint Constitutive Model for the Simulation of Anisotropic Rock Masses. Rock Mechanics and Rock Engineering, 50(6):1507–1528, February 2017.
- [336] Salamon, M. D. G. Energy considerations in rock mechanics: fundamental results. *Journal of the South African Institute of Mining and Metallurgy*, 84:233–246, 1984.
- [337] Saldivar, G. G. and Sánchez, F. A. Tunnels and Underground Cities: Engineering and Innovation meet Archaeology, Architecture and Art, chapter Comparative study on shotcrete performance in tunnels based on different constitutive approaches, pages 1–10. CRC Press, 1st edition, April 2019.
- [338] Sammis, C. G. and Biegel, R. L. Fractals, fault-gouge, and friction. *Pure and Applied Geophysics PAGEOPH*, 131(1-2):255–271, 1989.
- [339] Sausgruber, T. and Brandner, R. The Relevance of Brittle Fault Zones in Tunnel Construction—Lower Inn Valley Feeder Line North of the Brenner Base Tunnel, Tyrol, Austria. *Mitteilungen der Österreichischen Geologischen Gesellschaft*, 94:157–172, August 2003.
- [340] Saw, H. A., Villaescusa, E., Windsor, C. R., and Thompson, A. G. Non-linear, elastic-plastic response of steel fibre reinforced shotcrete to uniaxial and triaxial compression testing. In Amberg, F. and Garshol, K. F., editors, Shotcrete for Underground Support XI, ECI Symposium Series, pages 1–18, June 2009.
- [341] SBT 1.1 Tunnel Gloggnitz: ARGE. Semmering Base Tunnel, construction lot SBT 1.1, tunnel Gloggnitz—Daily construction records. Project document (in german), Joint venture (ARGE): Implenia Österreich GmbH, HOCHTIEF Infrastructure GmbH, THYSSEN SCHACHTBAU GMBH, 2016.
- [342] SBT 1.1 Tunnel Gloggnitz: ARGE. Semmering Base Tunnel, construction lot SBT 1.1, tunnel Gloggnitz—Daily construction records. Project document (in german), Joint venture (ARGE): Implenia Österreich GmbH, HOCHTIEF Infrastructure GmbH, THYSSEN SCHACHTBAU GMBH, 2017.
- [343] SBT 1.1 Tunnel Gloggnitz: PGST. Semmering Base Tunnel, construction lot SBT 1.1, tunnel Gloggnitz—Tender documents: Geotechnical prognosis underground. Project document (in german), Austrian Federal Railways, 2014. Planungsgemeinschaft Semmering-Basistunnel neu Tunnelbau (PGST).
- [344] SBT 1.1 Tunnel Gloggnitz: site team. Semmering Base Tunnel, construction lot SBT 1.1, tunnel Gloggnitz—Presentation for the 13th meeting on the geotechnical conditions. Project document (in german), 2016.

BIBLIOGRAPHY 310 of 498

[345] SBT 1.1 Tunnel Gloggnitz: site team. Semmering Base Tunnel, construction lot SBT 1.1, tunnel Gloggnitz—Report on the site decisions on support. Project document (in german), 2016.

- [346] SBT 1.1 Tunnel Gloggnitz: site team. Semmering Base Tunnel, construction lot SBT 1.1, tunnel Gloggnitz—Report on the site decisions on support. Project document (in german), 2017.
- [347] Schädlich, B. and Schweiger, H. F. Shotcrete Model: Implementation, validation and application. Internal technical report, Graz University of Technology, Graz, Austria, October 2016.
- [348] Schädlich, B. and Schweiger, H. F. A new constitutive model for shotcrete. In Hicks, M. A., Brinkgreve, R. B. J., and Rohe, A., editors, Numerical Methods in Geotechnical Engineering Proceedings of the 8th European Conference on Numerical Methods in Geotechnical Engineering, NUMGE 2014, volume 1, pages 103–108, Delft, Netherlands, June 2014. Taylor & Francis Group, London, UK.
- [349] Schädlich, B., Schweiger, H. F., Marcher, T., and Saurer, E. Application of a novel constitutive shotcrete model to tunnelling. In *Rock Engineering and Rock Mechanics:* Structures in and on Rock Masses, pages 799–804. CRC Press, May 2014.
- [350] Schanz, T., Vermeer, P. A., and Bonnier, P. G. The hardening soil model: Formulation and verification. In *Proceedings of the 1st PLAXIS symposium: Beyond 2000 in Computational Geotechnics-10 Years of PLAXIS*, pages 1–16. Balkema: Rotterdam, 1999.
- [351] Scheiner, S. and Hellmich, C. Continuum Microviscoelasticity Model for Aging Basic Creep of Early-Age Concrete. *Journal of Engineering Mechanics*, 135(4):307–323, April 2009.
- [352] Scheydt, J. C. Influence of the reactive Components on Shotcrete Performance. *Tunnel*, (3):22–27, 2015.
- [353] Schlicke, D. Mindestbewehrung für zwangbeanspruchten Beton: Festlegung unter Berücksichtigung der erhärtungsbedingten Spannungsgeschichte und der Bauteilgeometrie. In Monographic Series TU Graz, Schriftenreihe des Instituts für Betonbau, volume 4. Verlag der Technischen Universität Graz, Graz, Austria, 2nd edition, 2016.
- [354] Schlicke, D. Personal communication, February 2018.
- [355] Schlicke, D. Personal communication, June 2020.
- [356] Schmid, S. M. and Handy, M. R. Controversies in Modern Geology. Evolution of Geological Theories in Sedimentology, Earth History and Tectonics., chapter 16. Towards a Genetic Classification of Fault Rocks: Geological Usage and Tectonophysical Implications, pages 339–361. Academic Press Limited, London, 1991.
- [357] Schön, J. H. Developments in Petroleum Science. In Physical Properties of Rocks-Fundamentals and Principles of Petrophysics, volume 65. Elsevier B.V., 2nd edition, December 2015.
- [358] Schubert, P. Beitrag zum rheologischen Verhalten von Spritzbeton. Felsbau, 6(3):150–153, 1988.

BIBLIOGRAPHY 311 of 498

[359] Schubert, P., Hölzl, H., Sellner, P., and Fasching, F. Geomechanical knowledge gained from the Paierdorf investigation tunnel in the section through the Lavanttal main fault zone. *Geomechanics and Tunnelling*, 3(2):163–173, April 2010.

- [360] Schubert, W. Erfahrungen bei der Durchörterung von Störzonen bei österreichischen Tunneln. In Proceedings of the "Nachdiplomkurs in angewandten Erdwissenschaften: Herausforderung Geologie im Untertagebau", pages 1–10, CSF Monte Veritá, Ascona, Switzerland, May 1996. ETH Zurich.
- [361] Schubert, W. Experience of tunnel construction in weak ground. Geomechanics and Tunnelling, 4(3):211–220, June 2011.
- [362] Schubert, W. and Riedmüller, G. Geotechnisches Gutachten zum Verbruch Galgenbergtunnel / Vortrieb Leoben Ost Sta. 1326 bis 1333,6. Technical report, The Austrian Federal Railways, Graz, Austria, April 1995. Unpublished.
- [363] Schubert, W. and Riedmüller, G. Geotechnische Nachlese eines Verbruches Erkenntnisse und Impulse. In Semprich, S., editor, *Proceedings of the 10th Christian Veder Colloquium: Innovation in der Geotechnik Entwicklungen der letzten Jahre*, number 13 in Mitteilungshefte, pages 59–68, Graz, Austria, 1995. Institute of Soil Mechanics and Foundation Engineering, Graz University of Technology.
- [364] Schubert, W. and Riedmüller, G. Tunnelling in Fault Zones State of the Art in Investigation and Construction. Felsbau, 18(2):7–15, 2000.
- [365] Schubert, W., Brandtner, M., Schweiger, H. F., Helmberger, A., Marcher, T., and Radončić, N. Proposed design strategy for tunnels. In Schubert, W. and Kluckner, A., editors, Proceedings of the ISRM Regional Symposium EUROCK 2015 & 64th Geomechanics Colloquium— Future Development of Rock Mechanics, pages 37–47, Salzburg, Austria, October 2015. Austrian Society for Geomechanics.
- [366] Schubert, W., Blümel, M., Brunnegger, S., Staudacher, R., and Sellner, P. J. Aspekte des Ausbaus. In Schubert, W. and Kluckner, A., editors, *Proceedings of the Workshop on Tunnelbau in Störungszonen—Eine Herausforderung*, pages 49–62, Graz, Austria, November 2016. Institute of Rock Mechanics and Tunnelling, Graz University of Technology.
- [367] Schubert, W., Blümel, M., Staudacher, R., and Brunnegger, S. Support aspects of tunnels in fault zones. *Geomechanics and Tunnelling*, 10(4):342–352, August 2017.
- [368] Schütz, R., Potts, D. M., and Zdravković, L. Advanced constitutive modelling of shotcrete: Model formulation and calibration. *Computers and Geotechnics*, 38(6):834–845, September 2011.
- [369] Schütz, R. Numerical Modelling of Shotcrete for Tunnelling. PhD thesis, Imperial College London, London, UK, February 2010.
- [370] Sercombe, J., Hellmich, C., Ulm, F.-J., and Mang, H. A. Modeling of early-age creep of shotcrete. I: Model and model parameters. *Journal of Engineering Mechanics*, 126(3): 284–291, 2000.
- [371] Sezaki, M., Kibe, T., Ichikawa, Y., and Kawamoto, T. An experimental study on the mechanical properties of shotcrete. *Journal of the Society of Materials Science*, 38(434): 1336–1340, 1989.

BIBLIOGRAPHY 312 of 498

[372] Sibson, R. H. Fault rocks and fault mechanisms. *Journal of the Geological Society*, 133(3): 191–213, March 1977.

- [373] Sibson, R. H. Structural permeability of fluid-driven fault-fracture meshes. *Journal of Structural Geology*, 18(8):1031–1042, August 1996.
- [374] Simo, J. C., Kennedy, J. G., and Govindjee, S. Non-smooth multisurface plasticity and viscoplasticity. Loading/unloading conditions and numerical algorithms. *International Journal for Numerical Methods in Engineering*, 26(10):2161–2185, October 1988.
- [375] Skempton, A. W. Residual strength of clays in landslides, folded strata and the laboratory. *Géotechnique*, 35(1):3–18, March 1985.
- [376] Sönmez, H., Gokceoglu, C., Tuncay, E., Medley, E. W., and Nefeslioglu, H. A. Relationships between Volumetric Block Proportions and Overall UCS of a Volcanic Bimrock. *Felsbau*, 22(5):27–34, 2004.
- [377] Sönmez, H., Tuncay, E., and Gokceoglu, C. Models to predict the uniaxial compressive strength and the modulus of elasticity for Ankara Agglomerate. *International Journal of Rock Mechanics and Mining Sciences*, 41(5):717–729, July 2004.
- [378] Sönmez, H., Gokceoglu, C., Medley, E. W., Tuncay, E., and Nefeslioglu, H. A. Estimating the uniaxial compressive strength of a volcanic bimrock. *International Journal of Rock Mechanics and Mining Sciences*, 43(4):554–561, June 2006.
- [379] Sönmez, H., Kasapoglu, K. E., Coskun, A., Tunusluoglu, C., Medley, E. W., and Zimmerman, R. W. A conceptual empirical approach for the overall strength of unwelded bimrocks. In Vrkljan, I., editor, Proceedings of the 2009 Regional Symposium of the International Society for Rock Mechanics (EUROCK 2009)—Rock Engineering in Difficult Ground Conditions Soft Rocks and Karst, pages 357–360, Dubrovnik, Croatia, October 2010. Taylor & Francis: London.
- [380] Stadlmann, T., Vanek, R., and Goricki, A. Semmering Base Tunnel, construction lot SBT 1.1, tunnel Gloggnitz—Tender documents: Rock mass types. Project document (in german), Austrian Federal Railways, 2014.
- [381] Staudacher, R. F. Anschlüsse für Arbeitsfugen bei Spritzbetonauskleidungen. Master's thesis, Graz University of Technology, Graz, Austria, November 2016.
- [382] Steindorfer, A. F. Short Term Prediction of Rock Mass Behaviour in Tunnelling by Advanced Analysis of Displacement Monitoring Data. PhD thesis, Graz University of Technology, Graz, Austria, November 1997.
- [383] Stini, J. Tunnelbaugeologie Die geologischen Grundlagen des Stollen- und Tunnelbaues. Springer Vienna, 1st edition, 1950.
- [384] Swanson, M. T. Late Paleozoic strike-slip faults and related vein arrays of Cape Elizabeth, Maine. *Journal of Structural Geology*, 28(3):456–473, March 2006.
- [385] Tazawa, E.-i., editor. Autogenous Shrinkage of Concrete: Proceedings of the International Workshop, organized by the JCI (Japan Concrete Institute), Hiroshima, Japan, June 1999. Taylor & Francis.
- [386] Terzaghi, K. Theoretical Soil Mechanics. John Wiley & Sons, Inc.: New York, 1943.

BIBLIOGRAPHY 313 of 498

[387] Thomas, A. Numerical modelling of sprayed concrete lined (SCL) tunnels. PhD thesis, University of Southampton, Southampton, United Kingdom, 2003.

- [388] Thomas, A. Sprayed Concrete Lined Tunnels—An introduction. Taylor & Francis, 2009.
- [389] Thomas, A. Sprayed Concrete Lined Tunnels—second edition. CRC Press, 2020.
- [390] Thomée, B. *Physikalisch nichtlineare Berechnung von Stahlfaserbetonkonstruktionen*. PhD thesis, Technical University Munich, Munich, Germany, 2005.
- [391] Thornton, C. Numerical simulations of deviatoric shear deformation of granular media. *Géotechnique*, 50(1):43–53, February 2000.
- [392] Thuro, K., Plinninger, R. J., Zäh, S., and Schütz, S. Scale effects in rock strength properties. Part 1: Unconfined compressive test and Brazilian test. In Särkkä and Eloranta, editors, Proceedings of the 2001 Regional Symposium of the International Society for Rock Mechanics (EUROCK 2001)—Rock Mechanics A Challenge for Society, pages 169–174. Swets & Zeitlinger Lisse, 2001.
- [393] Tigges, V. E. Die Hydratation von Hüttensanden und Möglichkeiten ihrer Beeinflussung zur Optimierung von Hochofenzementeigenschaften. PhD thesis, Clausthal University of Technology, Clausthal-Zellerfeld, Germany, 2009.
- [394] Tourenq, C. and Denis, A. La resistance a la traction des roches. Rapport de Recherches 4A, Laboratoire Central des Ponts et Chaussées, Paris, France, 1970.
- [395] Traina, L. A. Experimental stress-strain behaviour of a low strength concrete under multiaxial states of stress. Technical report AFWL-TR-82-92, Air Force Weapons Laboratory, Kirtland Air Force Base, New Mexico, USA, 1983.
- [396] Tsesarsky, M., Hazan, M., and Gal, E. Estimating the elastic moduli and isotropy of block in matrix (bim) rocks by computational homogenization. *Engineering Geology*, 200:58–65, January 2016.
- [397] Twiss, R. J. and Moores, E. M. Structural Geology. W. H. Freeman and Company, New York, USA, 2nd edition, 2007.
- [398] Tziallas, G. P., Tsiambaos, G., and Saroglou, H. Determination of Rock Strength and Deformability of Intact Rocks. *Electronic Journal of Geotechnical Engineering (EJGE)*, 14 (G):1–12, 2009.
- [399] Ulm, F.-J. Couplages thermochémomécaniques dans les bétons: Un premier bilan. Monograph LCPC OA31, Laboratoire Central des Ponts et Chaussées, Paris, France, 1998.
- [400] Ulm, F.-J. and Acker, P. Le point sur le fluage et la recouvrance des bétons. *Bulletin Liaison des Laboratoires des Ponts et Chaussées*, (XX):73–82, 1998. Special issue.
- [401] Ulm, F.-J. and Coussy, O. Modeling of Thermochemomechanical Couplings of Concrete at Early Ages. *Journal of Engineering Mechanics*, 121(7):785–794, 1995.
- [402] Ulm, F.-J. and Coussy, O. Strength Growth as Chemo-Plastic Hardening in Early Age Concrete. *Journal of Engineering Mechanics*, 122(12):1123–1132, 1996.

BIBLIOGRAPHY 314 of 498

[403] Ulusay, R., Türeli, K., and Ider, M. H. Prediction of engineering properties of a selected litharenite sandstone from its petrographic characteristics using correlation and multivariate statistical techniques. *Engineering Geology*, 38(1-2):135–157, December 1994.

- [404] U.S. Department of the Interior Bureau of Reclamation. *Engineering geology field manual*, volume I. U.S. Government Printing Office, 2nd edition, 1998.
- [405] U.S. Department of the Interior Bureau of Reclamation. Glossary of commonly used terms by the Bureau of Reclamation. Electronical, 2016. URL https://www.usbr.gov/library/glossary/index.html. Last access: 20.12.2016.
- [406] van der Pluijm, B. A. and Marshak, S. Earth structure: an introduction to structural geology and tectonics. W. W. Norton & Company, Inc.: New York, 2nd edition, 2004.
- [407] Vanek, R. and Stadlmann, T. Semmering Base Tunnel new—Legal railway approval procedure documents: Report on the construction geology. Project document (in german), Austrian Federal Railways, May 2010.
- [408] Vanek, R., Fasching, F., and Fasching, A. Ingenieurgeologische Charakterisierung von Störungszonen. In Schubert, W. and Kluckner, A., editors, *Proceedings of the Workshop on Tunnelbau in Störungszonen—Eine Herausforderung*, pages 1–11, Graz, Austria, November 2016. Institute of Rock Mechanics and Tunnelling, Graz University of Technology.
- [409] VBE. Semmering Base Tunnel, construction lot SBT 1.1, tunnel Gloggnitz—Concrete test report. Project document (in german), Verein für Baustoffprüfung und -entwicklung (VBE), 2016.
- [410] Vermeer, P. A. and de Borst, R. Non-associated plasticity for soils, concrete and rock. HERON, 29(3):1–64, 1984.
- [411] Vlachopoulos, N. and Diederichs, M. S. Improved Longitudinal Displacement Profiles for Convergence Confinement Analysis of Deep Tunnels. Rock Mechanics and Rock Engineering, 42(2):131–146, April 2009.
- [412] Volpe, R., Ahlgren, C., and Goodman, R. Selection of engineering properties for geologically variable foundations. In *Proceedings of the 17th International Congress on Large Dams*, *Vienna:Paris*, pages 1087–1101. International Commission on Large Dams, 1991.
- [413] von Rabcewicz, L. Die Ankerung im Tunnelbau ersetzt bisher gebräuchliche Einbaumethoden. Schweizerische Bauzeitung, 75(9):123–131, March 1957.
- [414] von Terzaghi, K. *Ingenieurgeologie*, chapter Tunnelgeologie, pages 365–407. Julius Springer: Vienna, 1st edition, 1929.
- [415] Wagner, L. Concept and realisation of a distributed fibre-optic sensing system for direct and continuous strain measurement in a shotcrete lining. Master's thesis, Graz University of Technology, Graz, Austria, September 2017.
- [416] Wagner, L., Kluckner, A., Monsberger, C. M., Wolf, P., Prall, K., Schubert, W., and Lienhart, W. Direct and Distributed Strain Measurements Inside a Shotcrete Lining: Concept and Realisation. *Rock Mechanics and Rock Engineering*, 53(2):641–652, August 2019.

BIBLIOGRAPHY 315 of 498

[417] Wen-jie, X., Zhong-qi, Y., and Rui-lin, H. Study on the mesostructure and mesomechanical characteristics of the soil—rock mixture using digital image processing based finite element method. *International Journal of Rock Mechanics and Mining Sciences*, 45(5):749–762, July 2008.

- [418] Wen-Jie, X., Qiang, X., and Rui-Lin, H. Study on the shear strength of soil—rock mixture by large scale direct shear test. *International Journal of Rock Mechanics and Mining Sciences*, 48(8):1235–1247, December 2011.
- [419] Wesche, K. Baustoffe für tragende Bauteile—Band 2: Beton, Mauerwerk. Bauverlag GmbH: Wiesbaden, Berlin, 3rd edition, 1993.
- [420] Wibberley, C. A. J., Yielding, G., and Toro, G. D. Recent advances in the understanding of fault zone internal structure: a review. *Geological Society, London, Special Publications*, 299(1):5–33, 2008.
- [421] Wittmann, F. Bestimmung physikalischer Eigenschaften des Zementsteins. In *Deutscher Ausschuss für Stahlbeton*, number 232. Wilhelm Ernst & Sohn, Berlin, 1974.
- [422] Wuilpart, M. Advanced Fiber Optics: Concepts and Technology, chapter Rayleigh scattering in optical fibers and applications to distributed measurements, pages 1–56. EPFL Press, Lausanne, Switzerland, 1st edition, 2011.
- [423] Wullschläger, D. Ein Verbundwerkstoffmodell für die Systemankerung im Tunnelbau. PhD thesis, Universität Karlsruhe, Karlsruhe, Germany, 1988.
- [424] Yin, J. Untersuchungen zum zeitabhängigen Tragverhalten von tiefliegenden Hohlräumen im Fels mit Spritzbetonausbau. PhD thesis, Technische Universität Clausthal, Clausthal-Zellerfeld, Germany, February 1996.
- [425] ZAMG. Zentralanstalt für Meteorologie und Geodynamik: Klimamonitoring. Electronical, 2021. URL https://www.zamg.ac.at/cms/de/klima/klima-aktuell/klimamonitoring/?view=fullscreen¶m=t&period=period-ymd-2016-11-17&ref=3. Last access: 02.12.2021.
- [426] Zhang, H.-Y., Xu, W.-J., and Yu, Y.-Z. Triaxial tests of soil—rock mixtures with different rock block distributions. *Soils and Foundations*, 56(1):44–56, February 2016.
- [427] Zhao, X. G. and Cai, M. A mobilized dilation angle model for rocks. *International Journal of Rock Mechanics and Mining Sciences*, 47(3):368–384, April 2010.
- [428] Zi, G. and Bažant, Z. P. Continuous Relaxation Spectrum for Concrete Creep and its Incorporation into Microplane Model M4. *Journal of Engineering Mechanics*, 128(12): 1331–1336, December 2002.

Appendix B: Some mechanical properties of rocks

This appendix comprises information completing Chapter 3 (p. 19). For clarity, the section titles are identical.

B.1 Tensile strength

The following subsections list published test data referring to the tensile strength of rocks and to correlations of the tensile strength with the uniaxial peak compressive strength. Fig. 3.8 (p. 31) graphs the data.

B.1.1 Johnston (1985)

Johnston (1985) [183] compiled about 1700 results from various laboratory tests (triaxial compression, uniaxial compression, uniaxial tensile) on different groups of rock types (note the range of the uniaxial peak compressive strength, σ_c , different for each group):

- Group a: Carbonate materials with well-developed crystal cleavage (e.g., dolomite, limestone, and marble); 20 MPa $< \sigma_c < 600$ MPa;
- Group b: Lithified argillaceous materials (e.g., mudstone, shale, slate, and clay); $6 \text{ kPa} < \sigma_c < 200 \text{ MPa}$;
- Group c: Arenaceous materials with strong crystals and poorly developed crystal cleavage (e.g., sandstone and quartzite); 8 MPa $< \sigma_c < 200$ MPa;
- Group e: Coarse-grained polyminerallic igneous and metamorphic materials (e.g., amphibolite, gabbro, gneiss, granite, norite, and granodiorite); 100 MPa $< \sigma_c < 400$ MPa.

And for each group Johnston performed a best curve fit (Fig. B.1; observed difference between measurement and prediction max. 16%). With the fittings of the failure envelope, it is also possible to predict the uniaxial peak tensile strength, σ_t , for a given uniaxial peak compressive strength, σ_c . These predictions are added to the graph in Fig. 3.8 (p. 31). Johnston disregarded data sets if they did not satisfy several (quality) criteria. He, for example, studied the failure modes involved at the individual uniaxial compression tests. If tensile splitting dominated failure rather than shear failure along a plane inclined to the specimen axis, then the test result remained unconsidered. The peak load (i.e., uniaxial compressive strength) is lower in the former case than in the latter and, thus, underestimating the shear strength of the particular rock ([183, p. 732]). Predictions of σ_t have been verified by the author comparing them with results from Brazilian

and direct uniaxial tensile tests. [183, p. 739] comments that the correlation for group e may be inadequate as one dominant data set used for the fitting featured unusual values.

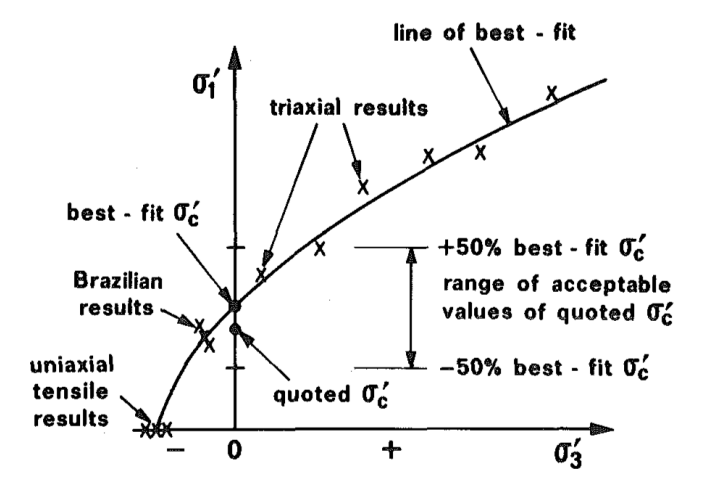


Figure B.1: Fitting of results from various laboratory tests in the σ'_3 - σ'_1 plane (from [183, Fig. 2, p. 733]). Fitting method: method of least squares. Fitting equation: $\sigma'_{1n} = (M \cdot \sigma'_{3n}/B + S)^B$ ([183, Eq. 1, p. 731] with S=1 for intact materials; similar to the Hoek-Brown criterion, cf. [181, Eq. 4.26, p. 96]). $\sigma'_{1n} = \sigma'_1/\sigma'_c$, $\sigma'_{3n} = \sigma'_3/\sigma'_c$: normalised effective principal stresses at failure; intact material parameter B: describes the non-linearity of the failure envelope; intact material parameter M: describes the slope of the failure envelope at $\sigma'_{3n} = 0$. Symbols with apostrophe refer to effective stresses or to effective or drained strength parameters.

B.1.2 Kluckner (2012)

For the determination of characteristic ground types according to [290], Kluckner (2012) [199] analysed results from various laboratory tests (e.g., triaxial compression, uniaxial compression, Brazilian) on different rock types from the Semmering Base Tunnel project. Next to checking the photographs of the test specimens for failure along pre-existing planes of weakness, he applied following thresholds referring to the test specimen size and shape and published in standards to increase the comparability of the results ([199, p. 16ff]; l ... specimen length, d ... specimen diameter):

- Brazilian test: $d \ge 50$ mm ([223, p. 624]), $l/d = 0.5 \pm 0.2$ ([223, p. 624]);
- Triaxial compression test: $d \ge 47$ mm ([15, p. 4]), $2 \le l/d \le 2.5$ ([15, p. 4]; for the compilation in Fig. 3.8 on p. 31, the lower limit is relaxed to have results from tests on specimens with a l/d ratio below but close to 2 included; those results are marked accordingly);
- Uniaxial compression test: $d \ge 50$ mm ([111, p. 285]), $1 \le l/d \le 2.5$ ([272, Tab. 1, p. 828]); if l/d < 2, reduction of strength according to Eq. 16 in [272, p. 827] (from [285]).

The characteristics of the remaining test data are listed in Tab. B.1. For Fig. 3.8, the splitting tensile strengths, $\sigma_{t,sp}$, from Brazilian tests on specimens of a particular rock type recovered from a particular depth below surface (with core drillings) have been linked to uniaxial peak compressive strengths, σ_c , from uniaxial compression tests or triaxial compression tests (utilising the Hoek-Brown criterion, cf. [181, p. 96]) on specimens of the same rock type recovered from a similar depth. These pairs of σ_c and $\sigma_{t,sp}$ values are added to Fig. 3.8 (p. 31).

If rocks feature a pronounced foliation, their behaviour is anisotropic. Thus, when analysing results from tests on rock specimens with such a feature, the orientation of the weakness planes

Table B.1: Data from laboratory tests on rock specimens from the *Semmering Base Tunnel* project (from [199]).

Test type			Dolomite	Gneiss	Rock type Limestone	Phyllite	Schist
Brazilian	$n \\ d \\ l/d \\ \sigma_{t,sp}$	mm - MPa	6 {51.4; 102.0} [0.48;0.53] [2.19;10.49]	51 [51.2;102.2] [0.42;0.58] [1.57;14.25]	3 51.4 [0.55;0.60] [4.65;7.83]	15 [51.2;102.0] [0.41;0.58] [1.87;29.36]	24 [51.2;102.5] [0.47;0.54] [1.13;15.42]
Uniaxial compression	$n \\ d \\ l/d \\ \sigma_c$	mm - MPa	6 {51.4; 102.0} [1.36;2.00] [23.07;107.96]	24 [51.2;102.1] [1.06;2.00] [24.62;126.44]	1 51.4 2.01 98.68	8 [51.2;102.0] [1.22;2.00] [15.66;241.71]	14 [51.2;102.5] [1.07;2.01] [1.98;170.10]
Triaxial compression	n d l/d σ_c	mm - MPa	1 51.3 2.01 34.92	12 [51.2;83.6] [1.99;2.01] [43.31;109.40]	1 51.4 1.99 86.39	5 [51.2;51.4] [2.00,2.01] [17.69;215.39]	5 [51.2;51.5] [1.89;2.01] [35.89;253.34]

n ... number of specimens, l ... specimen length, d ... specimen diameter, $\sigma_{t,sp}$... splitting tensile strength, σ_c ... uniaxial peak compressive strength

relative to the load direction must be considered.² [75], who simulated uniaxial compression tests on anisotropic specimens numerically, observed different failure mechanisms involved depending on the dip, α , of a single weakness plane passing through the specimen centre ([75, p. 6407]):

- $\alpha = 0^{\circ}$: tensile and shear failure in the intact rock;
- $\alpha = 30^{\circ}$, $\alpha = 75^{\circ}$: both slip along the weakness plane and tensile failure in the intact rock;
- $\alpha = 45^{\circ}$, $\alpha = 60^{\circ}$: mainly slip along the weakness plane;
- $\alpha = 90^{\circ}$: splitting of the weakness plane and tensile failure in the intact rock.

The lowest uniaxial compressive strength resulted for the case where the weakness plane dips at 60° (cf. Fig. B.2). The highest values resulted for $\alpha=0^{\circ}$ (i.e., axial load direction normal to the weakness plane) and $\alpha=90^{\circ}$ (i.e., axial load direction parallel to the weakness plane). These findings match with other literature. [181, p. 104f] reports that depending on the orientation of planes of weakness, failure will either occur along a plane of weakness or along a plane within the intact rock. [130, p. 95] confirms that the strength is usually higher when the loading is parallel to the weakness planes than when the loading is perpendicular them (cf. Fig. B.2). He also reports a similar dependency of the behaviour on the orientation of weakness planes for triaxial compression tests (cf. [130, p. 94]).

Thus, [199] divided compressive strength data into three groups relating to the dip of the weakness planes: $\alpha \leq 20^{\circ}$ (weakness planes sub-perpendicular to the axial load direction), $20^{\circ} < \alpha < 70^{\circ}$ (weakness planes inclined to the axial load direction), $\alpha \geq 70^{\circ}$ (weakness planes sub-parallel to the axial load direction). These groups are marked accordingly in Fig. 3.8. Where weakness planes are inclined, slip along those planes might dominate the failure resulting to a low peak compressive strength of the rock specimen. This might explain why some data points of specimens with inclined weakness planes align far left of the majority in Fig. 3.8. Results from Brazilian tests also depend on the orientation of weakness planes relative to the major principal stress. Tests on specimens with weakness planes perpendicular to the load direction normally yield the highest tensile strengths; they are lowest for tests on specimens with weakness

²For all tests described here (Brazilian, uniaxial compression, triaxial compression), it is the direction of the load applied to the top and bottom of the test specimen.

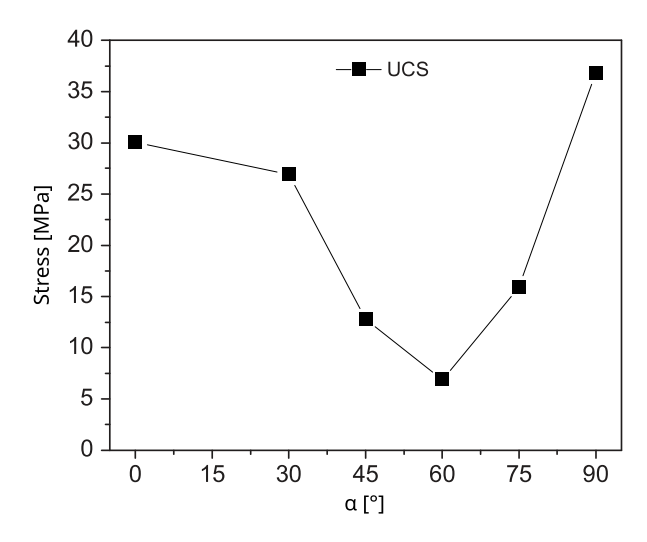


Figure B.2: Influence of the dip of a single weakness plane, α , passing through the specimen's centre on the peak strength (i.e., UCS ... uniaxial compressive strength) at numerical uniaxial compression tests (modified from [75, Fig. 5, p. 6408]).

planes parallel to the loading ([223, p. 625]). Here, no distinction is made for the plot in Fig. 3.8. Considering only strength pairs from tests featuring a similar loading direction relative to the dip of the weakness planes, very few data would remain.

B.1.3 Rostami et al. (2016)

Rostami et al. (2016) [329] have compiled more than 1800 pairs of uniaxial peak compressive strength, σ_c , and splitting tensile strength, $\sigma_{t,sp}$, values from laboratory tests on different rock types with a wide range of σ_c :

- Colorado School of Mines (CSM): n = 182; $\sigma_c = [1.3; 468.5]$ (in mega-pascal); mainly welded tuff, granite, sandstone, limestone, and argillite;
- Pennsylvania State University (PSU): n = 198; $\sigma_c = [8.1; 247.0]$ (in mega-pascal); mainly limestone, sandstone, claystone, siltstone, shale, and gneiss;
- Istanbul Technical University (ITU): n = 158; $\sigma_c = [3.6; 174.0]$ (in mega-pascal); mainly sandstone, limestone, shale, marl, and silt-claystone;
- University of Melbourne (UM): n = 1202; $\sigma_c = [0.2; 458.5]$ (in mega-pascal); no information on rock type available;
- Nidge University (NU): n = 122; $\sigma_c = [2.2; 210.6]$ (in mega-pascal); mainly limestone, travertine, granite, pyroclastics, marble, and metallic ores.

The authors performed a fitting with the method of least squares for each data set utilising a linear or exponential relation between σ_c and $\sigma_{t,sp}$. The correlation coefficient of the best fits range between 0.54 and 0.89 for linear relations and between 0.61 and 0.90 for exponential relations. Before fitting, the authors disregarded data from tests on specimens which featured a plane of weakness prior to the test having adverse effects on their behaviour during the test (e.g., failure along weakness plane) ([329, p. 148]). Fig. 3.8 illustrates the relations with the higher correlation coefficient (either linear or exponential) for each data set.

B.2 Dilation angle (zone failure, disintegration)

Section B.2.1 addresses the puzzling wording for volume change upon failure, and Section B.2.2 details results of shear tests on weak rock material.

B.2.1 Terminology

[410, p. 6] associate the term dilatancy (short for shear dilatancy) with volume changes which accompany plastic shear distortion. These volume changes can be negative or positive, i.e., resulting to a decrease or an increase in volume, respectively. A material which changes its volume upon shear distortion is called a dilatant material, independent of whether the volume decreases or increases (as the dilatancy angle used to characterise a dilatant material can be negative or positive; cf. [410, p. 7, 27]). If it preserves its volume, it is a non-dilatant material ([410, p. 8]). The process associated with a decrease in volume is termed contraction (the material contracts). In case of an increase in volume, it is termed dilation (or dilatation; the material dilates; cf. [410, p. 42]).

[427, Fig. 4, p. 371] use the terms contraction and dilation in the same way. [130, p. 70] explicitly relates the term dilatancy to volume increase associated with cracking (i.e., plastic deformation) only. However, somehow inconsistent, he uses this term also as a general term for volume change (cf. Fig. 3.9b on p. 34 in this document, or other Figures in [130], e.g., Fig. 3.9 on p. 73). Adding more confusion, in [11, p. 169], dilatancy is associated with volume increase only, and dilatation (or dilation) is used as a general term for volume change. And for [181, p. 85], dilatancy is the "phenomenon by which the volume of the rock decreases under the action of an additional compressive stress", but it also describes the phenomenon when "the total volume will in fact increase" (cf. [181, p. 266] referring to [82]). Further, it is a dilatant material if the dilatancy angle is positive, and it is contractant if it is negative ([181, p. 267]).

For this study, dilatancy is used as a general term describing volume change upon deviatoric loading. The dilatancy angle quantifies the volume change. Contraction refers to volume decrease (negative dilatancy), dilation (or dilatation) to volume increase (positive dilatancy). Thus, a material either contracts or dilates. Volume increase (i.e., dilation), however, occurs only at frictional sliding. And this is possible only in case of plastic (i.e., unrecoverable) deformation. This definition agrees, for example, with [166, p. 249] who quote that at "failure, the rock will dilate (increase in volume)". The dilation angle (not the dilatancy angle), therefore, quantifies volume increase only and equals the dilatancy angle if the latter is positive. A material is dilatant, if it changes its volume upon loading, and it is non-dilatant, if it preserves its volume.

B.2.2 Kluckner (2012)

In the course of his investigations, [199] examined also some laboratory direct shear tests on weak intact rock material (from which specimen preparation for triaxial compression tests was not possible). The data set (n = 23) comprises results from tests on phyllites, schists, carbonates, and gneiss, most of them in the form of breccias, cataclasites, or tectonites. The material has been recovered from depths of 20 m to 609 m below surface. The tests have been performed under constant normal stiffness (CNS) conditions with the external stiffness $K \approx \infty$ ([41]) (i.e., vertical displacement of shear box fully constrained, thus, no dilation possible; for details, cf., e.g., [310, 312]). The initial normal load, $\sigma_{n,0}$, ranges from approx. 0.3 MPa to approx. 0.85 MPa depending on the material tested. The shear area of all specimens was greater than 80 cm² exceeding the lower limit of 19 cm² according to [14, p. 4] by far. The values for the dilation

angle, ψ , range from 0.1° to 10.7°, those for the internal angle of friction, φ , from 30.9° to 61°, and those for the cohesion, c, from 0 MPa to 0.33 MPa. The data is included in the graph in Fig. 3.5 (p. 25). The difference between φ and ψ is 23.8° at minimum. The residual values are $\varphi_r = [25; 45.4]$ (in degrees) and $c_r = [0; 0.08]$ (in mega-pascal). Note that the analysis of the test results lacks a differentiation regarding the shear direction relative to the orientation of weakness planes (if present; e.g., foliation planes).

B.3 Poisson's ratio

Fig. B.3 compares the Poisson's ratio, ν , with the Young's modulus, E, and the uniaxial peak compressive strength, σ_c , of some rock specimens. The data is from [130, 199].

In the top graphs, the data from [199] is coloured according the upper value $\sigma_{1,u}$ of the axial stress range $\{\sigma_{1,u};\sigma_{1,l}\}$ within which the unloading-reloading loop has been performed prior peak load to determine E and ν at the compression tests. If the developments of E and ν with axial strain shown in Fig. 3.10b/c (p. 35) generally apply to rocks, then each data in Fig. B.3 is valid for one particular material state (e.g., accumulated axial strain) only. Then, for example, data points in the top right graph from unloading-reloading loops where $\sigma_{1,u} > 15$ MPa probably would be closer to the bottom right corner of the graph in case the loops would have been performed at a lower stress level (e.g., $\sigma_{1,u} = 10$ MPa). Considering only data with the same $\sigma_{1,u}$, no clear trend can be identified, or too few data points exist. Being unaware of the stress levels the parameters cited in [130] have been determined at, no correlations in the bottom graphs can be constructed either. Note that other factors like differences in the testing procedure also contribute to the data scatter. Anyway, all graphs in Fig. B.3 show that independent of E and σ_c , ν varies within the natural range for real materials of $0 < \nu < 0.5$ (cf. Section 3.2.7 on p. 33). Most values are below 0.3.

B.4 Young's modulus

Both Fig. B.4 and Fig. B.5 plot data of sedimentary and metamorphic rocks from [199]. The former compares the Young's modulus, E, with the uniaxial peak compressive strength, σ_c . In the latter, E is compared with the deformation modulus, V. E is the secant modulus determined at an unloading-reloading loop, and V is the secant modulus determined at the virgin loading curve (cf. Fig. 3.13 on p. 38). For the determination of both E and V, the same axial stress levels are used between which the secants are constructed. The legend in the figures cites the upper bound $\sigma_{1,u}$ of the stress range $\{\sigma_{1,l}; \sigma_{1,u}\}$.

Because the data is limited, no trend can be constructed in Fig. B.4 regarding l/d, α , or $\sigma_{1,u}$. But most data pairs are above the 200 : 1 line and below the 1000 : 1 line. Fig. B.5 suggests that for less-stiff rocks, the increase from the modulus at the virgin loading curve, E, to the modulus at the unloading-reloading curve, V, is larger. This implies that at high-stiff rocks, the difference between E and V is less.

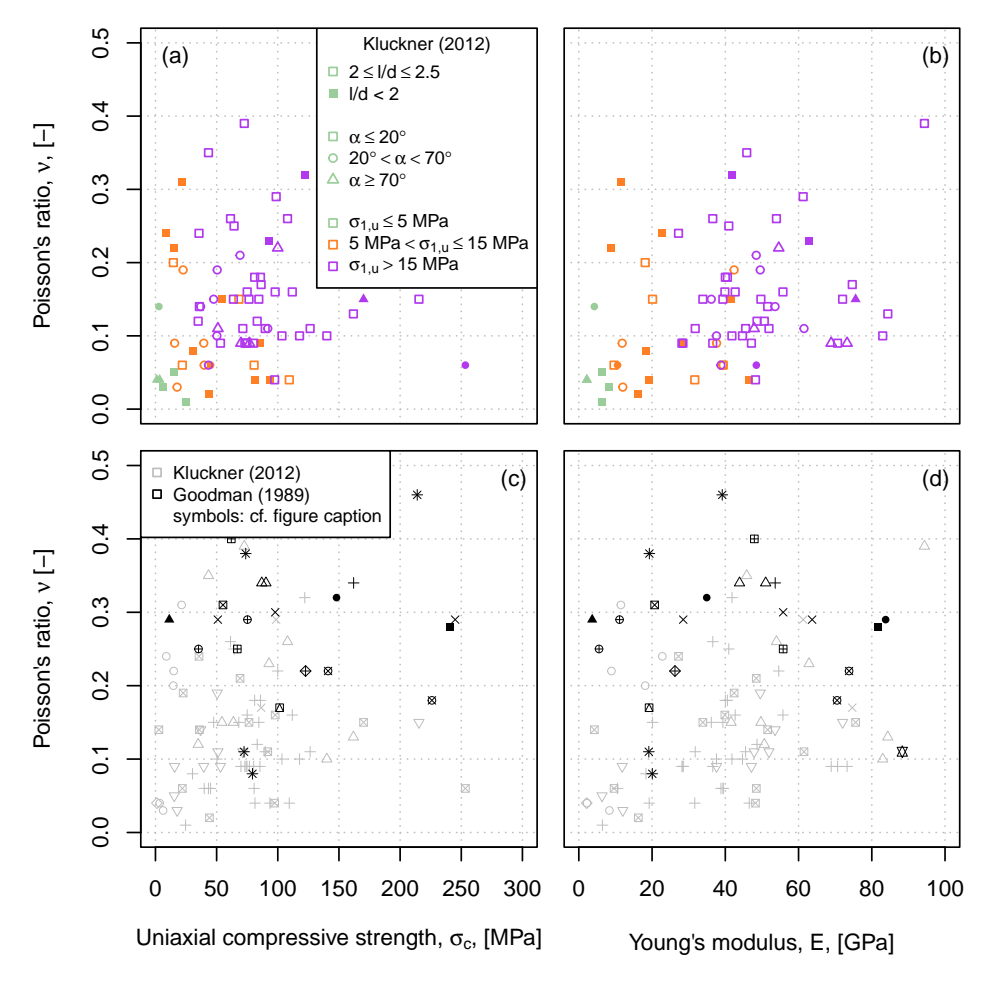


Figure B.3: Comparison of the Poisson's ratio, ν , with the uniaxial peak compressive strength, σ_c , (left column) and Young's modulus, E, (right column) of some rock specimens. Kluckner (2012) [199]: data from the Semmering Base Tunnel project (cf. also Section B.1.2); secant modulus from the unloading-reloading loop; l/d ... specimen length to specimen diameter ratio, α ... dip of weakness planes (if existing; if not: $\alpha = 0^{\circ}$), $\sigma_{1,u}$... upper bound of axial stress range within which the unloading-reloading loop has been performed to determine E and ν . Goodman (1989) [130, Tab. 3.1, p. 61; Tab. 6.1, p. 186]: for the origin of the data, cf. reference list in [130, Footnote c, p. 62]; tangent modulus from the virgin loading curve (stress level for determination is not reported). Symbols in bottom graphs: \mathbf{o} breccia (n=6), Δ dolomite (n=11), + gneiss (n=34), + limestone (n=5), + cataclasite (n=1), + phyllite (n=10), + schist (n=14), + sandstone (n=4), + siltstone (n=1), + shale (n=2), + quartzite (n=1), + marble (n=2), + granite (n=2), + tonalite (n=1), + diabase (n=1), + basalt (n=2), + tuff (n=1).

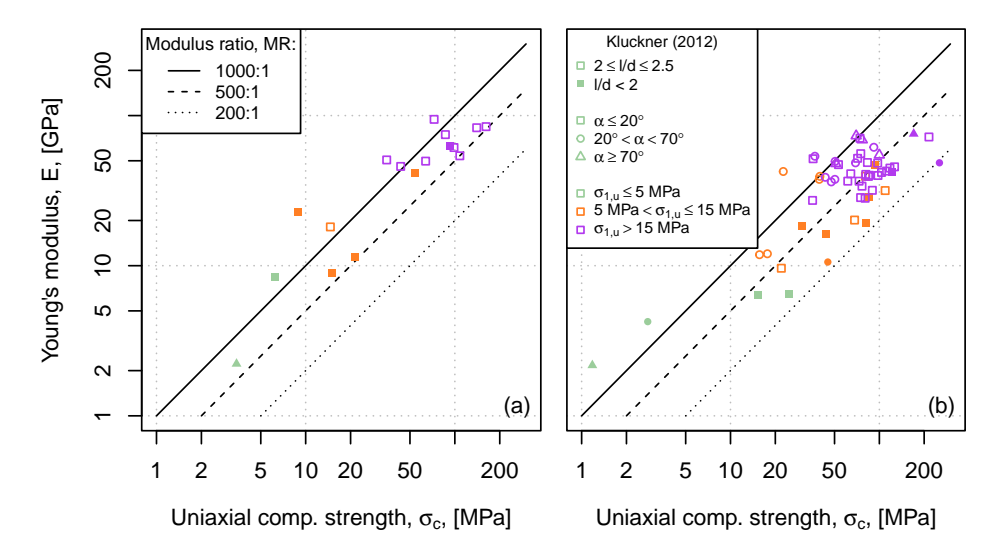


Figure B.4: Comparison of the Young's modulus, E, with the uniaxial peak compressive strength, σ_c , of some rocks. Log-log plot. (a) Sedimentary rocks: breccia, dolomite, limestone; (b) metamorphic rocks: gneiss, cataclasite, phyllite, schist. Kluckner (2012) [199]: data from the Semmering Base Tunnel project (cf. also Section B.1.2); secant modulus from the unloading-reloading loop; l/d ... specimen length to specimen diameter ratio, α ... dip of weakness planes (if existing; if not: $\alpha = 0^{\circ}$), $\sigma_{1,u}$... upper bound of axial stress range within which the unloading-reloading loop has been performed to determine E.

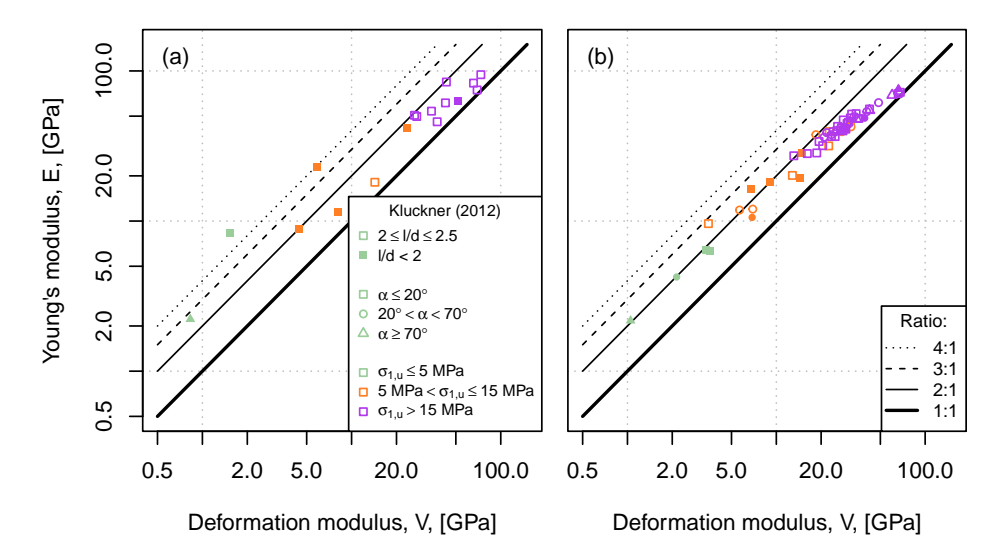


Figure B.5: Comparison of the Young's modulus, E, with the deformation modulus, V, of some rocks. Log-log plot. (a) Sedimentary rocks: breccia, dolomite, limestone; (b) metamorphic rocks: gneiss, cataclasite, phyllite, schist. Kluckner (2012) [199]: data from the Semmering Base Tunnel project (cf. also Section B.1.2); E ... secant modulus from the unloading-reloading loop; V ... secant modulus from the virgin loading curve; l/d ... specimen length to specimen diameter ratio, α ... dip of weakness planes (if existing; if not: $\alpha = 0^{\circ}$), $\sigma_{1,u}$... upper bound of axial stress range within which the secant moduli are determined.